Title
Cultivating and Characterizing Electroactive Microbial Communities using Bioelectrochemical Systems and Metagenomics

Author
Arbour, Tyler

Publication Date
2017

Cultivating and Characterizing Electroactive Microbial Communities using Bioelectrochemical Systems and Metagenomics

by

Tyler Joseph Arbour

A dissertation submitted in partial satisfaction of the

requirements for the degree of

Doctor of Philosophy

in

Earth and Planetary Science

in the

Graduate Division

of the

University of California, Berkeley

Committee in charge:

Professor Jillian Banfield, Chair
Professor James Bishop
Professor Ronald Gronsky

Spring 2017

ABSTRACT

Cultivating and Characterizing Electroactive Microbial Communities using Bioelectrochemical Systems and Metagenomics

by

Tyler Joseph Arbour

Doctor of Philosophy in Earth and Planetary Science

University of California, Berkeley

Professor Jillian F. Banfield, Chair

Certain microbes have the remarkable ability to form direct electronic connections with their extracellular environment, harnessing existing redox gradients to drive their own life processes. The recognition of extracellular electron transfer (EET) as a widespread microbial phenomenon that plays an important role in biogeochemistry is recent, and is accompanied by new understanding of how this process impacts physical and chemical characteristics of the environment. Our current knowledge of the mechanisms and the microbial physiology behind EET is based largely on studies of two well studied isolates, *Geobacter sulfurreducens* and *Shewanella oneidensis*. Nevertheless, nature is not well represented by isolated organisms. Identification of the larger set of "electroactive" microbes from across much of the phylogenetic spectrum is critical for complete understanding of microbial controls on redox chemistry in natural environments. Genomic information for these organisms has the potential to expand our understanding of the mechanisms of growth that rely upon EET. This information should be particularly useful if it is obtained in an experimental setting that enables manipulation of redox potential.

In this doctoral dissertation, microbial electrochemical cells (MXCs) are employed as a tool to select for and characterize the subset of electroactive microbial community members. The main advantage of MXCs is that they use a solid, inert electrode in place of natural minerals as the terminal electron acceptor (TEA) for microbial metabolism. This enables direct control over the redox potential and overcomes the chemical heterogeneity and variation in surface reactivity of natural minerals. Experiments are inoculated using microbial communities from subsurface sediments sampled from a major Department of Energy research site near the town of Rifle, Colorado, USA. This site has general relevance as a riparian zone aquifer; prior research has generated thousands of microbial genomes from samples collected across multiple subsurface environment types and impacted by a variety of experimental manipulations (including acetate amendment). Complex electroactive microbial communities, including anode-associated biofilms, are cultivated in the MXC experiments using the sediment inoculum and acetate as the electron donor. Experiments include two independent MXCs with duplicate compartments.

In Chapter 1, we subjected the biofilms and associated planktonic cells to large changes in anode redox potentials and characterized the responses of these organisms using electrochemical methods. Community composition was documented using 16S rRNA gene-based surveys. Our results strongly suggested that TEA redox potential is an important determinant of the makeup of mineral-respiring communities.

Chapter 2 tested the hypothesis that microbes populating anode-associated biofilms electrochemically adapt to imposed redox conditions on a short timescale (minutes). Through a series of cyclic voltammetry experiments, the overall biofilm responses to changing redox potential were observed. The voltammetry data suggested inherent redox flexibility in the microbial EET network, very likely conferred by multiheme *c*-type cytochromes known to be critical for extracellular respiration in most known electroactive organisms. We performed a series of experiments that allowed us to rule out within-biofilm pH changes as the cause for the observed shifts.

In Chapter 3, metagenomic methods were employed to genomically characterize the MXC microbial communities. Genome-resolved metagenomics enabled the recovery of comprehensive genetic information for the majority of community members without the requirement for isolation of individual organisms. Hundreds of near-complete genomes were reconstructed and used to compare biofilm and planktonic organisms across experimental systems. Specifically, biofilm *vs*. planktonic growth preferences for most organisms were defined. Importantly, genomes were used to predict genes that could enable growth on electrodes. Biofilm-associated bacteria are known to have genomes that are strongly enriched in multiheme cytochromes and to have associated outer-membrane porins implicated in electron transfer complexes. In addition to organisms related to known electroactive species, several novel organisms (from an expected undiversity of phyla) were implicated in electrode growth. The extensive metagenomic data assembled previously from the Rifle site was used to link specific organisms enriched in the MXCs to those from Rifle, and thereby yielding insights into their roles in the natural environment.

Coupling electrochemical methods with genomic and metagenomic DNA sequencing provided new information about microbial growth in MXCs and the response of the overall microbial community to imposed changes in redox potential. The hypothesis that TEA (and by proxy, mineral) redox potential shapes community composition was supported. The question of adaptation of microbes to changing environmental redox conditions was investigated in community context, without reliance on isolation methods. The findings suggested that large multiheme cytochromes evolved to cope with intrinsic mineral redox heterogeneity and fluctuating redox conditions. Finally, genome-resolved metagenomics enabled the identification of novel, putatively electroactive organisms functioning as part of complex microbial consortia, with widely different metabolisms from those of the well-studied type strains. This contributes to basic knowledge of EET in natural systems, and opens new avenues for the application of electroactive organisms in biologically-based technology, engineering and remediation.

TABLE OF CONTENTS

ACKNOWLEDGEMENTS

While few eyes will ever see this, it is important to me to acknowledge and thank those who helped shape me into the person and scientist I am today. Starting with teachers: From elementary through high school, there were many committed individuals that fostered my curiosity and went the extra mile to excel in one of the most crucial roles in our society and world. You all do not get the credit or salaries that you deserve, and I will fight throughout my life to change that.

Next to Montana State University. First and foremost, to my college roommate and one of my best friends, Luke Oltrogge, and to his wonderful family that more or less adopted me during that time: I am not sure I would have discovered the unending joys of a life in science had we never met. To the undergraduate Chemistry professors who became my research advisors for over two years: Trevor Douglas and Robert Szilagyi. The opportunities you gave me, and the fantastic lab culture you fostered in your groups, propelled me on the path to graduate school. Other professors and teachers at MSU who showed me the best side of academia, and whose enthusiasm for their research and teaching inspire my own: Richard Gillette in the Math department, and Pat Callis, David Singel, and Hien Nguyen in my home Department of Chemistry and Biochemistry. Finally, the University Honors Program provided an amazingly rich, well-rounded college education that far surpasses what most state schools provide, and opened my rural-Montana eyes to a much wider world.

Deutschland! Ich liebe dich. Professor Jörg Enderlein, thank you for having me in your lab and for outstanding scientific mentorship, as well as ongoing friendship. My time in Germany was the most unforgettable of my life, and I am so excited to be heading back across the pond for a postdoc! Marie-Luise und die ganze Familie Klotz: you will always among the most special people in my life. Mary, during our time together here in the East Bay, you did more than anyone else in my life to help me recognize and take action in overcoming the worst of my insecurities and fears that prevented me from being the person I strive to be. I will forever be both extremely grateful and sorry.

Berkeley, California and UC Berkeley, you get a bad rap among us Montana folk, but I now know what a special place you are, and that it is entirely undeserved. There are so many people and places I have come to know over these past nearly *eight* years (sorry Jill!) that mean so much to me. John and Pat Rea, I can never repay your gratitude and support. To so many in my home Department of Earth and Planetary Science, especially fellow grad students who became the friends with which I shared this fantastic and arduous journey, and who supported each other along the way. Thank you to the Berkeley undergrads I have had the privilege to serve as a "GSI" (TA) or Berkeley Connect mentor; you helped to remind me how much I love learning, and why I decided to pursue this PhD thing. To the inspiring faculty who I have been fortunate to have as teachers, top among them Phill Geissler, Ron Gronsky and Gary Sposito.

My sincere thanks to Leighton Fong, who has loaned me his old cello for the entirety of my long graduate career, and given me many lessons in exchange for kid-sitting his wonderful daughter, not to mention a fair number of tickets to performances of the one and only *Left Coast Chamber Ensemble*. Thank you to Renato and Sonya Rodolfo-Sioson, my house mates, landlords and good friends for the past... wow, how many years now? Thanks for making me feel like much more than just your tenant. And it would be disingenuous of me to neglect my friends in the Bay Area craft beer world: you all helped to keep me balanced, and to get outside of my (wonderful) academic bubble now and then. In particular, I want to acknowledge Jen Muehlbauer, Heather

Clegg-Haman, and the wonderful human beings on the other side of the bar at Sierra Nevada's *Torpedo Room*.

To my parents and step-parents, thank you for your love and support throughout my life. Marmalade and RandyDad, thank you for working with me to nurture our relationships, which are thriving more than ever; I cannot express how much this means. Thank you to all of my siblings, especially the Tate family who made sure I had a home away from home for the family holidays I missed in Montana. Also to my extended family—aunts, uncles, cousins—who always have a place for me to stay when bouncing around the Big Sky State, and whose remote support through Facebook or email has helped me through some tough times.

The Banfield Lab: what an incredible group of people. So many current and former Banfielders (and significant others) I want to thank. Sue and Jay Spaulding, Chris Miller, Ryan Mueller, Anders Norman, Chris Brown and Emily Thompson, Joanne Emerson, Karen Andrade, Christine Sun, Alex Probst, Rose Kantor, and seriously everyone else. You inspire me. Thank you for your help and friendship.

Finally, and most of all, to my academic advisors Ben Gilbert and Jill Banfield. Ben, it has been so much fun working with you in and outside of the lab. Thank you for being so generous with your time. I have learned a lot from working with you that will be a great help going forward. And Jill: a mother, artist, teacher and the most hard-working, passionate, devoted scientist and advisor that I have ever had the privilege to know. This is no exaggeration, as anyone in the Banfield-lab family can attest. I do not have the words right now to express how much your too-many years of support means to me, and how fortunate I feel to have been a member of your group. Despite a slow start, I feel very well prepared for the next stage of my career. I hope to make you proud.

CHAPTER 1

Cultivation and Characterization of Anode-Respiring Biofilms Subjected to Changing Redox Conditions

Abstract

Certain microorganisms use solid minerals as electron acceptors for respiration. Unlike soluble electron acceptors such as oxygen or nitrate, minerals are heterogeneous in redox potential and often dissolve upon reduction. There are many open questions concerning the competitiveness of mineral-reducing microorganisms in anaerobic communities when presented with substrates at different redox potentials, and the mechanisms by which these organisms adapt to changes in electron-acceptor potential. To address these questions, we used a microbial electrochemical cell, in which a solid graphite electrode is used in place of natural mineral electron acceptors, to cultivate an anode-respiring biofilm community and precisely control redox conditions. As described in this Chapter, we investigated the controls of electron-acceptor redox potential by subjecting the growing biofilm to large shifts in anode potential, and characterized the response using electrochemical methods and 16S rRNA-based surveys of microbial community composition. Our observation that red-colored biofilm regions dominated by *Geobacter* species developed only after switching to an unfavorable potential (from +410 to -190 mV) after three months of continuous operation is strong evidence that these organisms outcompete other electroactive bacteria in unfavorable redox conditions, *i.e.*, where growth is just thermodynamically possible. We performed electrochemical analysis of the *Geobacter*-dominated biofilm as a basis for studies of anode-potential variation, described in Chapter 2.

Introduction

Microbial metabolism involving iron- and manganese-oxide minerals has been shaping Earth's mineralogy and geochemistry since at least the oxygenation of the atmosphere (Nealson & Myers 1990; Konhauser et al. 2005) around 2.4 billion years ago (Partin et al. 2013; Lalonde & Konhauser 2015), and likely far earlier (Vargas et al. 1998; Kim et al. 2013; Manzella et al. 2013; Weber et al. 2006; Harel et al. 2014). In low-oxygen environments, dissimilatory metal-reducing (DMR) microorganisms can capture energy released from the oxidation of a variety of organic and inorganic electron donors using insoluble, redox-active minerals as an electron sink (DiChristina et al. 1988; Myers & Nealson 1988; Lovley & Phillips 1988; Nealson & Little 1997). A wide and ever expanding variety of bacteria and archaea are being shown to be capable of DMR (Weber et al. 2006; Sturm et al. 2012), and thereby influence the geochemistry and mineralogy of their surroundings. Two important and contrasting examples are the reductive dissolution of iron(III) oxides, causing the release of surface-adsorbed contaminants such as arsenic (Islam et al. 2004), versus immobilization of toxic, highly soluble uranium(VI) upon reduction and precipitation as insoluble U(IV) oxides (Lovley et al. 1991; Anderson et al. 2003; Kostka & Green 2011).

Many interrelated factors influence the bioavailability of an iron oxide mineral as an electron acceptor, including its structure and composition (Thamdrup 2000; Majzlan 2012), grain size (Langmuir & Whittemore 1971; Navrotsky et al. 2008), specific surface area (Roden & Zachara

1996; Roden 2006) and solubility (Bonneville et al. 2004; Bonneville et al. 2009). However, the redox potential (*E*h) for the relevant Fe(III)-reduction reaction remains a fundamental thermodynamic constraint on the amount of energy that can be conserved in extracellular mineral respiration. The *E*h range of the many forms of naturally occurring iron oxides (Cornell & Schwertmann 2003) spans nearly 500 mV (Thamdrup 2000), and this heterogeneity therefore represents a particular challenge for these organisms.

DMR microorganisms present in anaerobic environments will readily utilize solid electrodes in place of natural minerals as an electron sink, assuming a sufficient free-energy difference exists (Reimers et al. 2001; Tender et al. 2002). This bio-electrochemical interaction is the basis for microbial fuel cell (MFC) technology (Potter 1911; Disalvo & Videla 1979; Wingard et al. 1982; Bennetto 1984). MFCs, and more generally microbial electrochemical cells (MXCs), are now being widely used in the cultivation and study of EET-active microorganisms (Bond et al. 2002; Bond & Lovley 2003; Kim et al. 2004; Logan et al. 2006; Wrighton et al. 2008). The use of a potentiostat in MXCs allows for precise control of electrode potential (Bond & Lovley 2003; Logan et al. 2006), which makes them an ideal tool to investigate the effects of electron-acceptor *E*h on EET activity (Aelterman et al. 2008; Marsili, Rollefson, et al. 2008; Torres et al. 2009; Wagner et al. 2010; Wei et al. 2010), and avoids the complexity and heterogeneity inherent to natural minerals.

In this study, we used a custom MXC combined with a potentiostat to investigate the effect of a large change in imposed *E*h on replicate anode-biofilm communities enriched from subsurface aquifer sediment. We observed a significant change in the magnitude of the maximum current the biofilms were able to produce after poising at *E*h each condition. We also observed a concomitant change in the appearance of the anode biofilms, which developed segregated regions of different color. We therefore characterized the community composition of each biofilm region, as well as of cells in the planktonic solution, using 16S rRNA gene clone library analysis.

Materials and methods

Preparation and inoculation of microbial electrochemical cells

A custom three-electrode cell with a shared cathodic chamber between duplicate anodic chambers (**Figure 1.1**) was prepared with graphite working electrodes (2.5 × 2.5 × 1.0 cm, McMaster-Carr). The unpolished graphite surfaces were rubbed with a soft sponge in water to remove loose flakes, rinsed, and sonicated in 5% bleach for 5 min. This was followed by three rounds of sonication (5 min each) in fresh DI water and then soaking overnight. Electrodes were rinsed and soaked several more times with DI water before installation. A Pt-mesh counter electrode (~1.5 × 1.0 cm) was used in the cathodic chamber for dual-anode chronoamperometry, and additional Pt-wire counter electrodes were inserted into anodic chambers for single-anode CV analysis. Pt electrodes were cleaned by soaking overnight in 1.0 N HCl. Reference electrodes were Ag/AgCl type (3 M KCl, Microelectrodes, Inc. model MI-403; +210 mV vs. SHE for standard conditions). Nafion 117 (DuPont) was used as the proton exchange membrane separating anodic and cathodic chambers, and membranes were soaked several times in DI water before cell assembly to dilute the acidity of the hydrated material.

The assembled electrochemical cell was filled with DI water and sterilized by autoclaving. DI water in anodic chambers was replaced with sterile, anaerobic (N_2-flushed) phosphate-buffered media, pH 7.2, containing the following per 1 L: NaH_2PO_4 plus Na_2HPO_4 (anhydrous; 0.38 g and

0.97 g, resp. for 10.0 mM total phosphate buffer), KCl (0.10 g, 1.3 mM), NH_4Cl (0.25 g, 4.7 mM), and previously described vitamin and mineral mix (10 mL each) (Lovley et al. 1984). Anaerobic conditions were maintained in anodic chambers by constant flushing with ultrahigh purity N_2 gas passed through an oxygen trap (Alltech OxiClear) and 0.2 μm filters. The same media recipe was used for aerobic cathode media, except the initial buffer was Tris-HCl (4.7 g/L, 30 mM, pH 7.2); at 35 days, we switched to media with an increased phosphate buffer concentration of 50 mM, and used this for cathodic as well as anodic chambers. Oxygen served as the electron acceptor at the cathode and was supplied by a steady stream of humidified air passed through a 0.2 μm filter.

Prior to inoculation, the anode potential was poised using a PAR VersaStat MC potentiostat to establish baseline current. The anodic compartment was amended with sodium acetate (10 mM initial concentration), which was used as the electron donor throughout the experiment. Anodic chambers were inoculated with subsurface sediment obtained from a major Department of Energy field site located at Rifle, CO, USA. This sample ("BH 3.2.11") was recovered from alluvium at the bottom of a freshly-dug trench with a depth of *ca.* 3.5 m below ground surface (co-located with the depth to groundwater). The trench was located in an area of "background sediment" not subjected to prior acetate amendments. Alluvium was passed through a <2.5 mm sieve, added to no-headspace Mason jars and saturated with groundwater from the trench. Samples were stored at 4 ºC in the dark until inoculation (6.5 months). The sediment-groundwater sample was shaken to mix and then introduced into anodic chambers through the MXC sampling ports using a sterile spatula for the coarser sediment grains, and a sterile, N_2-flushed syringe for the fine-grain/groundwater suspension.

The poised-anode MXC was operated at ambient temperature, which was constantly monitored (5 min intervals) and ranged from 18-24 ºC. Current readings were taken at 5-min intervals for the entire experiment except when performing voltammetry or other electrochemical measurements. The electrogenic cultures were maintained in a fed-batch manner and supplied with acetate in amounts that maintained the concentration in the range of 1-10 mM, with occasional periods of substrate limitation.

Calculating of Coulombic efficiency

We calculated CE for a given acetate-amendment peak in chronoamperometry data by integrating the peak (minus baseline current) to obtain the total charge in Coulombs, and comparing this to the theoretical amount of charge released in the complete oxidation of the acetate added (Lovley 1991): (mol Ac added) × (8 mol e^- per mol Ac) × (96,485 C per mol e^-).

Cyclic voltammetry

After confirming that voltammetry curves from the two independent anodes were indistinguishable aside from a difference in the absolute current (by a factor of 1-2 over the months of study), most slow-scan cyclic voltammetry (SSCV) was performed with both anodes connected, using the Pt-mesh electrode in the cathodic chamber as counter electrode. Scan rates as low as ~0.05 mV/s were required in order to obtain reversible, sigmoid-shaped CVs for mature biofilms. In most cases, additional SSCV scan parameters were: $E_{initial}$ = prior poising potential, E_{an}; $E_{vertex,1}$ = -0.5 V; $E_{vertex,2}$ = +0.4 V (all values vs. SHE).

Sampling of planktonic and biofilm communities

At four months post-inoculation, planktonic media (30 mL, Anode 1 compartment only) was removed and passed through a 0.2 μm filter. The filtrate was centrifuged for 7 min at 9000 × *g* and

the supernatant discarded. The same day, DNA from both the filter (>0.2 μm) and filtrate (≤0.2 μm) fractions was extracted, quantified and amplified by PCR (see next section). After 10 months of continuous operation with electrodes poised mostly at -190 mV (a value corresponding to half-maximal current), each of the graphite electrodes were briefly removed and exposed to ambient air to sample the anode-associated biofilms for 16S rRNA gene clone library analysis. Sterilized razor blades were used to gently remove biomass from the graphite surface, and biomass was then flushed into 2-mL centrifuge tubes using a small amount of sterile anaerobic media. Tubes were sealed with Parafilm and immediately placed in N_2-flushed 50-mL centrifuge tubes and stored at -80 ºC within 30 minutes. Electrodes were replaced immediately after sampling and chronoamperometry was resumed, allowing biofilms to recolonize anode surfaces.

At 21 months of stable operation, one electrode (Anode 1) was again removed to collect samples for protein gel electrophoresis and scanning electron microscopy (SEM) imaging. A sterilized razor blade was used to remove intact pieces of graphite-associated biofilm for SEM samples, which were immediately fixed in 2% glutaraldehyde in 0.1-M sodium cacodylate buffer, pH 7.2 and stored overnight at 4 ºC for further analysis. From the remaining biofilm, two replicate samples for gel electrophoretic analysis were collected as described above and stored on ice for same-day analysis (see below).

Nucleic-acid isolation and phylogenetic analysis (4- and 10-month samples)

Genomic DNA was isolated from planktonic (>0.2 μm filter fraction only as nucleic acid concentration in the ≤0.2-μm filtrate was below the limit of detection) and anode biofilm samples using the PowerSoil DNA Isolation Kit (MO BIO Laboratories, Inc.) following the manufacturer's protocol. PCR amplification using universal bacterial primers 27f and 1492r (Weisburg et al. 1991) was conducted with TaKaRa Ex Taq polymerase (Takara Bio, Otsu, Shiga, Japan) with steps as follows: 95 °C for 2 min., 95 °C for 30 s, 52 °C for 30 s, 72 °C for 90 s, 72 °C for 10 min, with steps 2-4 repeated 28 times. Clone libraries were created using the TOPO TA Cloning Kit for Sequencing (Invitrogen) according to manufacturer protocol and submitted for sequencing at the UC Berkeley DNA Sequencing Facility using M13 vector specific primers. The Anode 1 red and colorless biofilm samples (see *Results*) were sequenced bi-directionally, while the Anode 1 planktonic and Anode 2 red biofilm samples were sequenced with forward primer.

Sequences were quality-filtered and trimmed using Phred, vector-screened with Cross_match, and assembled into contigs with Phrap. Contigs less than 300 bp were discarded. Contigs were clustered at 99% 16S rRNA gene identity using UCLUST (Edgar 2010) and checked for chimeras using three methods: 1) UCHIME (Edgar et al. 2011) with the uchime_ref option vs. both Greengenes and SILVA; 2) uchime_denovo, which uses only the sequences in the clone library; 3) DECIPHER (Wright et al. 2012) (http://decipher.cee.wisc.edu). If results between different methods were ambiguous, the contig in question was examined manually.

Taxonomy for each sequence was assigned based on the following phylogenetic analysis: Closely related reference sequences were chosen based on best hits in the GreenGenes (downloaded 9/2013) and Ribosomal Database Project (RDP, downloaded 9/2013, type strains only, good quality) databases identified from USEARCH (-ublast) sequence similarity searches (Edgar 2010). Sequences, including an archaeal outgroup sequence, were aligned using SSU-ALIGN (Nawrocki 2009) (http://selab.janelia.org/software/ssu-align), and a maximum-likelihood phylogeny was inferred using RAxML (Stamatakis 2006) (http://sco.h-its.org/exelixis/index.html) with the GTRGAMMA model of evolution and 100 bootstrap re-samplings.

Protein gel electrophoresis (21-month red biofilm)

After determining protein concentration using a Qubit Protein Assay Kit and Fluorometer (Invitrogen), raw-biofilm samples were heated for 5 min at 95 ºC. A NuPAGE 4-12% Bis-Tris Gel with MES SDS Running Buffer (Invitrogen) was prepared. The heat-denatured sample was divided into two sets, one for Coomassie-blue-type staining (Bradford 1976) and the other for TMBZ staining and heme peroxidase activity (Thomas et al. 1976). NuPAGE LDS Sample Buffer was used for both sets of samples, but NuPAGE Reducing Agent (containing dithiothreitol (DTT)) was added only to samples to be Coomassie-stained, and omitted for those to be TMBZ-stained according to Thomas et al. (1976). Reduced and non-reduced samples were loaded onto opposite halves of the gel with empty lanes separating them, and a lane of ColorBurst Electrophoresis Marker (M.W. 8,000 - 220,000; Sigma) on each half. Proteins were separated by applying 150 V for ~1.5 hrs.

After three rinses for 5 min each with DI water, the gel was cut in half to separate reduced and non-reduced samples for the different staining procedures. Reduced samples were stained with SimplyBlue SafeStain (Life Technologies) to visualize all proteins. Non-reduced samples were treated with the following solutions under gentle agitation using a shaker: equilibration with sodium acetate (250 mM, pH 5.0) for 30 min; incubation with 3,3',5,5'-tetramethylbenzidine dihydrochloride hydrate (TMBZ, 4 mM; Sigma-Aldrich) in 30:70 vol% ethanol:sodium acetate (250 mM) for 30 min; addition of hydrogen peroxide (to give ~30 mM final concentration); incubation in 30% isopropanol to quench the reaction.

Results

Potential-dependent development of anode biofilms

Following inoculation of the three-chamber electrochemical cell (**Figure 1.1A**), we detected no current while the anode potential (E_{an}) was poised for seven days at +10 mV (all values vs. SHE). Three days after changing E_{an} to +410 mV, we observed a transient current that increased to 1.5 mA (~20 μA/cm^{2‡}) upon the replenishment of acetate (**Figure 1.2A**). This initial current peak was the highest value observed during poising at E_{an} = +410 mV, or the first three months of the study. The Coulombic efficiency (CE) during this period ranged from 26% to 63% (mean of 42% for n = 8); these values were calculated based on the sum current from both anodes, and are therefore an average of the two.

The switch to E_{an} = -190 mV at three months post-inoculation was accompanied by a steady increase in current from ~0.25 to above 2.5 mA over a period of three weeks (**Figure 1.2B**). During this time, thicker, reddish biofilm became evident on well-defined regions of both anodes, and in the same relative spatial location within both anodic chambers (**Figure 1C**). A red or pink color in anode-respiring biofilms is usually associated with a high concentration of *c*-type cytochromes.

We estimate a CE for a time near the end of this three-week period for the anode producing the most current (~2.0 mA vs. ~0.5 mA) of at least of 86%, which was the highest observed in the study; CE for the second anode could not be similarly estimated because we did not allow acetate

‡In converting absolute current to current density, we multiply the geometric surface area by a factor of three to account for the surface roughness of unpolished graphite based on work by Marsili *et al*. (Marsili et al. 2008).

to become depleted. After three weeks, switching from -190 mV back to a highly positive E_{an} (+250 mV) to allow for maximum rates of current generation resulted in a sustained current of more than 5 mA (~60 μA/cm^2 for total anode S.A.), the highest observed in this study. After this test, the anode was once again poised at -190 mV, and was held at this potential for most of the remaining study period (21 months in total).

Slow-scan CV of the community biofilm

Despite the presence of species from several different bacterial phyla in the anode biofilms (see below), their electrochemical characteristics were mostly indistinguishable from those of *Geobacter* and other known iron-reducing species (Srikanth et al. 2008; Fricke et al. 2008; Xing et al. 2008; Marshall & May 2009). Specifically, the results of slow-scan cyclic voltammetry (SSCV) performed under conditions of excess substrate, which reveals the dependence of metabolic current on E_{an}, showed a characteristic increase in current from zero to saturating across a potential window of -200 to 0 mV (**Figure 1.3A**). Also consistent with previous studies of *Geobacter* biofilms, complete exchanges of the medium did not cause a drop in current (Bond & Lovley 2003).

In addition to the main window of current onset, two smaller features appeared in SSCV, best seen in the first-derivative SSCV spectrum, **Figure 1.3B**, as peaks located at *ca.* -260 and +240 mV. The low-potential peak was observed only in the first cycle, and its presence in this and other SSCVs we acquired appeared to require acetate concentrations above a certain threshold (we estimate between 0.5 and 1.0 mM). Notably, the position of this peak overlapped with the measured open-circuit potential (OCP) of -266 mV that developed in the presence of excess acetate (following an extended period at E_{an} = -190 mV). The apparent dependence of this feature on acetate concentration prompted us to conduct a separate experiment that showed OCP to decrease by ~75 mV after adding acetate to an initially substrate-limited biofilm (**Figure 1.4**). The acetate-saturated OCP value of -266 mV lies within the range reported for several *G. sulfurreducens* strains (Bonanni, Schrott, Robuschi, et al. 2012; Malvankar, Mester, et al. 2012), and is only ~25 mV more positive than the standard electrochemical potential for acetate oxidation under similar conditions (Torres et al. 2010).

Biological analysis and imaging of anode biofilms

We confirmed the presence of *c*-type cytochromes in the red biofilm sample from Anode 1 by protein gel electrophoresis of raw biofilm extract, which revealed at least 16 distinct bands in the heme-stained portion (**Figure 1.5**). The range of molecular weights confirmed the presence of MHCs that are likely associated with EET specialists such as *Geobacter* spp. Low-resolution SEM images of red biofilm sampled from Anode 1 showed a dense and continuous biofilm over the spatial scales imaged (~1 mm), with an approximate thickness of 60-80 μm (**Figure 1.6A**). Higher-resolution SEM imaging revealed a diversity of cell morphologies that were closely integrated throughout the biofilm (*e.g.*, **Figure 1.6B**).

Composition of planktonic and anode-biofilm communities

16S rRNA gene clone library results (**Figure 1.7**) showed that red biofilm regions of both anodes were dominated by Deltaproteobacteria within family Geobacteraceae (58/71 clones for Anode 1, 76/86 clones Anode 2). Almost all of these sequences were 97-98% similar to members of *Geobacter* "subsurface clade 2" (Holmes et al. 2007), which includes *G. psychrophilus*, *G.*

thiogenes, *G. chapellei* and *Pelobacter propionicus* (Coates et al. 2001). Other taxonomic groups present in the red biofilm at lower abundance were Bacteroidetes and Betaproteobacteria.

The colorless biofilm (Anode 1) showed a more even distribution of several phyla. Geobacteraceae were far less abundant (20%) than in red regions, with Betaproteobacteria (33%) and Bacteroidetes (25%) making up the largest proportions. Tenericutes (5/61), Actinobacteria (3/61), Clostridia (2/61) and single sequences of other taxa were also present. The community composition of this colorless-biofilm sample was much more similar to that of a planktonic medium sample collected earlier in the study (at 4 months), which 16S rRNA gene clone library analysis showed to contain Betaproteobacteria (44%), Bacteroidetes (38%), Tenericutes (11%) and Gammaproteobacteria (6%) (**Figure 1.7A**). Maximum-likelihood phylogenetic trees including closest hits from databases of both cultured and uncultured organisms are included in **File S1**.

Overall, sequences classified as Betaproteobacteria showed high similarity to several type species (avg. 97.8% for 34 sequences), with *Azospira oryzae* by far the most abundant (17/34) and most similar at 99.9-100%. Other examples included *Simplicispira metamorpha* and *S. psychrophila* (both 97.6%), and *Rhodoferax ferrireducens* (97-99%). All of these organisms are classified as strictly respiratory, and known to oxidize more complex substrates using oxygen or nitrate as electron acceptors (Reinhold-Hurek & Hurek 2000; Grabovich et al. 2006). Additionally, *R. ferrireducens* is an EET-active species known to reduce Fe and Mn oxides (Finneran 2003) and electrodes (Chaudhuri & Lovley 2003). In contrast to the Betaproteobacteria, Bacteroidetes were on average only 84.5% similar to cultured representatives, but identity to uncultured organisms, most from the same subsurface aquifer that was the source of the inoculum used in this study, was much higher at 98.9% (accession numbers JX223673 and HQ260947). This was also the case for the Tenericutes clones, which were on average 96.6% similar to uncultured organisms from genus *Acholeplasma* (JX225403; DQ337019).

Discussion

Biofilm community composition and inferred metabolic interdependencies

The communities of planktonic and electrode-associated bacteria enriched from Rifle, CO background sediment (**Figure 1.7**) were broadly taxonomically similar in composition to those characterized in many previous MXC studies (Tender et al. 2002; Bond et al. 2002; Lee et al. 2003; Holmes et al. 2004; Kim et al. 2004; Jung & Regan 2007; Richter et al. 2009; Torres et al. 2009; Kan et al. 2011; Jung & Regan 2011; Malvankar, Lau, et al. 2012; Yates et al. 2012; Ishii et al. 2014; Zhu, Yates, Hatzell, Ananda Rao, et al. 2014). Enrichment for members of the family Geobacteraceae in anode biofilms is a common observation that demonstrates their specialization in respiration using insoluble electron acceptors (LaBelle & Bond 2009). This enrichment is especially pronounced when non-fermentable substrates such as acetate, butyrate or propionate are used, as was the case in this study (Jung & Regan 2007).

Other organisms abundant in the MXC, including members of the Bacteroidetes, Betaproteobacteria, Tenericutes and others, likely gain energy principally through fermentation of more complex forms of carbon. Because acetate is the only added energy source, these more complex forms must ultimately be derived from the biomass that constitutes or is produced by acetate-respiring community members. This is similar to the indirect 'priming' effect (Bianchi 2011) that has also been proposed to explain the subsequent increase in abundance of fermentative bacteria following acetate amendments to the terrestrial subsurface aquifer at Rifle, CO (Wrighton

et al. 2014). However, the prevalence of species from taxa Bacteroidetes, Betaproteobacteria, and others in electrogenic biofilms, along with their generally low 16S rRNA gene sequence identity to cultured organisms, leaves open the possibility that some may be able to gain energy from anode respiration, and thus contribute to current production (White et al. 2009; Zhang et al. 2009; Jung & Regan 2011; Ha et al. 2012; Ishii et al. 2014; Chae et al. 2009).

In summary, the persistence of at least 10 phyla over the course of more than 10 months using acetate as the only substrate suggests an interdependent microbial community that includes a wide variety of metabolisms. This finding highlights the importance of investigating EET-active species in a community context in order to understand their interactions in and implications for the natural environment.

Unfavorable electrode potential allowed the proliferation of Geobacteraceae

The influence of anode potential in determining community composition has been a topic of recent debate (Commault et al. 2014; Zhu, Yates, Hatzell, Rao, et al. 2014). Our observation that the red-colored, *Geobacter*-dominated biofilm regions developed only after switching to an unfavorable potential (from +410 to -190 mV) at three months is strong evidence that this caused a substantial increase in the overall proportion of Geobacteraceae in anode biofilms. This is further supported by the concomitant increases in both current-production capacity (**Figure 1.1**) and Coulombic efficiency, which indicates that more of the acetate is being consumed by anode-respiring specialists at -190 mV than at +410 mV. These observations are in line with previous results suggesting that many *Geobacter* spp. (or strains) are most competitive in unfavorable redox conditions, including low electrode potentials in MXCs (White et al. 2009; Yi et al. 2009; Torres et al. 2009; Bond 2010; Jung & Regan 2011). Our results strongly support the hypothesis that anode potential can affect biofilm community composition at a course taxonomic level.

The localization of the red, Geobacteraceae-dominated regions at the same relative position on two independent electrodes (**Figure 1.1B**) suggests that *E*h is more favorable at this location within the chamber, likely as a result of higher average rates of diffusion (and therefore lower ohmic resistance) of counterions from anode biofilm to cathode. This effect could likely have been eliminated by stirring the anode-chamber medium.

Biofilm redox properties are dominated by a Geobacter-like EET network

The electrochemical data and protein gel electrophoresis are consistent with the biofilm being comprised of an extensive electrically conductive network containing a high concentration of multiheme cytochromes. Although the SEM imaging and 16S RNA gene clone library analyses showed the biofilm to comprise a rich diversity of species, the dominant metabolism was associated with electrode reduction. Moreover, slow-scan CV (SSCV) of the community biofilm (**Figure 1.3**) was indistinguishable from data previously published from studies of *Geobacter* pure culture. The electrochemical data showed that the electroactive microorganisms can couple acetate oxidation to anode reduction over a wide range of thermodynamic conditions that matches the redox potentials for environmental iron oxides.

Additional details of the metabolic range can be seen from the high- and low-potential features of the SSCV. The high-potential peak at +240 mV, which has been observed in at least one other study of *G. sulfurreducens* (Fricke et al. 2008), suggests the presence of reductases that may be specifically used for electron transfer to higher-potential electron acceptors such as manganese oxide minerals or nitrate (Lovley et al. 2004; Kashima & Regan 2015). The low-potential shoulder at -250 mV is interpreted to represent the fully reduced state of extracellular reductases present at

the electrode surface—likely multiheme cytochromes. The competitive advantage of *Geobacter* spp. at low potentials is most likely due to their ability to use low-potential redox proteins to sustain metabolic turnover given only a small potential energy difference between donor (acetate) and acceptor (minerals or the electrode) redox potentials (Bond 2010). This requires extracellular reductases with low redox potentials approaching the thermodynamic limit.

Conclusion

We established an anaerobic microbial community biofilm within a bioelectrochemical system in which the primary metabolism was acetate respiration coupled to anode reduction. Visual observation and electrochemical measurement of metabolic current showed that anode potential exerted strong control on the development of the biofilm community composition at a taxonomic level. The highest current production followed the imposition of a low, unfavorable anode potential. This potential switch correlated with and likely caused the establishment of a colored, cytochrome-rich biofilm shown by 16S rRNA gene clone libraries to be dominated by Geobacteraceae. The variation of biofilm current with anode potential (slow-scan cyclic voltammetry) showed the rate of microbial metabolic turnover (current production) to increase over a range of more than 200 mV, a relationship that is explored in more detail in Chapter 2.

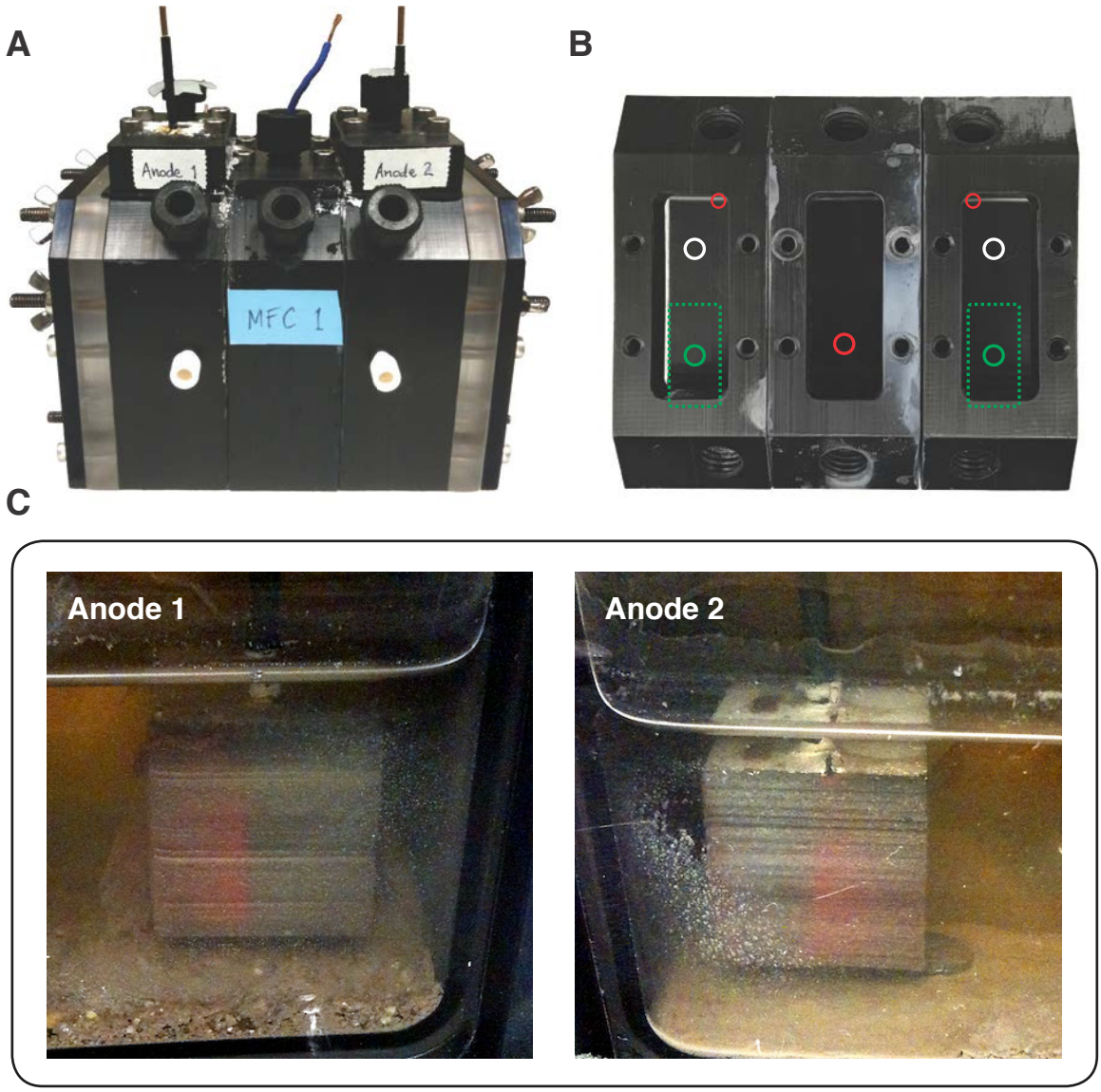

Figure 1.1 – Microbial electrochemical cell (MXC) and biofilm-covered anodes. (**A**) Front view of the MXC, which contains two identical anodic chambers sandwiching the shared cathodic chamber. (**B**) Top view of the main body of the MXC showing the approximate electrode positions within each compartment: ***green circles and dashed lines*** = graphite anodes (working electrodes); ***white circles*** = Ag/AgCl reference electrodes; ***red circles*** = cathode (central chamber) and additional counter electrodes (outer chambers) used for most cyclic voltammetry analyses. (**C**) Images showing sharply defined red/pink and nearly colorless regions of the anode biofilms. Both anodes were completely covered with a visible biofilm. The red-colored regions developed after switching the maintenance potential from +410 to –190 mV vs. SHE starting ~3 months after inoculation, and they formed in the same relative location within each anodic chamber. These images were taken at 9.5 months total enrichment time.

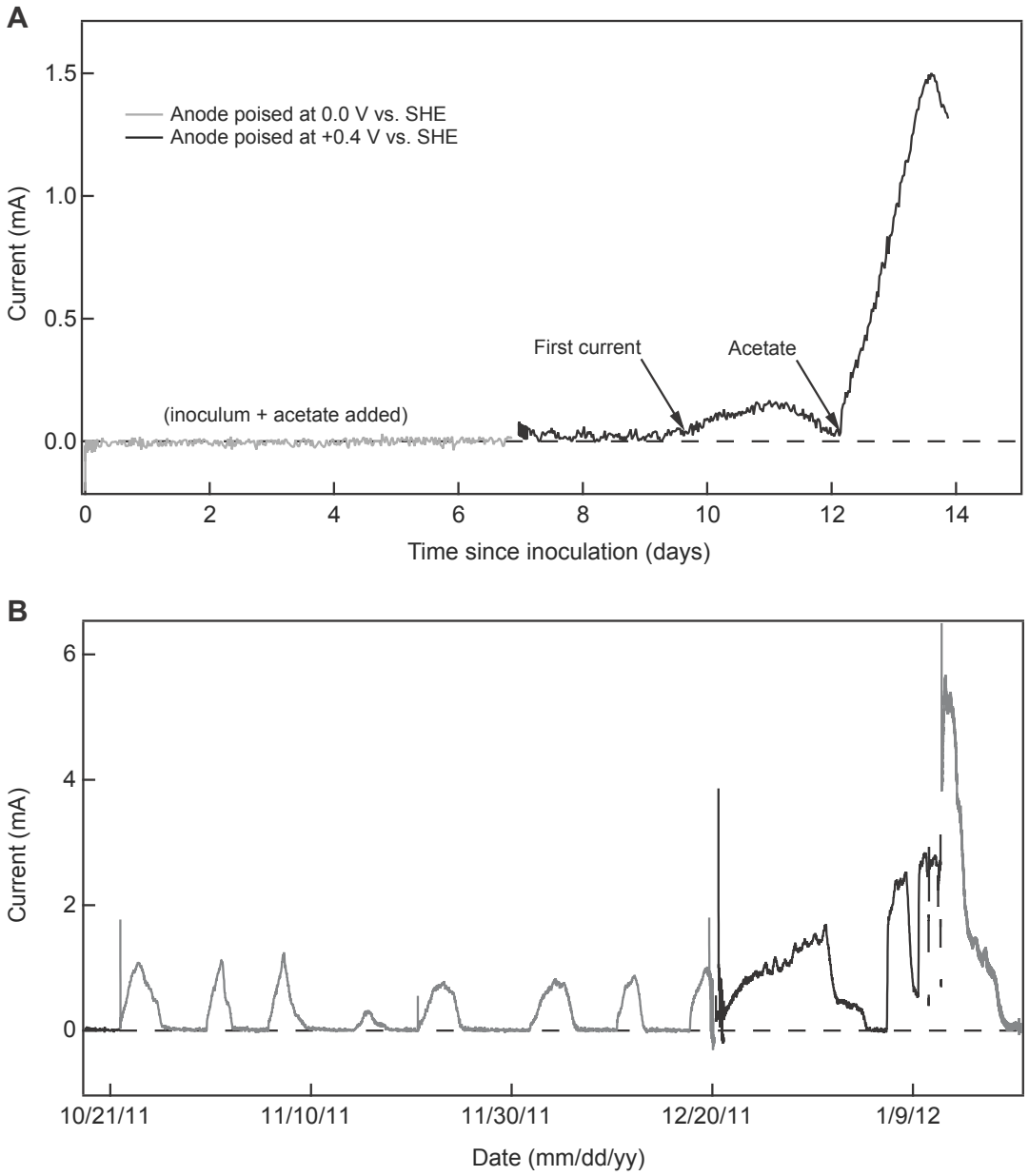

Figure 1.2 – Current produced by MXC microbial communities at different anode potentials for two different time periods. (**A**) The sum current (from both of the duplicate anodes) during the initial two weeks of the study. Anode potential was made more favorable at day 7. After a small increase and subsequent decay in current between days 9 and 12, a second acetate addition led to a substantial increase in microbially produced current. (**B**) Sum current over a period of 2.5 months. Zero current corresponds to periods of substrate limitation, and periodic current peaks correspond to acetate amendments. The gray traces indicate poising the anodes at highly favorable potentials (+410 or +250 mV vs. SHE), and the black trace indicates poising at -190 mV for the first time in the study (3 months post-inoculation).

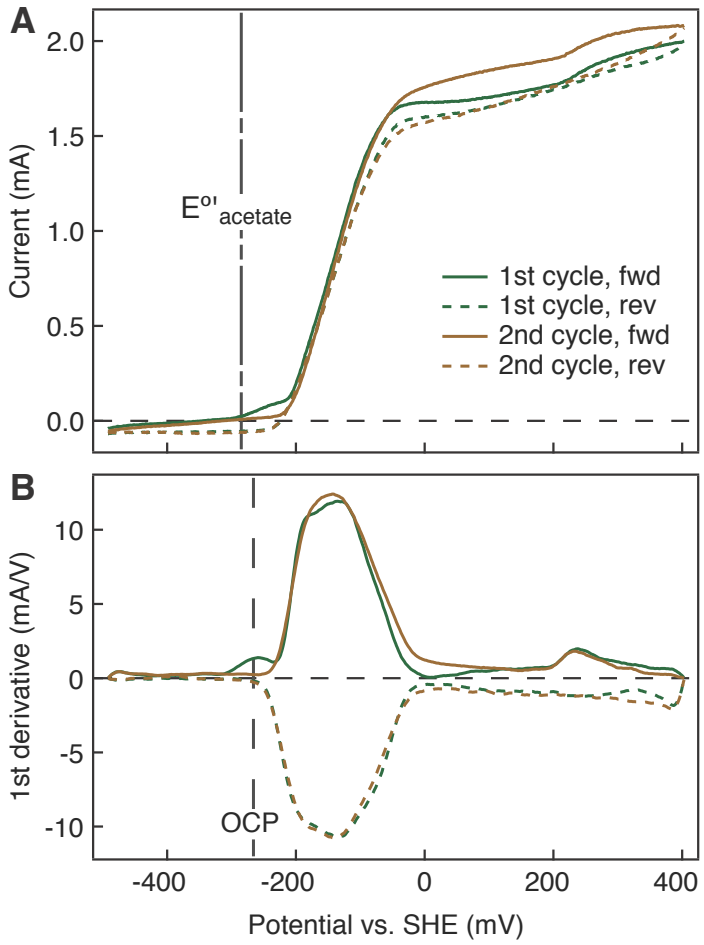

Figure 1.3 – Slow-scan cyclic voltammetry (SSCV) of anode biofilms. (**A**) Two consecutive slow-scan cycles acquired at 0.02 mV/s (250 times slower than the CV data shown in Chapter 2) for the mature biofilm after more than 3 months with E_{an} = -190 mV. One complete cycle at this scan rate takes 25 hours. (**B**) First derivative of (A), showing the broad potential range over which current increases (main peak), with other distinct features at *ca.* -250 and +240 mV. Forward (oxidative) sweeps are shown as solid lines, and reverse (reductive) as dashed. Vertical dashed lines in (A) and (B) indicate the calculated potential for acetate oxidation under relevant conditions, and the open-circuit potential (OCP) that developed when no current was allowed to flow, respectively.

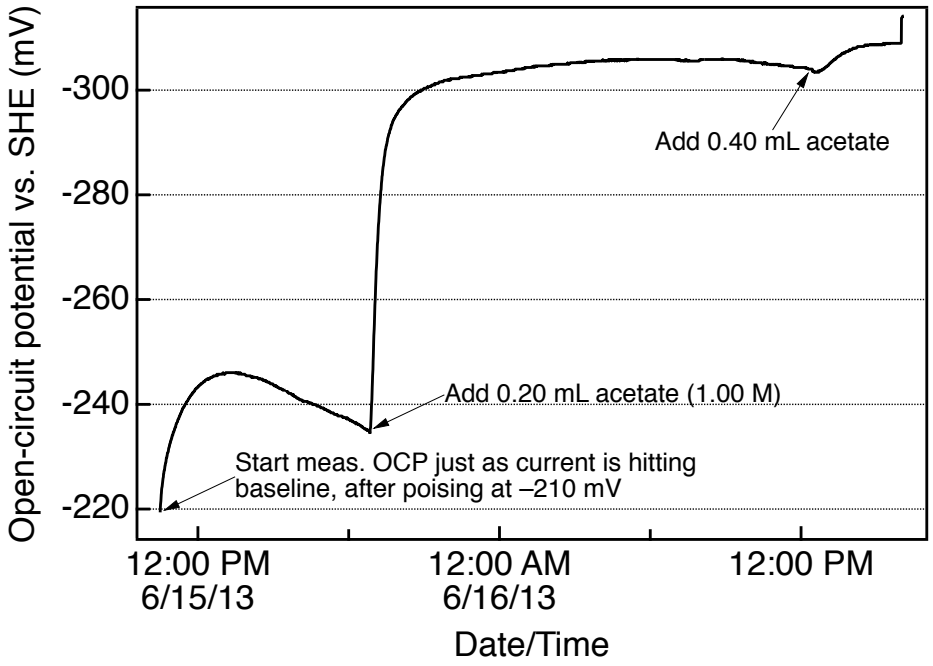

Figure 1.4 – Evolution of the measured open-circuit potential (OCP) for the initially substrate-limited biofilm following two subsequent additions of acetate. The volume of medium in anodic chambers was approximately 100 mL; adding 0.20 mL of 1.00 M acetate therefore raised the concentration from ~zero to 2 mM. A subsequent addition of 0.40 mL (giving a concentration of ~6 mM) had little effect, indicating that a concentration of 2 mM is already at or near the level needed to saturate the metabolism of the electroactive organisms, allowing them to fully reduce extracellular reductases. We note that the apparent OCP measured at the time of this experiment is more negative than the standard reduction potential of acetate (~285 mV), and also than the value we measured at an earlier time (-266 mV, see main text). This value is likely inaccurate and an indication that reference electrode needed to be calibrated, or of uncompensated resistance that was not taken into account.

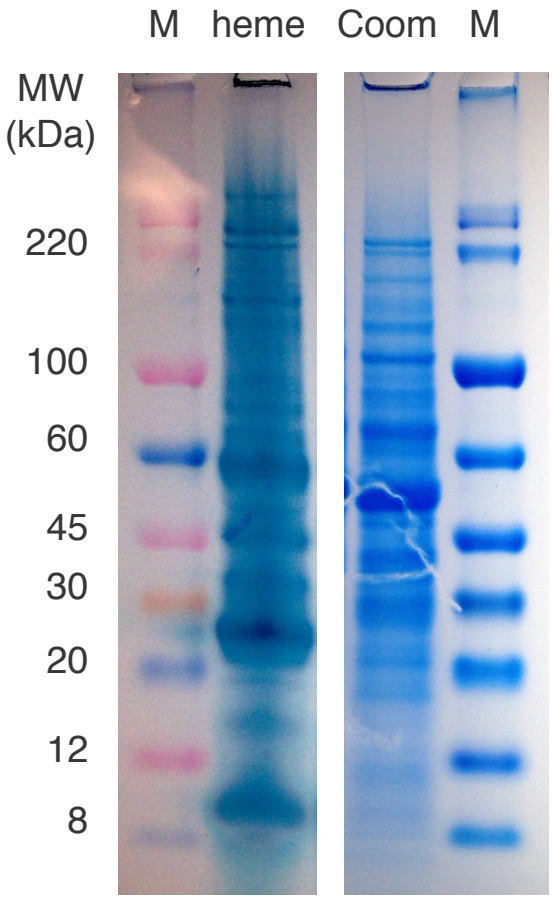

Figure 1.5 - Gel electrophoresis of denatured protein extract from red biofilm. (**Left**) Sample plus the marker, "M", with *c*-type heme-specific stain. (**Right**) Sample stained with non-specific Coomassie blue stain for all proteins. These biofilm samples were collected along with those for scanning electron microscopy at 21 months post-inoculation.

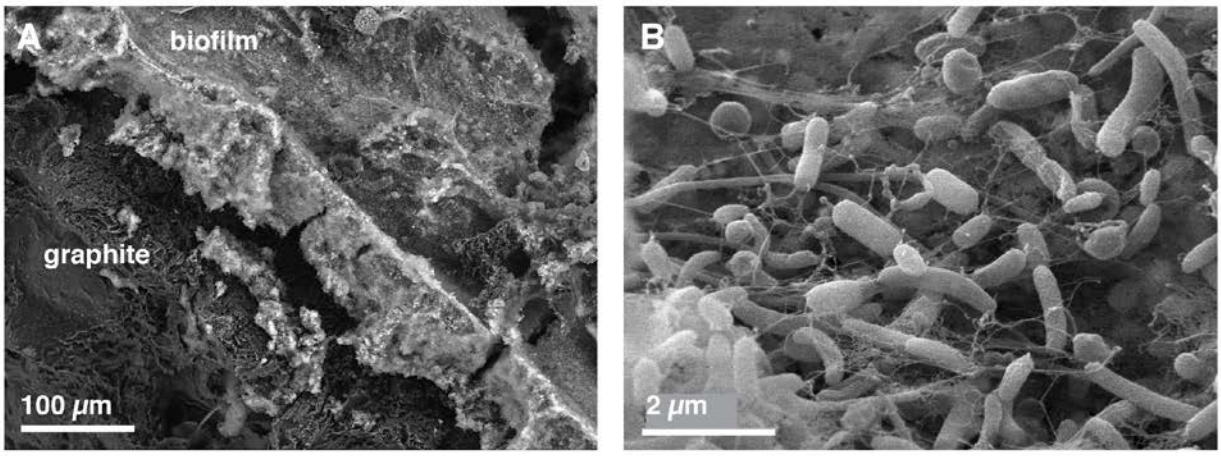

Figure 1.6 – Scanning electron microscopy (SEM) images of a sample of the thick, red-colored biofilm from Anode 1 collected at 21 months of enrichment. (**A**) Low-resolution SEM shows the biofilm in cross-section. (**B**) Higher-resolution SEM of cells near the electrode surface in a region where most of the bulk biofilm had detached. A variety of cell morphologies (rods, filaments, cocci) are consistent with a diverse microbial community.

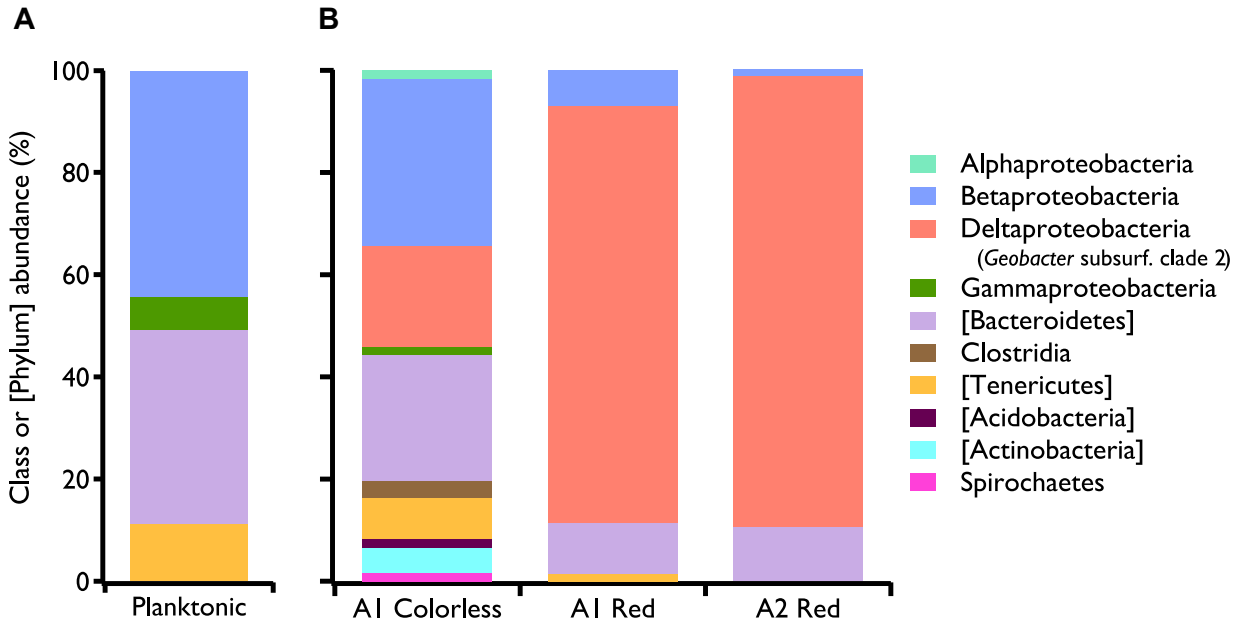

Figure 1.7 – Microbial community composition of anode biofilm samples based on 16S rRNA gene clone library sequencing and analyses. (**A**) Planktonic community composition for a sample collected from Anode 1 and four months. (**B**) Composition of 'Red' and 'Colorless' biofilm regions that developed on both graphite-block anodes. 'A1' and 'A2' refer to the duplicate anodes (see Figure 1.1). Taxonomic breakdown is given at the Class or [Phylum] (square brackets) level. Biofilm samples were harvested after 10 months of enrichment.

CHAPTER 2

Rapid Redox Flexibility in an Anode-Respiring Biofilm Community in Response to Changing Electrode Potential

Abstract

In many anaerobic environments of Earth's surface and subsurface, microorganisms gain energy by coupling breakdown of simple organic or inorganic compounds with the reduction of abundant, redox-active minerals—mainly iron- and manganese-oxides. This process requires extracellular electron transfer (EET) via a network of redox molecules to couple intracellular substrate oxidation to mineral surface reduction. Microbes that rely on this respiratory strategy face the challenge of substantial heterogeneity in mineral redox potential, which for the iron oxides spans almost half a volt. Yet, little is known about how mineral-reducing microorganisms respond to different redox potentials, especially within microbial communities found in subsurface sediments. Here we present cyclic voltammetry data from anode-respiring, sediment-derived biofilms that shows the redox state of the EET network to rapidly adapt to the steady-state anode potential over a redox range corresponding to the iron oxides. The continuous nature and fast timescale (minutes) of the voltammetry response suggest a passive form of redox "tuning" that is a property of the biofilm EET network itself. We propose that this is a very effective strategy for enabling optimal use of minerals as electron acceptors, in particular because it can accommodate changes in both substrate and mineral redox potential. Because most known EET networks are composed largely of multiheme cytochromes (MHCs), and because these enzymes themselves display broad windows of redox activity, we provide a conceptual model based on MHCs to explain the observed redox response. Our results and model may help answer the longstanding question of why MHCs are so important to most mineral-respiring microbes.

Introduction

Microorganisms capable of using extracellular minerals or aqueous metal species as electron acceptors are significant drivers of the geochemical cycles involving iron, manganese, and many trace metals, including several that are toxic to humans (Weber et al. 2006; Lovley 1991; Nealson & Little 1997; Roden 2012). The unique ability of these dissimilatory metal-reducing (DMR) microorganisms to interact electronically with their extracellular environment is the basis for promising biotechnological applications in fields of wastewater treatment, bioremediation of metal-contaminated sites, and microbial electrosynthesis (Logan & Rabaey 2012; Anderson et al. 2003; Nevin et al. 2010).

The field has made significant progress in understanding the pathways for extracellular electron transfer (EET) (Shi et al. 2016). Most of this knowledge has been generated from studies of two model organisms (*Geobacter sulfurreducens* and *Shewanella oneidensis*), including structural and electrochemical studies of their proteins that facilitate charge transport from the inner membrane to extracellular electron acceptors in the environment. The mechanism of long-distance EET has been a subject of considerable debate for several years (Malvankar & Lovley 2012; Snider et al. 2012). However, it is now clear that multiheme *c*-type cytochromes (MHCs)

are key components of the EET networks that connect intracellular metabolism to insoluble electron acceptors outside the cell. This has been shown by many studies of *Geobacter* (Leang et al. 2003; Lloyd et al. 2003; Butler et al. 2004; Chung et al. 2005; Shi et al. 2007; Shi et al. 2009; Lovley et al. 2011; Levar et al. 2012), *Shewanella* (Beliaev & Saffarini 1998; Myers & Myers 1997; Myers & Myers 2001; Myers & Myers 2003; Bretschger et al. 2007; Hartshorne et al. 2007; Bouhenni et al. 2010; Bücking et al. 2010; Coursolle et al. 2010; Mitchell et al. 2012; Bücking et al. 2012), and a growing number of other organisms (Wrighton, Engelbrektson, et al. 2011; Sturm et al. 2012).

The remarkable abundance of distinct genes encoding for MHCs in these species (Heidelberg et al. 2002; Heidelberg et al. 2004; Methé et al. 2003; Thomas et al. 2008; Butler et al. 2010; Sharma et al. 2010) indicates their critical role in extracellular metal reduction, but just how they confer an advantage remains a matter of speculation. One general property that suggests a role in accommodating environmental redox heterogeneity is broad redox activity: Voltammetry and redox titrations of purified MHCs from DMR and sulfate-reducing microbes typically exhibit reversible transitions between fully reduced and oxidized states over redox windows of 350 to 500 mV (Hartshorne et al. 2007; Moreno et al. 1991; Valente et al. 2001; Reis et al. 2002; Firer-Sherwood et al. 2008; Inoue et al. 2010; Bodemer et al. 2010; Qian et al. 2011; Clarke et al. 2011; Santos et al. 2015); these windows largely overlap with each other (Firer-Sherwood et al. 2008) and with the *E*h range of the iron oxides (Cornell & Schwertmann 2003; Thamdrup 2000).

Several research groups have used the electrochemical techniques afforded by BESs, most commonly cyclic voltammetry (CV), to seek evidence that DMR species can adapt their EET network to changes in anode potential, and by proxy to mineral redox potential, to gain an energetic advantage. These methods have been applied to both pure cultures (Busalmen et al. 2008; Marsili et al. 2010; Katuri et al. 2010; Zhu et al. 2012) and mixed communities (Torres et al. 2009; Commault et al. 2013; Zhu, Yates, Hatzell, Ananda Rao, et al. 2014). Surprisingly, no definitive signs of altered EET protein redox behavior were detected in the CV studies cited above. Two of these do report some differences in the CV spectra of biofilms grown at or exposed to different potentials (Busalmen et al. 2010; Zhu et al. 2012; Commault et al. 2013) but no conclusive interpretations about the biological underpinnings could be made. However, with the exception of two studies by Yoho et al., CV measurements of actively respiring biofilms have not been performed in a way that would capture rapid (*i.e.*, over minutes) changes in biofilm redox characteristics (Yoho et al. 2014; Yoho et al. 2015).

Here, we used CV at relatively fast scan rates of 5 mV/s, along with more typical slow-scan CV, to probe the redox response of an anode-respiring microbial community to changes in anode potential on timescales ranging from minutes to about a day. We cultivated the anode biofilms using a sediment inoculum obtained from a well-studied Department of Energy field site located at Rifle, CO, USA, with poised electrodes acting as the only added electron acceptor and acetate as the electron donor. We chose to study microbial communities instead of pure cultures to allow for inter-organism interactions that likely affect the performance of known DMR species like *Geobacter* in natural environments (Wrighton et al. 2014; Summers et al. 2010; Rotaru et al. 2012), and also to potentially expand the list of known EET-active species through follow-up isolation or metagenomics approaches (see Chapter 3).

Materials and methods

Preparation, inoculation and operation of microbial electrochemical cells

See Methods section of Chapter 1.

Cyclic voltammetry

The procedure for slow-scan cyclic voltammetry (SSCV) is described in Chapter 1. All "fast-scan" CV (FSCV) measurements were performed independently on both anodes, requiring the use of the additional Pt-wire counter electrode in the anodic compartments. The reference electrode was always placed in the same chamber as the anode biofilm being analyzed, and in an equivalent geometry with respect to working and counter electrodes. A scan rate of 5 mV/s was chosen for all FSCV (see *Results*) with the following additional settings: $E_{initial} = E_{an}$, or in some cases the negative vertex potential following a 30-s equilibration period; $E_{vertex,1} = -0.5$ V; $E_{vertex,2} = +0.3$ V; $E_{final} = E_{an}$. In preliminary FSCV experiments, multiple cycles were performed to check consistency between the first and subsequent oxidative and reductive sweeps. We found no significant differences between first and second cycles, and therefore subsequently performed only one complete cycle for each unique FSCV measurement in order to minimize perturbation of the biofilm. Electrochemical data was analyzed using custom routines in IGOR Pro (WaveMetrics).

Results

Slow-scan CV of the community biofilm

Despite the presence of species from several different bacterial phyla in the anode biofilms (see **Figure 1.7**), their electrochemical characteristics were mostly indistinguishable from those of *Geobacter* and other known iron-reducing species (Srikanth et al. 2008; Marsili et al. 2010; Fricke et al. 2008; Xing et al. 2008; Marshall & May 2009). Specifically, the results of slow-scan cyclic voltammetry (SSCV) performed under conditions of excess substrate, which reveals the dependence of metabolic current on E_{an}, showed a characteristic increase in current from zero to saturating across a potential window of -200 to 0 mV (**Figure 1.3**). Also consistent with previous studies of *Geobacter* biofilms, complete exchanges of the media did not cause a drop in current (Bond & Lovley 2003).

CV at faster scan rates reveals a shift in biofilm midpoint potential with anode potential

We used faster CV scan rates to obtain snapshots of biofilm redox signature after exposing the biofilm to different steady-state anode potentials. Our goal was to resolve hypothesized changes in EET networks of electroactive microbes that might be occurring on shorter timescales (minutes to ~an hour). CV performed at 5 mV/s revealed a ~100 mV shift in the major midpoint potential, E_{mid}, when the biofilm was equilibrated at an E_{an} of -190 mV *vs.* +210 mV for several hours each (*e.g.*, **Figure 2.1B**; see next section). This shift was completely reversible and repeatable for both anodes. A thorough literature review at that time did not reveal any prior observation or analysis of this phenomenon so we investigated in more detail. A series of faster-scan CVs (FSCVs) performed at progressively faster scan rates ranging from 2.5-20 mV/s showed a dependence of E_{mid} on scan rate (**Figure 2.2**), so we kept 5 mV/s as the scan rate for all FSCV experiments.

Timescale of the midpoint shift

In order to determine the timescale of the midpoint shift, as well as explore how the voltammetric response changes with E_{an} in more detail, we performed two series of FSCV experiments. The results are given in **Figure 2.1**, which is the key dataset of this study. The first series, shown in **Figure 2.1A**, includes FSCVs acquired as a function of time following a step-change from -190 to +210 mV and then back again. The corresponding derivative data (**Figure 2.1B**) illustrate the significant shift in E_{mid} between the endpoints of the experiment. **Figure 2.3** summarizes the rate of change in E_{mid} following the 400-mV forward and reverse E_{an} steps. The shift began immediately following a step in either direction, but was much more rapid for a jump to more positive potentials than for the reverse. Importantly, even the more rapid positive shift still required ~60 min to be complete, and the process underlying the observed shift should therefore not be significantly impacted by a 5-mV/s CV scan requiring less than three minutes.

Chronoamperometry data for the periods of poising between each FSCV is given in **Figure 2.3B**. The pulses of anodic (positive) current that take place at the beginning of each trace indicate accumulation of electrons in redox mediators near the electrode during the short period at open circuit condition following FSCV, which are rapidly discharged when the circuit is closed. The one exception is the trace after switching from +210 to -190 mV, which shows cathodic currents due to the flow of charge from the reducing electrode into a highly oxidized biofilm. Overall, the latter portions of the individual traces shows the current asymptotically approaching steady-state values over several hours. These chronoamperometry data reveal that the time required for the whole biofilm to attain redox equilibration after a large change in anode potential was about three hours.

The midpoint shift occurs continuously across a range of E_{an} conditions

In a second series of experiments, we collected FSCVs after poising at 10 different E_{an} values across the region of current increase observed in SSCV (-265 to +10 mV) (**Figures 2.1C** and **D**). We equilibrated the biofilm at each E_{an} by poising for at least 3 hours prior to CV. The dependence of E_{mid} on E_{an} is quantified in **Figure 2.4A** (dark triangles). The trend is approximately linear below *ca.* -115 mV, with a noticeable increase in slope around this potential. The steady-state current for each E_{an} condition is also plotted (open squares), and as expected closely matches SSCV data.

The total amount of charge transferred to the electrode during the anodic (oxidizing) sweep also varied with E_{an} in this series, as can be seen by the vertical offset between CV spectra in **Figure 2.1C**. To quantify this effect, we integrated the oxidative-sweep spectra from -0.215 V to the vertex potential of +0.310 V (indicated by vertical bars in the figure) to yield (after dividing by scan rate) the total charge transferred in Coulombs. The results of this procedure (**Figure 2.4B**, circles) reveal a non-monotonic relationship between E_{an} and discharge, with a peak around -200 mV.

The derivative spectra of both FSCV series contain a distinct low-potential peak that, unlike the main midpoint feature, was not dependent on anode potential and exhibited no splitting between oxidative and reductive peaks. The inset of **Figure 2.1B** shows the same data after fitting and subtracting an estimated background (capacitive) current for each oxidative sweep, in order to emphasize this low-potential feature.

pH changes within the biofilm are not the cause of the midpoint shift

A consequence of respiration that couples organic matter oxidation to the reduction of extracellular electron acceptors is a net production of protons inside of the cell; this is in contrast to the case of

soluble electron acceptors such as nitrate, sulfate, and fumarate, where the protons are consumed intracellularly (Mahadevan et al. 2006). Therefore, in an acetate-oxidizing, anode-reducing biofilm, protons must diffuse to the cathode to be finally reduced. As a result, pH gradients can develop within the biofilm (Torres et al. 2008; Franks et al. 2009; Beyenal & Babauta 2012). This makes the energetics of the overall reaction sensitive to pH as described by the Nernst equation. On the molecular level, pH can affect the midpoint potential of redox enzymes containing acidic residues through the electrostatic redox-Bohr effect (Papa et al. 1979; Reis et al. 2002; Morgado et al. 2010). Because current production, and therefore the rate of proton generation, ranged from near zero to maximal over the E_{an} range investigated (**Figure 2.1E**), and because the direction of the observed midpoint shift is consistent with a possible Nernstian or redox-Bohr effect, it was important to rule out within-biofilm pH changes as the main mechanism. We performed three sets of experiments to test this.

First, we adjusted the pH of the media itself by adding acid (HCl) or base (NaOH). After allowing current to reach steady state at a constant E_{an} of -215 mV, FSCV was collected at each pH condition (6.67, 7.02, and 8.00). We indeed found a strong dependence of E_{mid} (and also of steady-state current) on media pH, with a shift of 71 mV per pH unit for the oxidative peak in derivative CV, and 46 mV/pH using the average position of oxidative and reductive peaks (**Figure 2.5**). This confirmed the need to exclude proton accumulation within the biofilm as the primary cause of the shift.

To do so, we adopted the approach of Torres et al. to vary buffer concentration (Torres et al. 2008), since increasing buffer concentration should attenuate proton accumulation in the biofilm, and thus any pH-induced shift. We found that even at a current-saturating E_{an} of +10 mV, for which maximum metabolic turnover is expected, changing buffer concentration (25, 50, and 75 mM phosphate) had no effect on FSCV midpoint (**Figure 2.6A** and **B**). However, as observed by Torres et al., steady-state current did increase with buffer concentration (**Figure 2.6C**), meaning that the rate of proton transport may limit current.

As a final test, initial FSCVs were collected after allowing acetate to be depleted at two different potentials, -190 and +10 mV. At each E_{an} condition, acetate was added, and additional FSCVs were collected periodically as current increased and protons were presumably generated in the biofilm. The results (**Figure 2.7)** show two distinct midpoints—one for each E_{an} condition—that did not shift as current increased. In combination, the results of these three experiments show that pH was not a significant factor in causing the midpoint shift.

Discussion

Biofilm cyclic voltammetry performed at a relatively fast scan rate (5 mV/s) revealed a change in redox response of the biofilms as a function of anode potential. We posit that the continuous shift in midpoint corresponds to changing redox states of extracellular MHCs, which confers intrinsic redox flexibility to the EET network. In two other recent bioelectrochemical studies of *Geobacter sulfurreducens* and *Geoalkalibacter* and *Geoalkalibacter ferrihydriticus* pure cultures, which were also aimed at detecting changes in the biofilm CV redox signature as a function of anode redox potential, the authors observed similar shifts in biofilm midpoint potential that was interpreted as a switch between different EET pathways or proteins in these organisms (Yoho et al. 2014; Yoho et al. 2015). Indeed, subsequent genetic studies from another research group have indeed confirmed the existence of at least two distinct EET pathways that operate at distinct redox

potentials (Levar et al. 2014; Levar et al. 2017). However, as described below, features of our data indicate that they are not best interpreted as a transition between metabolic electron transfer pathways.

There are three key observations drawn from our data that suggest a passive, physical redox response to anode poising potential as the main explanation for the observed midpoint shift in this study (and perhaps also, at least in part, in the studies of Yoho et al.) First, the continuous, linear dependence of the apparent biofilm midpoint potential on anode poising potential across most of the redox-active range (**Figure 2.4A**) provides strong support for our interpretation. This response is more consistent with a passive, physical mechanism than a dynamic switch between EET pathways at a specific threshold. Second, the decrease in biofilm discharge (during anodic sweeps; see Results for how this value was measured) after poising at increasingly positive E_{an} values starting at *ca.* -200 mV (**Figure 2.4B**) indicates that the biofilm becomes progressively more oxidized under steady-state turnover conditions, with fewer electrons stored in the biofilm mediator pool. This finding is consistent with other studies of electron storage in *G. sulfurreducens* biofilms (Esteve-Núñez et al. 2008; Marsili et al. 2010; Schrott et al. 2011). Such a decrease in the concentration of reduced biofilm redox centers can also explain the increasing "peak-like" character in the oxidative FSCV sweep for more positive E_{an} values (**Figure 2.1E**) (Harnisch & Freguia 2012). The fact that this oxidation occurs in spite of increasing rates of microbial turnover (**Figures 2.1E** and **2.4**) suggests that neither electron transport through the near-anode biofilm, nor electron transfer at the electrode surface, are rate-limiting steps in overall current production, in agreement with findings by Richter et al. (2009) and Bonanni et al. (2012).

A third important observation is provided by data presented in Chapter 1, namely the dependence of the measured open-circuit potential (OCP) on acetate concentration (**Figure 1.4**). The OCP reflects the redox potential of extracellular reductases at the electrode surface when no current is allowed to flow. Because acetate itself is not redox active, the decrease in OCP to a more reducing potential when acetate is supplied to an initially substrate-limited biofilm must be driven by microbial metabolism. That is, electroactive microbes in the biofilm consume the acetate and deposit the electron byproducts to extracellular reductases (almost surely dominated by MHCs). The results in the Figure indicate that the redox potential of these reductases can vary continuously across a range of at least 80 mV.

A schematic illustrating how an anode-respiring biofilm containing MHCs can explain our observations—without invoking a switch in microbial EET pathways—is shown in **Figure 2.8**. This model builds upon that presented by Schrott et al. (2011). The schematic depicts the redox states of MHCs in the biofilm pool for two different E_{an} values during steady-state turnover conditions. MHCs are more oxidized when the electrode is held at a positive potential ($E_{an,2}$) than when the electrode is more reducing ($E_{an,1}$) (Millo et al. 2011; Liu et al. 2011; Virdis et al. 2012). The key property of MHCs in this context is a wide and continuous redox-active window of 350-500 mV (Moreno et al. 1991; Valente et al. 2001; Reis et al. 2002; Hartshorne et al. 2007; Firer-Sherwood et al. 2008; Inoue et al. 2010; Bodemer et al. 2010; Qian et al. 2011; Clarke et al. 2011), which results from close spacing and thus interaction between the multiple heme redox centers (Moreno et al. 1991; Paquete et al. 2014; Breuer et al. 2014; Santos et al. 2015). MHCs can therefore adopt a range of redox microstates differentiated by the particular combination of oxidized and reduced hemes.

The model distinguishes MHCs bound to the anode from those located farther into the biofilm because these two pools likely contribute distinct signals to the FSCV: The low-potential feature that appears in all FSCV spectra displays behavior consistent with redox centers bound to the

electrode (Busalmen et al. 2008; Schrott et al. 2011) that undergo complete oxidation and reduction during any CV scan. These behaviors include zero offset between oxidative and reductive peaks (Laviron 1979; Laviron & Roullier 1980; Bard & Faulkner 2001; Harnisch & Freguia 2012), and no dependence on steady-state E_{an}, in contrast to the main FSCV feature. The main peaks in the derivative FSCV, in contrast, display all the hallmarks of diffusive behavior (peak offsets, a nonlinear dependence of peak height on scan rate (data not shown), and a peak in the oxidative CV sweep.

Discrepancies between observations and expectations based on the simple physical model do suggest important roles for microbial physiology. Although the trend in anode potential vs. steady-state midpoint potential is linear across most of the range (**Figure 2.4A**), there is a discontinuity in the E_{mid} *vs.* E_{an} slope between -115 and -90 mV, which bracket the threshold potential at which Yoho et al. (2014) and Levar et al. (2014; 2017) find evidence for an intracellular pathway-switch in *G. sulfurreducens*; this is accompanied by the appearance of a distinctive feature in the reductive FSCV sweep (arrow in **Figure 2.1C**). These may be signatures of a similar phenomenon occurring in the Geobacteraceae strains present in the mixed-species biofilms studied here.

Also, we would not predict from the model that there would also be a decrease in biofilm discharge below about -200 mV in **Figure 5A**; instead, we should expect a plateau at an E_{an} value just low enough to fully reduce the biofilm EET pool. The discrepancy indicates that the activity of anode-respiring organisms diminishes significantly following prolonged exposure to unfavorable conditions (Marsili et al. 2010). Importantly, this deviation also suggests that the electrode itself cannot effectively reduce mediators in the biofilm pool, leaving microbial metabolism as the sole source of reducing power. This is likely a result of electron-transfer in microbial EET pathways that are nearly or totally irreversible, perhaps those between periplasmic cytochromes (such as PpcA of *G. sulfurreducens* (Lloyd et al. 2003; Ding et al. 2008; Liu et al. 2011; Bonanni, Schrott & Busalmen 2012) and extracellular mediators. This observation explains the difference in timescales for the positive *vs.* reverse midpoint shifts (**Figure 4A**): discharging of the EET network by the electrode after a switch to oxidizing conditions occurs more rapidly than recharging, or reduction, *via* microbial metabolism when reducing conditions are restored.

The hypothesis we propose has implications for EET in the environment. The production of an EET network whose components are useful over a broad redox window is an efficient strategy for handling the challenges of dissimilatory metal respiration in heterogeneous or fluctuating redox environments. For example, such a network would have the ability to transmit electrons from different inner-membrane pathways to the wide variety of iron-bearing mineral phases with diverse particle sizes, solubilities, and crystallinities—factors known to affect their redox potential. It was recently shown that *Geothrix fermentans* produces two different soluble extracellular redox shuttles with midpoint potentials of -0.2 V and +0.3 V, which may be another strategy to solve the same problem (Mehta-Kolte & Bond 2012). In comparison, the use of MHCs by *Geobacter* and other metal-reducing bacteria is likely important in that it confers a degree of passive, instantaneous redox tuning of the EET network to different electron donors and acceptors. This strategy avoids the need to biosynthesize and export different EET proteins as the cell moves from particle to particle, or as conditions fluctuate.

Acknowledgements

The work described in Chapters 1 and 2 was supported by the Director, Office of Science, Office of Basic Energy Sciences, Chemical Sciences, Geosciences, and Biosciences Division of the U.S. Department of Energy under Contract No. DE-AC02-05CH11231. T.J.A. was supported by a

fellowship from the Berkeley Connect program (UC Berkeley Dept. of Environmental Science, Policy and Management). Critical discussion and technical assistance by Christopher Brown, Alexander Probst, Laura Hug and Karthik Anantharaman is sincerely acknowledged. T.J.A. would like to thank Sudeep Popat for generous advice and discussions.

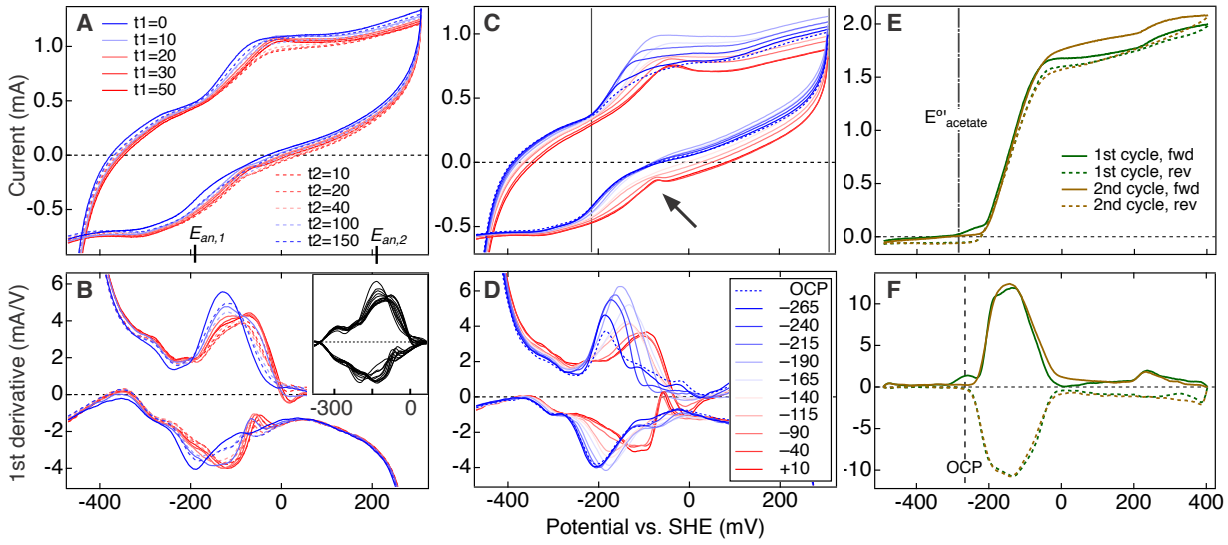

Figure 2.1 – Representative cyclic voltammetry (CV) of actively respiring anode biofilms using two very different scan rates. The top panels show the raw CV data, and the bottom panels show their derivatives, whose peaks correspond to the midpoint potentials of extracellular reductases able to transmit electrons to the electrode surface. Pairs (A/B) and (C/D) were collected using a scan rate of 5 mV/s, whereas (E/F) shows a scan at 0.02 mV/s (reproduced from Chapter 1). The "fast-scan" (FS) CV data, A and C, were collected separately for each of the duplicate anodes yielding qualitatively identical results, and the data for one anode is shown. These data were collected at 7.5 months of enrichment. The slow-scan (SS) CV in (E) was acquired with both anodes connected to the central cathodic electrode, and is therefore the sum current. The data shown were collected at 11 months. No significant changes in biofilm voltammetry response was observed during the intervening period. (**A**) Raw and (**B**) derivative FSCV data as a function of time (minutes) after changing anode potential from -190 to +210 mV (t_1 series, solid lines), and then back to -190 mV (t_2 series, dashed lines). **Inset**: background-subtracted version of the same derivate CV data that more clearly shows the presence of a static low-*E*h feature at *ca.* -270 mV. (**C**) Raw and (**D**) derivative FSCV data from the steady-state series, in which the biofilm was allowed to equilibrate at E_{an} values spanning -265 to +10 mV (see figure legend in (D)). See the text for the meaning of the vertical bars and the arrow in (C). (**E**) Two consecutive slow-scan cycles acquired at 0.02 mV/s for the mature biofilm after more than 3 months with E_{an} = -190 mV. One complete cycle at this scan rate takes 25 hours. (**F**) First derivative of (E), showing the broad potential range over which current increases (main peak), with other distinct features at *ca.* -250 and +240 mV. Forward (oxidative) sweeps are shown as solid lines, and reverse (reductive) as dashed. The open-circuit potential (OCP) that developed when no current was allowed to flow is also indicated.

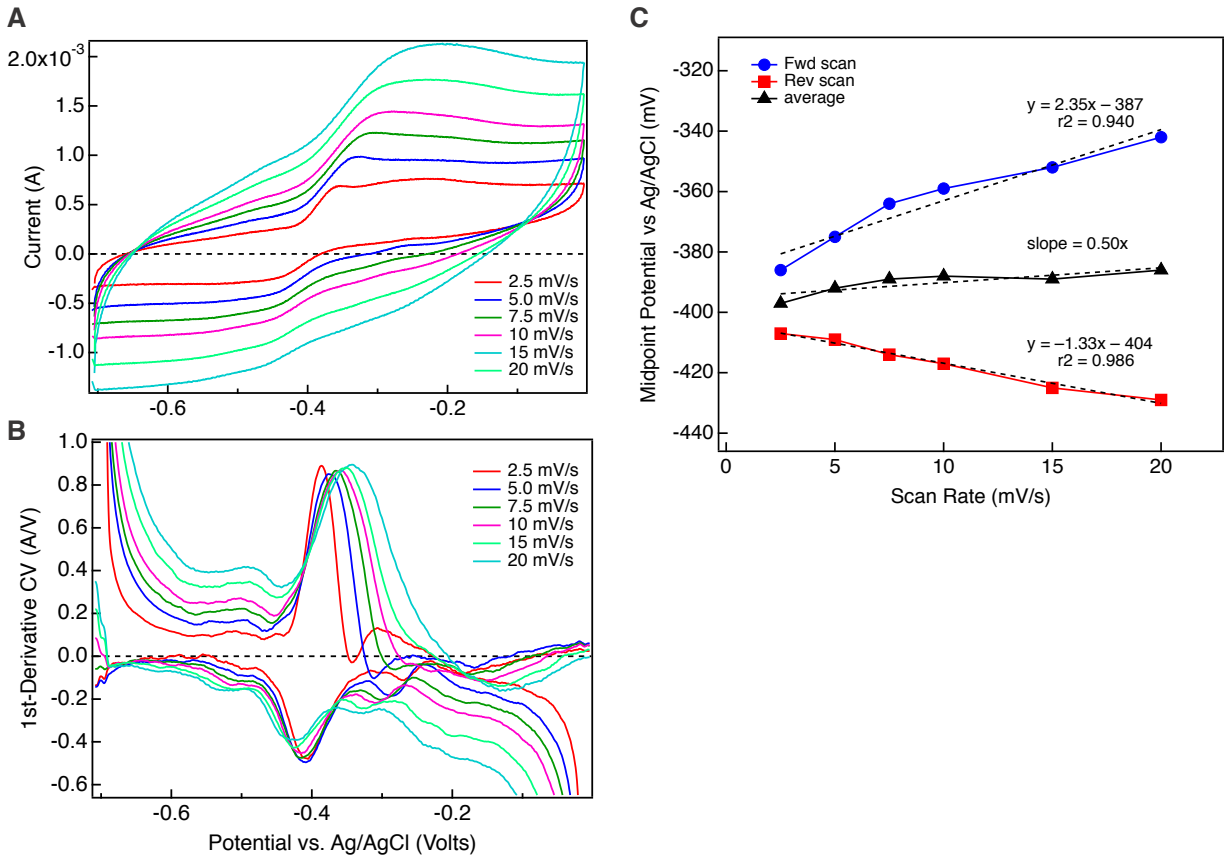

Figure 2.2 – Cyclic voltammetry scan-rate series including rates from 2.5-20 mV/s. Potential axes are in reference to the Ag/AgCl electrode (3-M KCl), which is +210 mV vs. SHE. (**A**) CV and (**B**) first-derivative CV spectra collected about 20 minutes apart, with a 10-15 minute recovery period at the long-term maintenance potential (E_{an} = -190 mV vs. SHE or -400 mV vs. Ag/AgCl) between each scan. The dCV spectra in (B) best show the shift in the oxidative (upper) and reductive (lower) main feature, which is quantified in (**C**). Data collected after 16.5 months of enrichment.

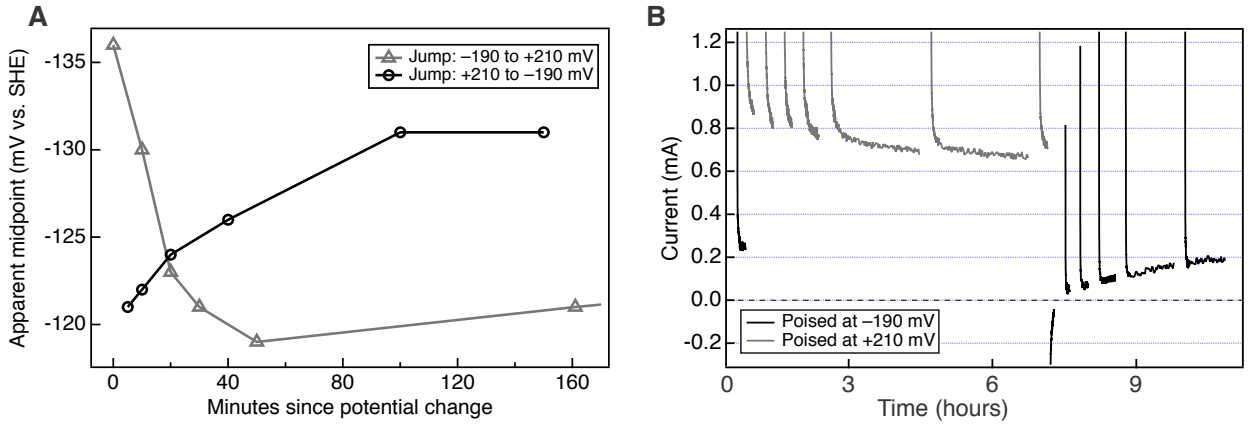

Figure 2.3 – Timescales of the apparent midpoint shift and of steady-state current re-equilibration following large changes in anode potential. (**A**) Time dependence of the shift in FSCV midpoint potential after positive and negative step changes in E_{an}. The trends are extracted from the oxidative-sweep dCV peaks of **Figure 2.1A**. The shift occurs much more rapidly following the jump to more positive potential than for the reverse. (**B**) Chronoamperometry data recorded between consecutive FSCV measurements showing the few-hour timescale required for current to reach steady state after the large E_{an} jumps. The spikes in current at the beginning of each trace reflect anodic discharge (and in one case cathodic electron flow) of electrons that had accumulated in the biofilm by the end of the CV measurement.

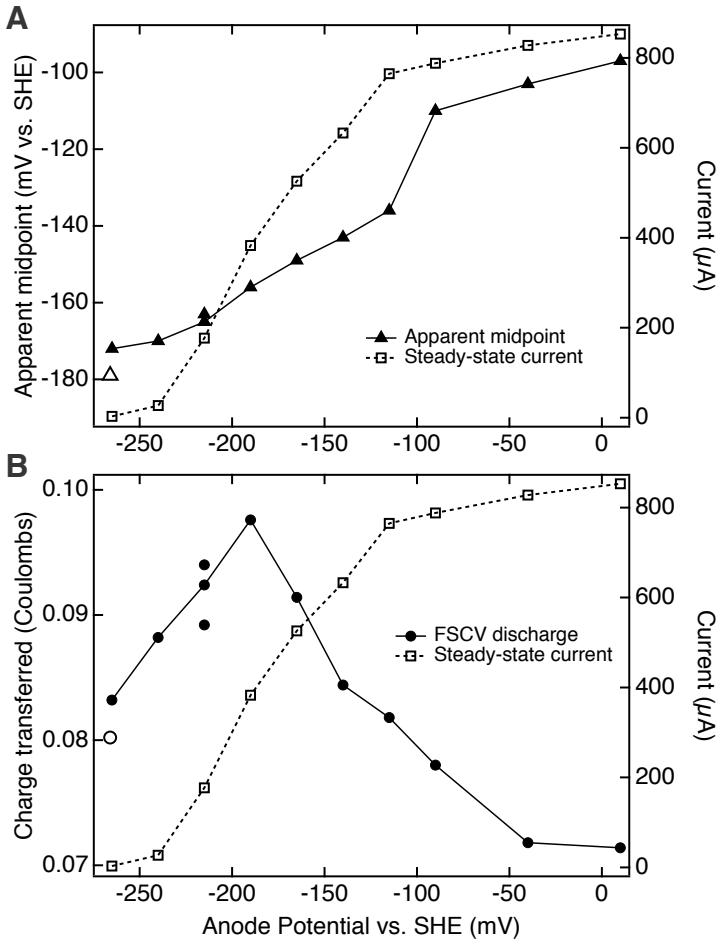

Figure 2.4 – Trends in biofilm redox response extracted from raw and derivative FSCV shown in Figures 2.1C and D. Both plots also include the steady-state current (right axis) measured at each potential prior to FSCV. (**A**) Apparent midpoint potential for the oxidative-sweep dCV peaks as a function of anode potential (solid triangles). The open triangle corresponds to the midpoint from CV performed after allowing the biofilm to reach open-circuit potential (-266 mV within 3 hr after poising at -190 mV). (**B**) Charge transferred to the electrode during the anodic (oxidative) sweeps of **Figure 2.1C** as a function of E_{an} (solid circles). As in (A), the open circle corresponds to the value measured from CV after the biofilm reached open-circuit equilibrium. The range of integration used to obtain charge transferred is indicated by the vertical bars in **Figure 2.1B**.

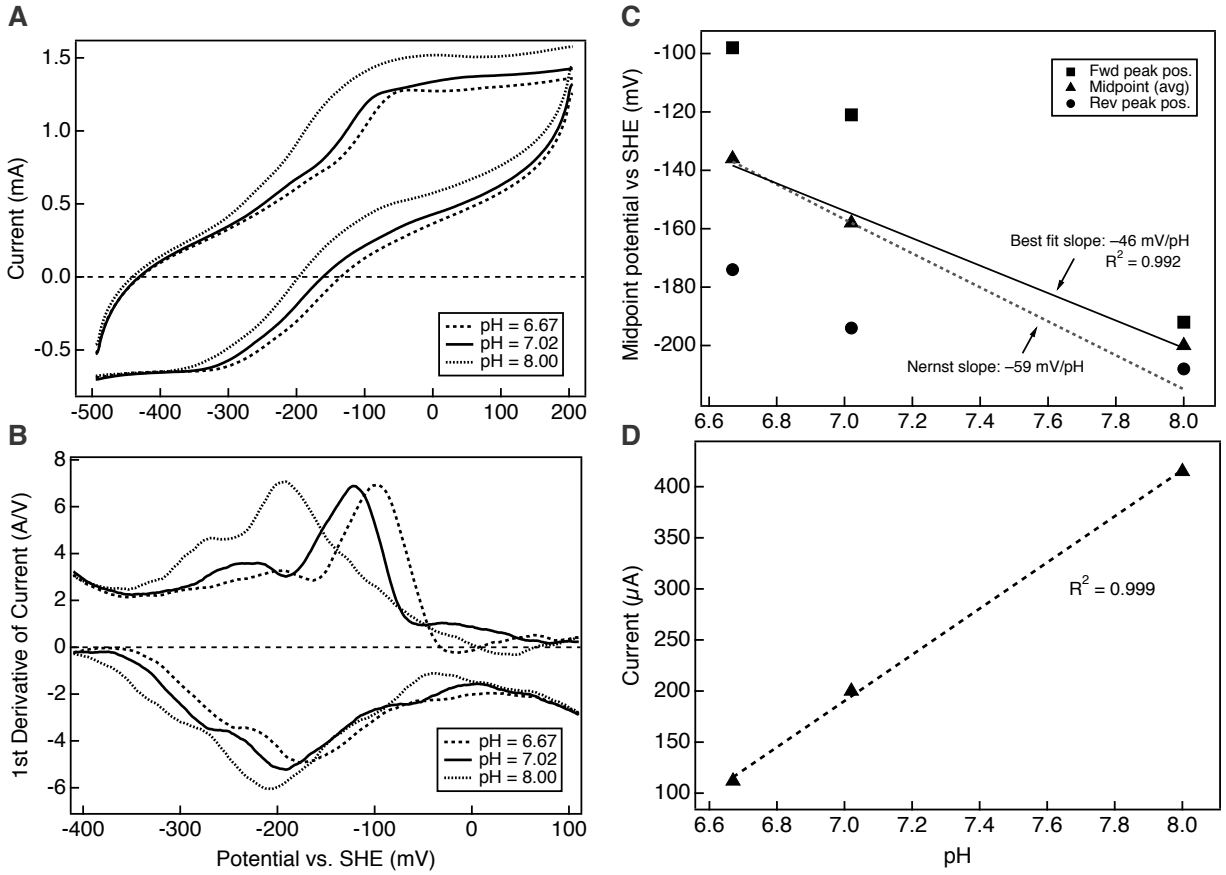

Figure 2.5 – Changes in fast-scan CV (5 mV/s) spectra and steady-state current in response to adjustment of media pH. (**A**) Raw CV and (**B**) first-derivative CV at three different media pH conditions. (**C**) Dependence of the apparent midpoint potential of the main CV feature on media pH. The midpoint was calculated using the dCV spectra in (B) by taking the average of the oxidative (upper curves) and reductive (lower curves) peak positions. The plot shows both the oxidative ('fwd') and reductive ('rev') peak positions in addition to their average. A linear fit to the average, or midpoint, data yields a slope of -46 mV per pH unit; the slope of the dashed line corresponds to the theoretical shift in midpoint of 59 mV per pH unit predicted by the Nernst equation. A linear fit to the oxidative-peak points only (not shown) gave a slope of -71 mv/pH unit. (**D**) Steady-state current at each pH condition. The anode potential throughout the experiment was -215 mV vs. SHE. Data collected after 12 months of enrichment.

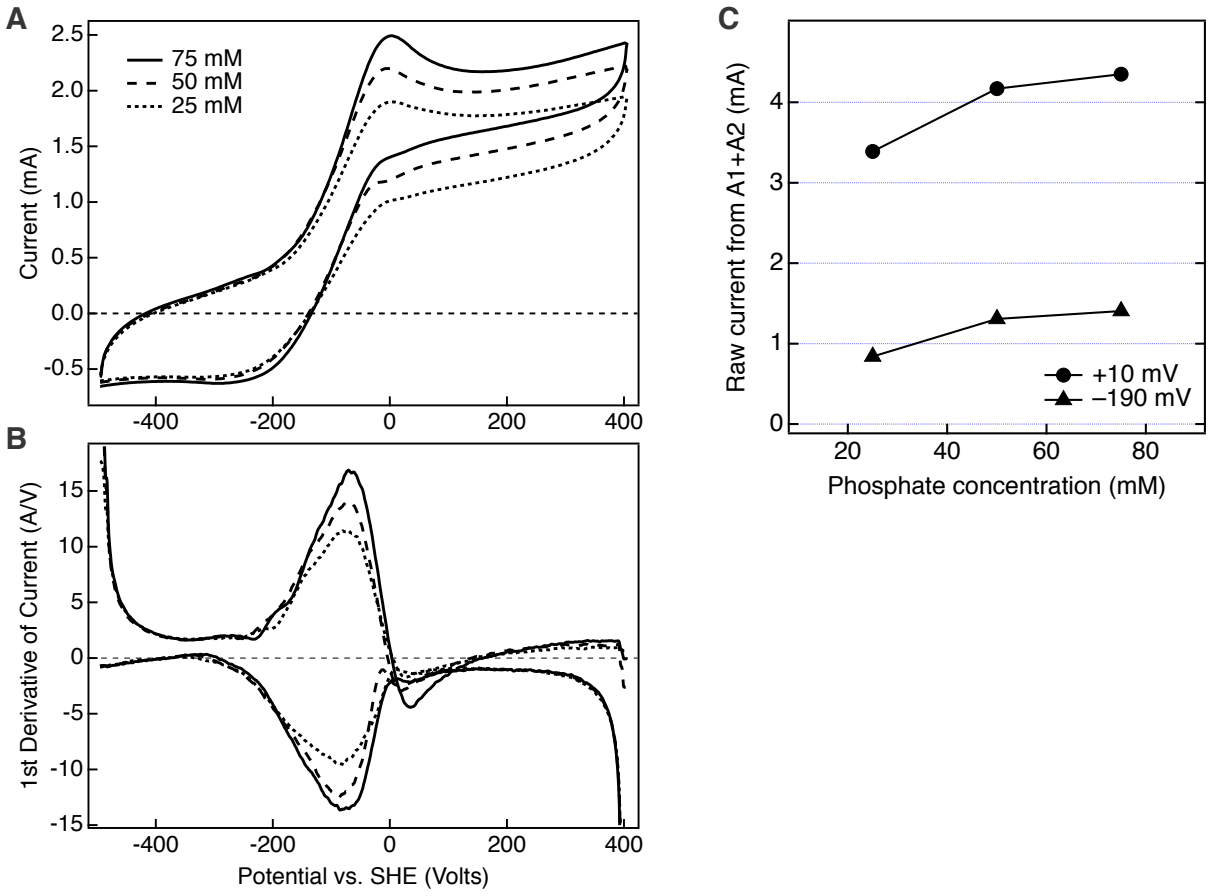

Figure 2.6 – Fast-scan CV (5 mV/s) spectra and steady-state current for three different phosphate buffer concentrations (25, 50, and 75 mM). (**A**) Raw CV and (**B**) first-derivative CV at each buffer concentration following steady state chronoamperometry at a set potential of +10 mV vs. SHE. Data shown corresponds to Anode 1, which had greater current production, but all CV experiments were performed for both anodes with similar results. (**C**) The effect of buffer concentration on steady-state current (after Torres et al. 2008) at two different anode potentials. Current is the sum from both MFC anodes. Data collected after ~10 months of enrichment.

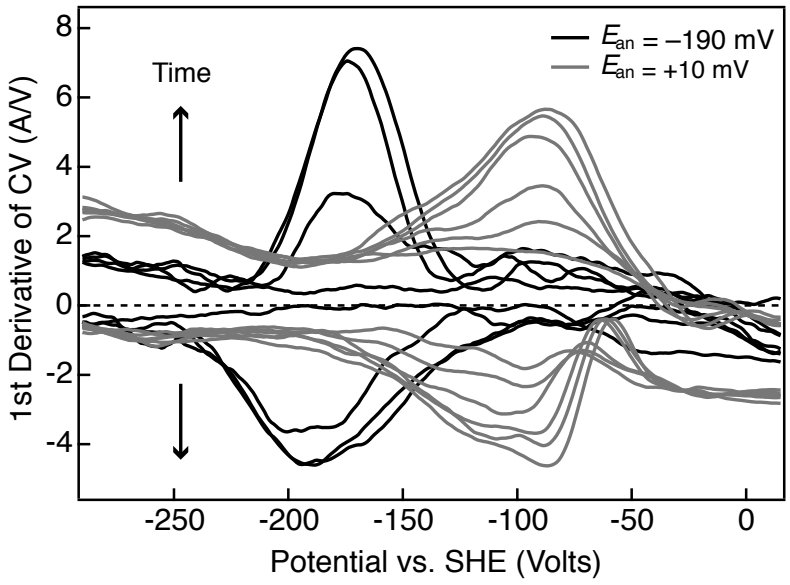

Figure 2.7 – Time series of fast-scan CV spectra (first derivative) collected after the addition of acetate to the substrate-limited biofilm. The experiment was carried out at two steady-state anode potentials. An initial scan under substrate-limiting conditions corresponds to lowest-amplitude peaks in each series above. After acetate addition, chronoamperometry was paused at the following (cumulative) times to collect subsequent scans: At E_{an} = -190 mV, t = 9, 30, and 55 min; at E_{an} = +10 mV, t = 5, 17, 37, 57, and 114 min. Different scan rates were used for the two series: 2.5 mV/s for E_{an} = -190 mV, and 5.0 mV/s for E_{an} = +10 mV; a scan rate series (next figure) showed an oxidative-peak offset of 12 mV for these two rates. Data collected after ~17 months of enrichment.

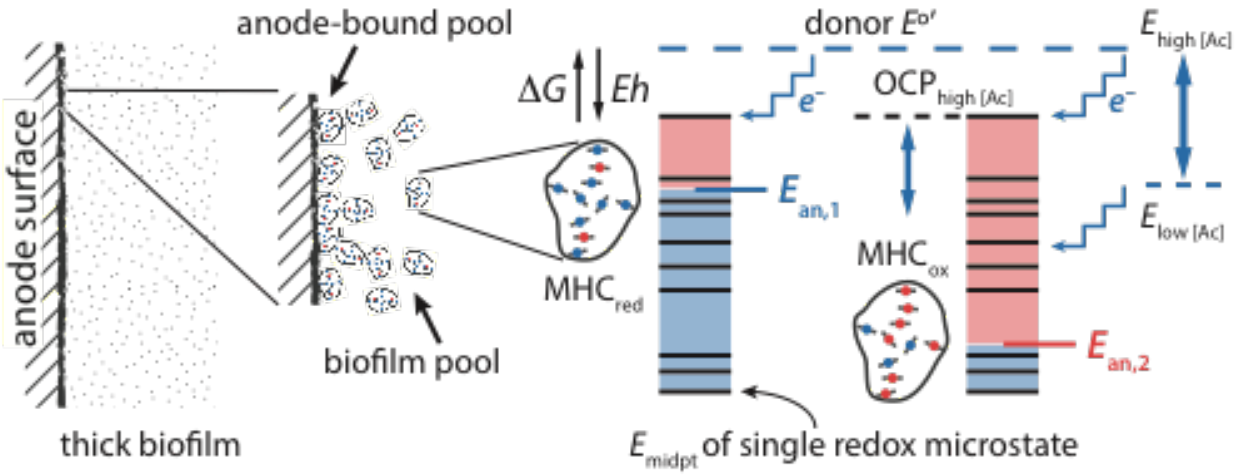

Figure 2.8 – Conceptual model proposing how the redox state of a thick, anode-respiring biofilm is affected by the steady-state poising potential, E_{an}, and can be measured by fast-scan CV. Left: Cartoon of a biofilm containing a conducting network of identical EET redox mediators, assumed to be multiheme cytochromes (MHCs). For clarity, bacterial cells and cell membranes are not shown. **Right:** Energy diagrams showing example redox microstates of the MHCs for steady-state current flow under two different E_{an} conditions. Near the electrode surface, MHC charge state, and thus the biofilm redox state, is determined strongly by E_{an} when acetate (Ac) is in excess, and by both E_{an} and Ac concentration, through the Nernst relation, under low electron-donor conditions. As described in the text, the redox state of the large, conductive biofilm-MHC pool is not significantly altered during a fast-scan CV sweep. The main current-onset (or "midpoint") potential thus reflects the average MHC redox state under the imposed E_{an} and substrate concentration.

CHAPTER 3

Identification of Diverse Potentially Electroactive Bacteria in Sediment and Groundwater Through Genomic Analysis of Consortia Enriched in Microbial Electrochemical Cells

Abstract

There is growing recognition of the ability of microbes to interact electronically with their external environment. Bioreduction of minerals and redox-active metals leads to dissolution or precipitation, processes that contribute to geochemical cycling. Here we used a bioelectrochemical system in which a solid electrode played the role of a redox-active surface to enrich for anode-respiring consortia. The system was inoculated with anaerobic sediment and groundwater from a genomically well-studied aquifer near Rifle, CO, and amended with acetate. Anode biofilms and planktonic samples were characterized by genome-resolved metagenomics. We reconstructed draft-quality or near-complete genomes for 84 Bacteria and 2 Archaea that represent the majority of organisms present in 28 samples. A novel *Pelobacter* sp. with 72 multiheme *c*-type cytochromes (MHCs) was the dominant electrode-attached organism. Other bacteria are now implicated in electrode respiration based on anode-association and genomes encoding cytochromes with ≥10 heme-binding motifs, as well as loci including porin cytochrome complexes. These include members of the Actinobacteria, Ignavibacteria, Chloroflexi, Acidobacteria, Firmicutes and Burkholderiales phyla. Interestingly, the number of heme-binding motifs in MHCs varied in closely related members of both the Anaerolineales and Burkholderiales. Organisms with multiheme cytochromes were at high abundance in the biofilms, but most remained at low abundance in the planktonic fraction over the two-year study period, consistent with the importance of these proteins for growth on electroactive surfaces. Our results identify a small subset of the vast diversity of organisms previously detected in this environment that may have the potential to mediate mineral redox transformations.

Introduction

Some members of microbial communities in the subsurface rely on extracellular minerals as either electron donors or acceptors as a respiratory strategy. Recently, it has also been shown that other organisms may play the role of metabolic electron-donating or -accepting partner in a form of electrochemical syntrophy. These types of biochemical redox interactions are known as extracellular electron transfer (EET) (Shi et al. 2016), and can drive major geochemical changes and cycles that shape Earth's bio- and geospheres (Nealson & Myers 1990; Roden 2012). In nearly all known cases of microbial EET, specialized electron-transfer proteins known as multiheme cytochromes (MHCs) have been shown to play a vital role (Leang et al. 2003; Lloyd et al. 2003; Butler et al. 2004; Kim et al. 2005; Shi et al. 2007; Lovley 2011; Levar et al. 2012; Beliaev & Saffarini 1998; Myers & Myers 1997; Bretschger et al. 2007; Hartshorne et al. 2007; Bouhenni et al. 2010; Bücking et al. 2010; Coursolle et al. 2010; Mitchell et al. 2012; Wrighton, Thrash, et al. 2011). Much of the knowledge gained about EET comes from studies of two of the early metal-respiring microbial species to be isolated in culture in the late 1980's to early 90's: *Geobacter sulfurreducens* of the Deltaproteobacteria, and *Shewanella oneidensis* within

Gammaproteobacteria (Myers & Nealson 1988; Lovley & Phillips 1988; Bond et al. 2002), which became and remain the model organisms for EET. Complete genome sequences for these organisms have been publicly available since the early 2000's, allowing a detailed look at their individual physiologies (Heidelberg et al. 2002; Methé et al. 2009).

Microbes able to perform EET have now been isolated from across the phylogenetic spectrum (Sturm et al. 2012; Gregory & Holmes 2011). EET has therefore recently been recognized as a widespread phenomenon with deep evolutionary history. However, the vast majority of organisms present in natural systems have not been isolated (Brown et al. 2015; Hug et al. 2016). This is almost certainly in large part due to the fact that in nature microorganisms exist and function as members of a community, relying on a number of complex interspecies interactions (Anantharaman et al. 2016). This hypothesis is supported by many laboratory-based enrichment experiments targeting electroactive microbes, which consistently result in diverse, stable populations of organisms from various phyla (Tender et al. 2002; Bond et al. 2002; Lee et al. 2003; Holmes et al. 2004; Kim et al. 2004; Jung & Regan 2007; White et al. 2009; Chae et al. 2009; Torres et al. 2009; Kan et al. 2011; Jung & Regan 2011; Malvankar, Lau, et al. 2012; Yates et al. 2012; Ishii et al. 2014; Zhu, Yates, Hatzell, Ananda Rao, et al. 2014). However, most of these studies to date have relied on phylogenetic profiling methods (either DGGE or 16S rRNA gene surveys) that do not provide information about metabolic capacities.

There is urgent need both for experimental systems that do not rely upon isolation of individual electroactive microbes in pure culture, and for complete genomic information that serves not only to identify members of the community, but also allows predictions about metabolic functions inferred from genomic content to be tested. Microbial electrochemical cells (MXCs) can address this need. In a MXC, an electrode can play the role of the mineral (or microbial) electron acceptor. Although minerals and electrodes should not be considered completely equivalent (Levar et al. 2017), this approach has several important advantages over using natural mineral electron acceptors. Minerals are reactive, as well as heterogeneous in redox potential and many other properties affecting bioavailability (Thamdrup 2000; Majzlan 2012; Langmuir & Whittemore 1971; Navrotsky et al. 2008; Roden & Zachara 1996; Bonneville et al. 2004; Bonneville et al. 2009). In an MXC, the redox conditions are defined by the voltage at the electrode, which can be precisely controlled, allowing for exploration of specific redox niches. These systems therefore provide an ideal way to enrich specifically for electroactive microbes and microbial communities, typically resulting in high cell densities in both the planktonic medium and, often, in the form of electrode-attached biofilms. With such high levels of biomass, near-complete genomes for the majority of organisms present in the system can be obtained from metagenomic sequencing and assembly of DNA reads, which is much more challenging when sequencing the subsurface environment directly.

In this study, we coupled an enrichment strategy using MXCs with genome-resolved metagenomics. The source of the inoculum used here was a major subsurface field research site (Rifle, CO) with a wealth of previous metagenomic studies (Hug et al. 2013; Wrighton et al. 2014; Anantharaman et al. 2016; Hug et al. 2016; Brown et al. 2015) that allowed us to compare our results to genomic information from Rifle. This approach made it possible to place the organisms studied in the fuel cells in environmental context. Overall, the results implicate a diverse consortium of bacteria and archaea, many with large MHCs and other EET-related genes, that are likely involved in electrode-based and by proxy mineral-based respiration. Some of these organisms are either not currently known to perform EET, or are vastly understudied relative to *Geobacter* and *Shewanella* species.

Materials and methods

Setup and operation of microbial electrochemical cells (MXCs)

"H-cell" type electrochemical cells with two duplicate anodic chambers on either side of a central, shared cathodic chamber (shown in **Figure 3.1**) were set up using unpolished graphite-block working electrodes (2.5 × 2.5 × 1.0 cm, McMaster-Carr) in anodic chambers, a platinum-mesh counter electrode (~1.5 x 1.0 cm) in the cathodic chamber, and additional platinum-wire counter electrodes in anodic chambers used for electrochemical characterization. Reference electrodes were either Ag/AgCl type (3 M KCl, Microelectrodes, Inc. model MI-403; +210 mV vs. SHE for standard conditions; used in MXC-1) or saturated calomel (Fisher Scientific Accumet; +242 mV vs. SHE for standard conditions; used in MXC-1.1). Nafion 117 (DuPont) was used as the proton exchange membrane separating anodic and cathodic chambers.

The first cell, MXC-1, was prepared as follows (Sept. 2011): Graphite electrodes were rubbed with a soft sponge in water to remove loose flakes, sonicated once in 5% bleach, then three times in fresh DI water (5 min each time), and stored in DI water until use. Pt electrodes were cleaned by soaking overnight in 1.0-N HCl. Nafion membranes were soaked several times in DI water before cell assembly to dilute the acidity of the hydrated material. The assembled reactor was sterilized by filling with DI water and autoclaving, using a liquid cycle with 20 min at 121 ºC. After cooling, DI water in anodic chambers was replaced with sterile, N_2-flushed phosphate-buffered medium, pH 7.2, containing the following per 1 L: NaH_2PO_4 plus Na_2HPO_4 (anhydrous; 0.38 g and 0.97 g, resp. for 10.0 mM total phosphate buffer), KCl (0.10 g, 1.3 mM), NH_4Cl (0.25 g, 4.7 mM), and vitamin and mineral mix (10 mL each) described in Ref. (Lovley et al. 1984). Anaerobic conditions were maintained in anodic chambers by constant flushing with ultrahigh purity N_2 gas passed through an oxygen trap (Alltech OxiClear) and 0.2-µm filters. The same media recipe was used for aerobic cathode medium, except the initial buffer was Tris-HCl (4.7 g/L, 30 mM, pH 7.2); at 35 days, we switched to a medium with an increased phosphate buffer concentration of 50 mM, and used this for cathodic as well as anodic chambers. Oxygen served as the electron acceptor at the cathode and was supplied by a steady stream of humidified air passed through a 0.2-µm filter.

MXC-1 anodic chambers were inoculated with a sediment-groundwater slurry obtained from the Department of Energy field research site at Rifle, CO, USA. This sediment sample (BH 3.2.11) was recovered from alluvium at the bottom of a freshly-dug trench with a depth of *ca.* 3.5 m below ground surface (co-located with the depth to groundwater) in March 2011. The trench was located in an area of "background sediment," i.e., not subjected to prior acetate amendments. Alluvium was passed through a <2.5 mm sieve, added to no-headspace Mason jars and saturated with groundwater from the trench. Samples were stored at 4 ºC in the dark until inoculation (6.5 months). Before inoculation, MXC-1 anodic chambers were amended with 10 mM sodium acetate, which was the electron donor used throughout the experiment. The sediment-groundwater sample was shaken to mix and then introduced into anodic chambers through the MXC sampling ports using a sterile spatula for the coarser sediment grains, and a sterile, N_2-flushed syringe for the fine-grain/groundwater suspension. The potential of graphite working electrodes was controlled using a potentiostat (PAR VersaStat MC). The startup potential was +10 mV (all values vs. SHE), but changed to a highly electropositive value of +410 mV after seven days with no observable increase in current. This electropositive potential was maintained for three months, at

which time the potential was poised at -190 mV, a value that gave approx. half-maximal current production.

A second cell, MXC-1.1, was prepared using the same procedure with the following modifications (June 2012): Graphite electrodes from above that had been stored in DI water were further cleaned by soaking for 9 hours in 1-N HCl, rinsed and then soaked in DI water for 30 min, soaked in 1 N NaOH for 15 min, rinsed and soaked in acetone for 5 min, then rinsed and stored in DI water until use, with at least two exchanges of the DI water; a rotator provided constant agitation during all of the above cleaning steps. For autoclave sterilization, the time at 121 ºC was 15 min. The phosphate-buffered medium (50 mM phosphate) described above was used in both the anodic and cathodic chambers from the outset. Saturated calomel-type references electrodes described above were used in conjunction with homemade salt bridges (aka "Luggin capillaries"), which were constructed as described in Marsili et al. (2008); salt bridges were filled with a 1.5% agar solution containing 0.5-M KCl as supporting electrolyte. Just prior to inoculation, anodic chambers of MXC-1.1 were amended with ~2 mM sodium acetate (consistent with prior studies of this type), which again was the sole electron donor used throughout the experiment. Both chambers were inoculated with 10 mL each of planktonic medium taken directly from the anodic compartments of MXC-1 (a total of 20 mL per chamber). The startup potential imposed at the graphite working electrodes was -190 mV.

Both MXCs were operated at ambient room temperature. Temperature was recorded at 5-min intervals with a data logger (HOBO Pendant, Onset), and ranged from 18-24 ºC. Current readings were taken at 5-min intervals for the entire experiment, except when performing voltammetry or other electrochemical measurements. Anode and cathode medium was exchanged periodically, and anaerobic 1.00-M sodium acetate was added using sterile, N_2-flushed 1-mL syringes after current dropped to baseline levels. Acetate concentrations varied due to microbial consumption, and we allowed occasional periods of substrate limitation. The maintenance anode potential for MXC-1 was -190 mV for most of the study. For MXC-1.1, the potential was also -190 mV for the first 6.5 months, and was set to increasingly negative values over time (-220 to -250 mV).

DNA sampling extraction

Biomass for preliminary 16S rRNA gene clone library analysis of the MXC-1 planktonic community in the Anode 1 (A1) chamber was collected at four months post-inoculation from 30 mL of A1 medium collected on a 0.2-μm filter. On the same day, DNA was extracted, quantified and amplified by PCR (see below for details). Further samples of the anode-attached biofilms of this MXC were collected after 10 months of continuous operation with electrodes poised mostly at -190 mV (a value corresponding to half-maximal current). Each of the graphite electrodes from A1 and A2 were briefly removed and exposed to ambient air while sampling. Sterilized razor blades were used to gently remove biomass from the graphite surface, and biomass was then flushed into 2-mL centrifuge tubes using a small amount of sterile anaerobic media. Tubes were sealed with Parafilm and immediately placed in N_2-flushed 50-mL centrifuge tubes and stored at -80 ºC within 30 minutes. Electrodes were replaced immediately after sampling and, allowing biofilms to recolonize anode surfaces. Genomic DNA was isolated from the 4-month planktonic and 10-month anode biofilm samples using a PowerSoil DNA Isolation Kit (MO BIO Laboratories, Inc.) following the manufacturer's protocol. Additional details for PCR amplification, sequencing, and bioinformatic analysis are given in the Chapter 1. Samples analyzing using metagenomics were collected and processed as follows. For planktonic samples (n = 26, collected from both MXCs), 40-45 mL of spent anode medium was collected in centrifuge

tubes and spun for 15 min at 5000 × *g* to pellet cells. The supernatant was discarded and cell pellets were stored at -80 ºC until DNA extraction. Biofilm samples (*n* = 2, replicate samples from MXC-1, A2) were collected as described above for the clone library. For all samples, DNA was extracted using a PowerBiofilm DNA Isolation Kit (MO BIO Laboratories, Inc.) and concentrations were quantified using a Qubit dsDNA High Sensitivity Assay Kit and 2.0 Fluorometer (Invitrogen).

Metagenomic sequencing, assembly and genome binning

DNA library preparation and metagenomic sequencing were performed by the UC Davis DNA Technologies Core (http://dnatech.genomecenter.ucdavis.edu/). Samples were prepared for sequencing on the Illumina HiSeq 3000 platform using paired-end reads with an average length of 150 base pairs target insert size of 350 base pairs. All 28 samples were run in a single lane. A fluidics problem occurred during the first run, and a second identical library and sequencing run was therefore performed. Fortunately, the data from both the first and second runs were deemed to be of sufficient quality and similar to one another, so reads from the two runs were pooled together for downstream analysis.

Metagenomic reads from each of the 28 samples were processed and assembled separately following our standard data preparation procedure for ggKbase (http://ggkbase-help.berkeley.edu/overview/data-preparation/). Briefly, forward and reverse reads were checked for Illumina adapters, PhiX, and other Illumina trace contaminants using BBTools (sourceforge.net/projects/bbmap). Sequences were trimmed using Sickle (https://github.com/najoshi/sickle). Reads were assembled using IDBA_UD (Peng et al. 2012) with the `--pre_correction` option. Resulting scaffolds ≥1 kb in length were mapped using Bowtie 2 (Langmead & Salzberg 2012) with default settings. Prodigal (Hyatt et al. 2010) was used for gene prediction, and similarity searches of the corresponding protein sequences were run against the KEGG (Kanehisa et al. 2016), UniRef100 and UniProt (Suzek et al. 2007) databases using USEARCH (Edgar 2010). The 16S and 23S rRNA sequences were identified using an in-house script that utilizes Infernal (Nawrocki & Eddy 2013) to perform hidden Markov model (HMM) searches based on databases from the SSU-ALIGN package (Nawrocki 2009); see Brown et al. (2015) for details. Prediction of tRNA genes was accomplished using tRNAscan-SE (Lowe & Eddy 1997).

Each of the 28 assemblies were binned separately. Manual binning was performed using the graphical interface on ggKbase (http://ggkbase.berkeley.edu/), which allows the user to select and bin scaffolds based on their GC content, average read coverage, predicted taxonomy based on gene annotations and single copy gene inventory.

Genome curation and de-replication

In order to identify and attempt to correct assembly and scaffolding errors, we used methods contained in an in-house script `ra2.py` (Brown et al. 2015). If errors could not be corrected, after these steps an error could not be corrected, NNNs were inserted. In the absence of paired read support for the join, the original scaffold was split.

Assessment of genome completeness was based on the presence or absence of genes deemed to be universal and present in a single-copy in most bacteria or archaea (Raes et al. 2007). Genomes were considered to be draft quality if at least 70% of these single-copy genes (SCGs) were present (36/51 for bacteria and 27/38 for archaea) and near-complete if ≥90% of the SCGs were identified.

Because many of the 28 samples were expected to contain the same organisms across time and in different MXC anodic chambers, genome de-replication across all samples was a critical step. Near-complete genomes from all samples were compared using an in-house script that generates an alignment of all scaffolds in each individual genomic bin to the scaffolds of every other bin using the NUCmer program (Delcher et al. 2002). For any sets of genomes that were at least 98% similar across 70% or more of the total alignment length (to be consistent with the 70% completeness threshold based on SCGs), a representative genome was selected based on the following criteria (in order of priority in cases of ties): (i) the highest number of non-redundant SCGs and lowest number of SCG multiples; (ii) the largest N50 contig length; (iii) total genome size (i.e., the sum of the lengths of all contigs in a bin).

Identification of multiheme cytochromes and porin-cytochrome complexes

Genes encoding multiheme *c*-type cytochromes (MHCs) were identified by searching the translated protein sequences of all genes for Cxx(xx)CH heme-binding motifs, where C is cysteine, H is histidine, and x's are any residue. An in-house script (`motif_search.py`) was used to perform the search using a regular expression as input ("C.{2,4}CH"). The motif CxxCH is by far the most common, but there are known cases of larger motifs residues (Stevens et al. 2004; Sharma et al. 2010), and we therefore allowed for 2-4 variable residues in the search. Proteins were categorized as MHCs if they contained three or more motifs.

Putative outer-membrane porin proteins that could be involved in extracellular electron transfer as part of porin-cytochrome complexes (PCCs) were identified using hidden Markov models (HMMs) (Eddy 2011). Four separate models were generated based on porin proteins from *Shewanella oneidensis* MR-1 and *Geobacter sulfurreducens* PCA: MtrB (SO_1776) (Hartshorne et al. 2009), OmbB (GSU2733), ExtB (GSU2644)/ExtE (GSU2726), and ExtI (GSU2939) (Liu et al. 2014; Chan et al. 2016). For each of the four groups above, protein BLAST searches (Altschul et al. 1990) against the NCBI non-redundant protein (nr) database (2017/03/25) were conducted to gather a set of the most closely related proteins currently represented in public databases. All hits with E-values less than 1e-20 to 1e-30 (minimum 26-27% identity) were retained for building the HMMs. Protein sequences were aligned using MAFFT v7.222 (Katoh & Standley 2013) with default parameters. The `hmmbuild` function of HMMER v3.1b2 (http://hmmer.org) was used with default parameters to construct HMMs, which were then used to search our curated metagenomic dataset for homologues with `hmmsearch`. Putative porin genes identified by the HMMs had to meet two criteria to be assigned as part of a putative PCC. First, the gene must be adjacent to or very near at least one MHC on the metagenomic scaffold; this was assessed visually in ggKbase for each candidate gene. Second, the protein must have a minimum of 14 predicted transmembrane domains (all but two cases had 16 or more domains). The number of transmembrane beta strands for each putative porin was predicted using the web-based PRED-TMBB with the default Viterbi method selected (http://bioinformatics.biol.uoa.gr/PRED-TMBB). For all of the putative porins meeting these requirements, protein BLAST searches were performed as described above to gather the most closely related sequences from the NCBI databases. A phylogenetic tree including all putative porins with these database top hits is included in the supplementary material.

Phylogenetic analysis

Two types of common marker genes, 16S rRNA and ribosomal protein S3 (rpS3), were used for phylogenetic analysis of genomes. Structure-based sequence alignments of 16S rRNA genes were

generated with SSU-ALIGN (Nawrocki 2009) (http://selab.janelia.org/software/ssu-align). A minimum aligned length of 800 bp was required for inclusion in construction of phylogenetic trees. Alignments of rpS3 sequences were performed using MUSCLE with default parameters (Edgar 2004). Sequences less than 50% of the aligned length were excluded. Maximum-likelihood phylogenies were inferred using RAxML version 7.2.8 (Stamatakis 2014) with either the GTRCAT (16S rRNA) or PROTCATJTT (rpS3) model of evolution and 100 bootstrap re-samplings.

Results

Enrichment of electroactive microbial consortia from the Rifle subsurface

A microbial electrochemical cell (MXC), MXC-1, was inoculated with an anaerobic sediment-groundwater slurry collected from the Rifle site in 03/2011 and maintained for almost four years at electrode potentials corresponding to the redox potential of iron- and manganese-oxide minerals (mostly around -0.2 V vs. SHE) and with periodic acetate addition. We used acetate as the electron donor because it is a well-known fermentation product linked to microbial community function at the site (Wrighton et al. 2014). Further, acetate has been used during *in situ* field experiments at the Rifle site and there is extensive data about microbial community responses, both in groundwater and sediments (Williams et al. 2011; Handley et al. 2013).

16S rRNA gene sequencing of planktonic cells from Anode 1 collected for preliminary microbial community compositional analysis at four months indicated the presence of organisms belonging to taxa Bacteroidetes, Betaproteobacteria, Tenericutes and Gammaproteobacteria (see **Figure 1.7A**) At nine months, planktonic medium samples from each of the MXC-1 anodic chambers were mixed and used to inoculate a second MXC, designated MXC-1.1, which was maintained for over four years (**Figure 3.1**). Over the experiment, the current production in both cells was similar for the same anode potentials. At the time of inoculation of MXC-1.1, distinct biofilms had formed on the electrodes of both chambers of MXC-1. The biofilms exhibited a color gradation from colorless to red with increasing proximity to the site where N_2 gas was bubbled into the system to maintain anaerobic conditions and ensure mixing (shown in **Figure 1.1**). 16S rRNA gene clone library analysis of colorless biofilm from one chamber and red biofilm regions from both compartments collected at 11 months revealed distinct differences in community composition (**Figure 1.7B**). Notably, the two red biofilm samples were dominated by *Geobacter*, whereas the colorless biofilm contained a more even distribution of taxa. Included in the colorless biofilm were taxa detected in the earlier planktonic 16S rRNA library, taxa found in the red biofilms, and additional groups (see Chapter 1). No visible biofilm developed on the electrodes in MXC-1.1, so we attribute current production in this system to planktonic cells.

To explore the planktonic community composition, we metagenomically sequenced samples collected from MXC-1.1 at a variety of time points within a few months of inoculation and near the end of the experiment (**Figure 3.1**). During the period of operation, MXC-1.1 experienced anode potentials ranging from -190 to -250 mV, and acetate was added periodically to maintain concentrations mostly at or below 2 mM. The experiment was conducted in this way to sample microbial community composition under a wide range of conditions. We also sampled the planktonic cells of MXC-1 at the end of the experiment to compare this community with that of MXC-1.1, as well as to the electrode-attached communities for which replicate samples were

collected from one anode of MXC-1. Details relating to DNA extraction and sequencing are provided in **Table S1**.

Genomic resolution of anode-biofilm and planktonic MXC communities

We reconstructed ~600 genome bins from the 28 independently assembled metagenomes using a combination of GC content, phylogenetic profile, coverage and single copy gene inventory. These were mostly bacterial, but some were for plasmids, phage and some archaea. After sequence curation (see Methods), genome bins were de-replicated, resulting in high quality draft genomes for 84 bacterial and 2 archaeal populations, 70 of which are considered near-complete (≥90% SCGs; **File S2**). These genomes accounted for between 70% and 91% of the reads from each sample (average 81.3%) (**Figure S1**).

Given that many bins lack 16S rRNA sequences, which do not assemble well in metagenomic reconstructions (Miller et al. 2011), genomes were assigned to organisms based on their phylogenetic profile and sequences of conserved (e.g., ribosomal) proteins. The overall community compositions of MXC-1 biofilms and planktonic samples, as well as MXC-1.1 planktonic communities, are shown in **Figure 3.2**.

The composition of the duplicate Anode-2 ("A2") biofilm samples is similar and quite distinct from that of any planktonic sample, in line with prior 16S rRNA gene clone library results (**Figure 1.7A**). Notable is the presence of a variety of distinct *Geobacter*/*Pelobacter* species, one of which comprises at least 69% of the electrode-associated community. In combination, six *Geobacter*/*Pelobacter* species comprised on average 73% of the cells in the biofilm. 16S rRNA gene sequences were recovered for two of the six near-complete and one partial *Geobacter*/*Pelobacter* genomes. Three additional *Geobacter* 16S rRNA sequences were from scaffolds not assigned to bins. Comparing these sequences with those from the original biofilm clone libraries (sampled 07/2012) showed that the dominant anode-attached *Pelobacter* organism from the late-2014 metagenomic samples was highly abundant in the clone libraries; the other 5 metagenomic *Geobacter* 16S rRNA sequences were not represented by clones (**Figure S2**).

Also among the top 10 most abundant biofilm organisms were two novel Bacteroidetes, an Acholeplasmatales (Tenericute), a Coriobacteriales (Actinobacteria), Ignavibacteria species, and one Chloroflexi. Six of these genomes contained a large number of multiheme cytochromes (MHCs; ranging from 18 to 37), which are fundamental in most known EET pathways. Genomic MHC content is described in more detail below. Notably, the 18th most-abundant (0.26% of mapped reads) organism in the biofilm was an archaeon whose 16S rRNA gene shares 99.8% identity with that from *Methanosarcina subterranea*. *Methanosarcina* and *Geobacter* spp. have been shown to form a syntrophic EET-based partnership in co-culture (Rotaru et al. 2014), and have also been shown to take up electrons from biocathodes (Bretschger et al. 2015).

Interestingly, the planktonic samples collected simultaneously from the two anodic chambers of MXC-1 ("A1" and "A2") showed systematic differences in community composition over the two-month sample timespan, including higher relative abundances of *Dechloromonas* (S9) Rhizobiales and *Delftia acidovorans* (S1) but lower abundances of *Azospira* (S23) and Bacteroidetes (S0_BJP) in A1 compared to A2 samples (**Figure 3.2A**). Overall, these data suggest quite stable populations over this timescale, which were robust to media exchanges and periodic acetate additions, the only major perturbations during this time period.

The planktonic community composition in MXC-1 was broadly similar to that of MXC-1.1 (**Figure 3.2B**, left group). Independent replicates collected simultaneously (or within two days in one case) from MXC-1.1 A1 and A2 are similar. However, more detailed examination reveals

intriguing community dynamics in MXC-1.1 across months to years. Specifically, over the first seven months (2012-2013 samples) there were replicated shifts in community composition in the independent chambers. This pattern persisted through the 2015 sampling period, although the populations diverged somewhat. Overall, the findings indicate that the community composition was largely dictated by experimental conditions.

We generated an overview of the planktonic organisms in MXC-1 and MXC-1.1 by focusing on the organisms that were among the top five most abundant in any of the samples across time (28 organisms in total; **Table S2**). One quarter of the most abundant organisms in MXC-1 were also abundant in MXC-1.1. Among the most abundant in both fuel cells were Bacteroidetes and Proteobacteria (see the supplementary Table). Notably, identical or highly-related strains (at least 98% similar across all contigs in a genome bin, on average) fell below our detection limit, but reemerged, demonstrating their persistence for years in this bioelectrochemical system. Of the abundant, persistent planktonic organisms, only Bacteroidetes (S9_GWE2) and *Azospira oryzae* (Betaproteobacteria S23) were also strongly detected in the biofilm community.

Genomes rich in multiheme cytochromes

Given that our objective was to identify potentially electroactive bacteria, we focused our genomic analysis on organisms in the anode biofilm. Of particular interest were organisms whose genomes contained many (or very large) multiheme *c*-type cytochromes (MHCs) that are implicated in electron transfer (**Table 3.1**). The number of MHCs (defined here as having three or more heme-binding motifs) encoded in Geobacteraceae genomes ranged from 16 to 81 with an average of 64. The most abundant of these, "S0_Deltaproteobacteria_53_40", has 72 MHCs, the largest of which has 45 heme-binding motifs. All *Geobacter*/*Pelobacter* species were detected in at least one of the MXC-1planktonic samples from A1 or A2, but five of the six were substantially more abundant in the biofilm (sample from A2). Abundant biofilm organisms outside of the Deltaproteobacteria with many MHCs included a Coriobacteriales whose genome encodes 37 MHCs, and two taxonomically distant Ignavibacteria whose genomes encode 18 and 20 MHC, the largest of which respectively contain 40 and 33 heme-binding motifs.

MHC-rich organisms most abundant in the planktonic MXC-1 samples (blue-shaded cells in the table) included a third ignavibacterium (S9, which shares an identical 16S rRNA sequence with S28_36_80), two Betaproteobacteria including a Burkholderiales with a 49-heme cytochrome, two highly similar Chloroflexi strains (order Anaerolineales), and a deltaproteobacterium from the *Desulfovibrio* genus. The organisms whose genomes are MHC-rich and that were found at highest abundance in MXC-1.1 planktonic samples were two Acidobacteria from genera *Geothrix* and *Holophaga*, a Burkholderiales sp. with 11 MHCs, a *Geobacter* sp., and a novel Firmicutes (genus *Desulfosporosinus*) that also has 11 MHCs.

We examined the relationship between the number of MHCs in a genome and the abundance of the corresponding organism in the biofilm (**Figure 3.3A**) and planktonic samples (**Figure 3.3B**) from MXC-1. Organisms present only at very low abundance levels were excluded from this analysis. The results show that genomes with high numbers of MHCs tended to be the most abundant biofilm species, whereas the most abundant planktonic organisms had relatively few MHCs.

Porin-cytochrome complexes in MXC genomes suggest EET capability

To support the genomic inference of EET capability based on MHC content, we examined genomic regions associated with MHCs for evidence of outer-membrane porin proteins. Together with

MHCs, these porins have been experimentally shown to form membrane conduits for electrons called porin-cytochrome complexes, PCCs (Liu et al. 2014). Known porin proteins identified in *Shewanella oneidensis* (MtrB) (Hartshorne et al. 2009) or *Geobacter sulfurreducens* (OmbB, ExtB/E, and ExtI) (Shi et al. 2014; Chan et al. 2016) were used to construct four separate hidden Markov models (HMMs) (Eddy 2011). Protein sequence alignments and phylogenetic trees suggest that these four proteins represent three or four evolutionarily independent families (**Figure S3**), which has been previously reported for some of these proteins (Shi et al. 2014; Chan et al. 2016). HMMs were then used to search MXC genomes for porin proteins. High-scoring candidate sequences were confirmed to be part of a putative PCC if they were adjacent or very close to at least one gene coding for a MHC, and if the sequence had at least 14 predicted transmembrane domains. Twelve of the 53 near-complete genomes that contain one or more MHCs from this study harbored at least one PCC (**Table 3.2**). All twelve are among the 21 organisms whose genomes were identified to be most enriched in MHCs (**Table 3.1**).

Geobacter/*Pelobacter* spp. had the greatest number and diversity of porin types, including proteins homologous to MtrB found in *Shewanella* spp. and in several other phyla (Shi et al. 2014). Interestingly, putative PCCs were also identified in an *acidobacterium* (genus *Holophaga*), three Betaproteobacteria (two of order Burkholderiales), and two Ignavibacteria. Gene diagrams for all putative PCCs from this study, as well as *Geobacter* and *Shewanella* type-strain examples, are grouped by porin family type in **Figure 3.4**. The *Holophaga* (S7) genome contained two PCCs, one sharing homology with MtrB, the other in the ExtB/E family. To our knowledge, this is the first report of a putative PCC in Acidobacteria.

Both Ignavibacteria genomes encoded OmbB-like PCCs, and one genome (S28) also contained a close MtrB homologue. *Geobacter*-like PCCs have been previously identified in the only two Ignavibacteria type strains *Melioribacter roseus* (Podosokorskaya et al. 2013) and *Ignavibacterium album* (Shi et al. 2014), and recently in metagenomics-derived environmental genomes from an iron-rich hot spring (Fortney et al. 2016). However, this is the first report of a PCC porin homologous to MtrB.

Porin-cytochrome complexes with porins homologous to MtrB have been found in a diversity of Betaproteobacteria including Fe(II) oxidizers such as *Sideroxydans lithotrophicus* and Fe(III)-reducing species like *Rhodoferax ferrireducens* (Shi et al. 2012). In addition to Mtr homologues, we found one case of a PCC similar to OmbB in a Burkholderiales MXC genome (S13) of genus *Hydrogenophaga*. The porin in this genome is preceded by two large MHCs containing 24 and 49 heme-binding motifs. A protein BLAST against the NCBI database revealed a highly related porin (Y695_01567) in the isolate genome of *Hydrogenophaga* sp. T4 (AZSO01000162). This putative porin gene from sp. T4 is adjacent to a MHC with seven heme-binding motifs, which is the only other open-reading frame on the short scaffold containing these two genes (see **Figure 3.4**).

The porin sequence from Burkholderiales S13 is most similar to sequences from two genomes assembled from Rifle metagenomic data (Anantharaman et al. 2016). These genomes also harbor the two large MHCs preceding the porin. The Rifle genomes have identical 30S ribosomal protein S3 (rpS3) sequences to one another, and differ only by a single residue from the S13 sequence. Interestingly, the homologous porin proteins and the smaller MHCs from these three genomes all had very high sequence similarity (96-98%), with very similar predicted porin transmembrane architecture and the same number of heme-binding motifs (24); the larger MHCs, however, were less similar (80-89%) due to apparent insertion or deletion of CxxCH-containing domains (**Figure 3.5**). Both MHCs display a remarkably tight packaging of hemes: the 24- and 49-motif cytochromes use only 22.4 and 23.4 residues per heme, respectively. These ratios are even lower

than for the decaheme periplasmic cytochrome MtrA from *Shewanella oneidensis* MR-1 (25.1 residues/heme), which is included in the Figure for reference.

We did not identify any PCCs in the Anaerolineales (Chloroflexi) genomes that encoded several large MHCs (**Table 3.1**), possibly due to the short length of the scaffolds containing these genes (i.e., the surrounding genomic context was not well reconstructed). These MHCs may function in EET, but the mechanism is less certain. Similar to the large MHCs from the Burkholderiales genomes described above, the sequences of the largest MHCs in the two Anaerolineales genomes vary in their number of heme-binding motifs. Given that the number of hemes should impact the redox properties of these proteins, we sought evidence for this as a more general phenomenon. A manually curated alignment of sequences from public databases confirmed this prediction (**Figure 3.6**).

Linking MXC and Rifle genomes

To evaluate whether organisms identified in MXC experiments are relevant in microbial communities present in the Rifle aquifer, we compared conserved marker gene sequences to all sequences from the 35 Rifle metagenomes, as well as to sequences in the NCBI database. This analysis used the 80 full-length and four partial rpS3 sequences from the 86 draft-quality to near-complete genomes. We also analyzed 16S rRNA sequences, although we recovered far fewer sequences encoding this gene (31 full-length and 4 partial). The Rifle comparison dataset contained a total of 17,056 rpS3 sequences (minimum 50 amino-acid length) and 5,598 16S rRNAs. A maximum-likelihood rpS3-based phylogenetic tree containing all MXC sequences and those from closely related-Rifle genomes is given in the supplementary material (**File S3**).

There were 38 MXC genomes whose rps3 protein sequences shared at least 96% identity with one or more genomes assembled from Rifle metagenomic data (**Table 3.3**). The Rifle sample type with the largest number of corresponding genomes was acetate-amended groundwater, followed by acetate-amended sediment and low-oxygen groundwater. Organisms from the Acidobacteria, Alphaproteobacteria, Betaproteobacteria, Deltaproteobacteria, Gammaproteobacteria, Bacteroidetes, Chloroflexi, Firmicutes, Ignavibacteria, and Spirochaetes taxa are represented. There were a total of 25 MXC genomes with ≥99% rpS3 amino-acid identity to one or more in a set of 47 unique Rifle genomes (**Table S3**). Additional statistics for MXC-to-Rifle genome linkages as inferred from rpS3 and 16S rRNA are given in the supplementary Table.

For MXC organisms potentially involved in current production based on MHC content, phylogenetic trees were constructed to place them in context with isolates and uncultured microbes previously detected at the Rifle site. The most abundant biofilm organism, S0_Deltaproteobacteria_53_40 (also present only at low levels in the planktonic fractions of both MXCs), is in the *Geobacter*/*Pelobacter* clade according to both rpS3 and 16S rRNA (**Figure S4**) gene sequence identity (Holmes et al. 2007). This organism shares 97.7% 16S rRNA gene nucleotide identity with that of *Pelobacter propionicus* DSM 2379, and 100% rpS3 amino-acid identity with sequences from several Rifle genomes from acetate-amended groundwater samples (**Figure S5**). Two other novel MXC *Geobacter* strains, S27 and S20 (with 81 and 80 total MHCs, the most of any genomes in this study), also shared 100% rpS3 amino-acid identity with a sequence from the genome of a *Geobacter* species sampled from acetate-amended groundwater at the Rifle site. Interestingly, these two strains had very different abundance patterns in the MXCs. S27 was the second most abundant Deltaproteobacteria in the (A2) biofilm and S20 was present at low levels in MXC-1 (biofilm and planktonic), but became relatively abundant in the MXC-1.1 planktonic samples early in the experiment (11/2012–04/2013). *Geobacter* sp. S28, which was

abundant in the biofilm, also shares 99.5% rpS3 sequence identity with a sequence from a Geobacter species from a sediment sample collected 19-ft deep below the ground surface and not subjected to acetate amendment.

The Coriobacteriales (Actinobacteria) genome that was the fourth most abundant in the biofilm, and harbored 37 MHCs, had no close relative in the Rifle metagenome. This genome was present only at low levels in planktonic samples from both MXCs. The most closely related sequences (97-98% 16S rRNA identity) come from uncultured species sampled from (deep) sediment or groundwater samples in redox zones associated with iron reduction (Kimura et al. 2010), and from the biocathode of a microbial electrolysis cell (Croese et al. 2011) (**Figure S6**).

16S rRNA sequences were recovered in all three MXC Ignavibacteria genomes, in addition to rpS3-coding genes. Genomes S28_36_80 and S9 have near identical 16S rRNAs, but very different abundance patterns in the MXCs: The former is abundant in the biofilm, detected at low levels in the MXC-1 A2 planktonic, and not detected in MXC-1.1; S9 is detected at low levels in the MXC-1 biofilm (A2), but much more abundant in the MXC-1 A1 planktonic samples from the 2015. No closely related organisms were found in the Rifle metagenome for these two strains, but there are closely related uncultured organisms (one with 99.8% 16S identity) from freshwater and marine sediments, as well as anaerobic bioreactors (**Figure S7**). The third MXC Ignavibacteria genome, S28_36_39, did have close relatives from Rifle background sediment (98.1% rpS3 amino-acid identity), and had a similar abundance pattern to S28_36_80 (most abundant in the biofilm). See the tree Figure for closest hits based on 16S rRNA.

Of the three Anaerolineales (Chloroflexi) genomes assembled from MXC samples, the one that was highly abundant in the biofilm (as well as the planktonic fraction of the same A2 chamber), S27, had no MHCs. In contrast, the two closely related S13 and S11 strains, which share identical rpS3 protein sequences and 14 total MHCs each, were more abundant in planktonic samples: S13 in both MXCs, and S11 only in MXC-1. There were no closely related isolate genomes in the NCBI databases (**Figure S8**). A 16S sequence was recovered for the S27 genome that is 99.5% similar to a Rifle-derived sequence. The shared rpS3 sequence for S13 and S11 is 96.4% similar to an unbinned Rifle groundwater sequence.

The three phylogenetically distinct Betaproteobacteria with MHC-rich genomes (**Table 3.1** and **Figures 3.3-3.5**) all had closely related Rifle genomes mostly derived from groundwater samples (**Table 3.3**; **File S3**), and thus were very likely enriched from the original sediment-groundwater inoculum. All three were detected at low abundance in the biofilm but were most abundant in planktonic samples of both MXCs, congruent with the sample types of the closely-related Rifle organisms. Burkholderiales S13 shares 97.6% rpS3 identity with *Hydrogenophaga taeniospiralis*, placing it in this genus. Burkholderiales S1 appears to fall within the *Rhodoferax* genus, which contains known iron-reducing species (Finneran 2003). Betaproteobacterium S12 is not closely related to any known organism (cultured or uncultured) outside of Rifle, and appears to place in the Nitrosomonadales or Rhodocyclales orders.

Some genomes from the phyla Acidobacteria, genera *Geothrix* and *Holophaga,* may also be electroactive. These include S15_Geothrix and S7_Holophaga, both of which have genomes with 12 MHCs. In the cases of S7 Holophaga, we also identified two PCCs. Very close relatives for both genotypes were detected in acetate amended sediment from the Rifle site.

Also of interest is the genome of a bacterium from the genus *Desulfosporosinus*. Organisms from this genus are known to reduce sulfate, and some have the capacity to reduce uranium (Suzuki et al. 2003). Some (e.g., *D. meridiei*) can reduce ferric iron and others (e.g., *D. acididurans*) are suspected to have this capacity. In neither case was a gene encoding dissimilatory ferric iron

reductase was detected. The S24_Desulfosporosinus_43_10 genome encodes eleven MHCs with up to eight heme-binding motifs, but no associated porins were identified. Some of the MHCs are annotated as nitrate reductase subunits. The organism was most abundant in the MXC-1.1, and related organisms (94.8 to 97.7% 16S rRNA gene sequence identity have been detected at the Rifle site.

The two archaeal *Methanosarcina* genomes recovered from the MXCs had opposite apparent preferences for biofilm vs. planktonic MXC environments: S28 was more abundant in the MXC-1 biofilm (A2), whereas S10 had much higher abundance in the A2 planktonic samples. Neither were present at significant levels in MXC-1 A1 or MXC-1.1 (planktonic) samples. A 16S rRNA gene sequence was recovered for S28 that was 97.8% similar to a Rifle genome from a 19-ft deep background sediment sample, and had even higher identity to isolate genomes *Methanosarcina lacustris* Z-7289 (99.1%) and *Methanosarcina subterranea* (99.8%). Closely-related uncultured archaeal 16S rRNA gene sequences were found in a deep sedimentary aquifer near Hokkaido, Japan (99.9%, AB288240) and a low-temperature biodegraded Canadian oil reservoir (99.7% AY570658). Given the close similarity between the 16S rRNA sequence of the MXC archaea and the *M. subterranea* and *M. lacustris* Z-7289 isolates, it is interesting that the rpS3 proteins from both MXC organisms were only 81-88% similar to those from the type strains.

Discussion

The favorable genome recovery statistics for all samples (on average of 81% of reads on mapped to high-quality draft genome bins) demonstrates the utility of metagenomic sequencing coupled to enrichment as a strategy to identify electroactive organisms in community context. We found that the composition of biofilm and planktonic samples differed substantially, suggesting different metabolic strategies predominate in these fractions (**Figure 3.2**). Notably, the strong correlation between the number of MHCs in MXC genomes and abundance in the biofilm (**Table 3.1** and **Figure 3.3**), underscores the importance of these proteins in growth on electrodes. Based on the findings, we identify a diverse group of bacteria that likely rely on extracellular electron acceptors for growth in sediments.

For the planktonic communities, we noted generally parallel changes in the microbial community composition in the two independent chambers of MXC-1.1 over more than four years (**Figure 3.2B**). From these observations, we infer that shifts in composition were not stochastic, as could have been the case given the initial high complexity of the inoculum. The main variables likely to be driving these changes are room temperature, slight differences in pH and media composition (dependent mostly on the time since the last media exchange or acetate addition). In addition, shifts may have been driven by the change of the anode potential (initially set at -190 mV vs. SHE) toward -250 mV later in the experiment.

The finding that a member of the Geobacteraceae made up ~70% of the biofilm population is not surprising, given that many prior enrichment studies that used iron oxides or electrodes as the electron acceptor and acetate as the substrate showed enrichment of *Geobacter* species (Bond et al. 2002; Tender et al. 2002; Lee et al. 2003; Holmes et al. 2004; Kim et al. 2004; White et al. 2009; Yi et al. 2009; Torres et al. 2009; Bond 2010; Jung & Regan 2011). However, the most closely related organisms from the Rifle metagenome all derived from acetate-amended groundwater samples, with no closely related species detected in the sediment. It has been shown that some *Geobacter* species can transfer electrons to other microbial species (Summers et al.

2010; Rotaru et al. 2014; McGlynn et al. 2015) and recent findings indicate that *G. sulfurreducens* uses different EET pathways when respiring minerals vs. electrodes (Chan et al. 2016). The distribution of the abundant MXC Geobacter in the environment may support the view that its natural electron acceptor is a planktonic organism.

There are a number of MXC biofilm organisms that we infer are likely to be capable of EET-based respiration. The Coriobacteriales S27 is only the second neutrophilic actinobacterium shown to encode MHCs in its genome. The only prior example was a genomically characterized strain from deep subsurface sediments (Hernsdorf et al. 2017). Until recently, the only Actinobacteria known to perform dissimilatory iron (or electrode) reduction were obligate acidophiles that do not encode MHCs in their genomes (Wrighton, Thrash, et al. 2011; Itoh et al. 2011; Bridge & Johnson 1998). However, neutrophilic Actinobacteria are commonly enriched in metal-reducing communities (Lentini et al. 2012; Wang et al. 2009) and are detected in 16S rRNA-based surveys of environments where iron reduction is likely occurring (**Figure S7**). One neutrophilic Actinomycetales, *Dietzia* sp. RNV-4, has been isolated from the anode of a sediment microbial fuel cell (Sacco et al. 2017). Overall, Actinobacteria may be far more common contributors to iron reduction than is currently realized.

Little is known about Ignavibacteria. Podosokorskaya et al. (2013) isolated the first species, *Melioribacter roseus,* and showed that it could grow by reducing Fe(III) as well as As(V) and nitrite. Ignavibacteria spp. are relatively abundant in anode biofilms from bioelectrochemical studies (Rimboud et al. 2015; Yoshizawa et al. 2014; Tian et al. 2015; Baek et al. 2016) and iron-reducing environments (Kato et al. 2015; Fortney et al. 2016). Our findings of Ignavibacteria genomes rich in large MHCs (**Table 3.1**) and porin-cytochrome gene clusters (**Table 3.2** and **Figure 3.4**) add further support for electroactivity by members of this group. By searching for porins using four separate HMMs, we could differentiate those homologous to porins from *Geobacter* and *Shewanella* spp., and thereby show the first case of an MtrB-like PCC in Ignavibacteria (see **Figure 3.4** and **Figure S4**).

The fact that the MHC-rich Anaerolineales (Chloroflexi) organisms from this study were more abundant in planktonic samples than in the biofilm makes it less clear whether they are able to use the electrode in a respiratory fashion. However, a Chloroflexi isolate that reduces ferric iron and nitrate (Kawaichi et al. 2013), isolates from iron-reducing environments (Hori et al. 2015), and observations that Anaerolineae organisms make up significant proportions of anode biofilms in MFC studies suggest this as a possibility (Ishii et al. 2008; De Schamphelaire et al. 2010; Cabezas et al. 2015). The investment by these organisms in very large MHCs (Hug et al. 2013) is consistent with the importance of EET-based metabolism for these bacteria (**Figure 3.6**).

MHC-containing MXC Betaproteobacteria were also more abundant in the planktonic compared to biofilm samples. Iron oxidation coupled to nitrate reduction is known for related organisms (Chaudhuri & Lovley 2003; Straub & Schink 2004), and there is some evidence suggesting iron-reduction ability in some species (Kato et al. 2010; Hori et al. 2010). *Delftia* and *Azonexus* spp. from a deep aquifer produced small amounts of current in MXCs (Jangir et al. 2016), and a *Hydrogenophaga* sp. grew in a syntrophic partnership with *G. sulfurreducens*, consuming H_2 and using the electrode as the electron acceptor. Our findings that the genome of S13 Burkholderiales places in the genus *Hydrogenophaga* and encodes large MHCs as well as PCCs, coupled with our identification of a putative PCC from the isolate *Hydrogenophaga* sp. T4, indicate that PCCs may exist in other members of this genus. Syntrophic growth with other MXC community members may be important for the growth of this bacterium in the planktonic fraction.

The large MHCs present in Burkholderiales and Anaerolineales genomes from this study serve as a case study for the topic of variability in the number of heme-binding motifs in homologous cytochromes from closely related species or strains (**Figures 5** and **6**). We find very little on this topic in existing research literature (Klotz et al. 2008), and highlight it as an exciting unexplored area in multi-domain protein evolution. The abundance of MHC-rich genomes from this study, combined with (in most cases) those from populations of closely related Rifle organisms, provides an ideal dataset to leverage in investigating this phenomenon in more detail.

The observation of similar current production from MXC-1.1 compared to MXC-1 despite a lack of any substantial (i.e, visible) biofilm on anodes of the former, raises the question of which organism or organisms in the planktonic fraction were responsible for the majority of the electrons liberated from acetate. Direct cellular contact with an electrode (or mineral) is not the only mode of EET-based respiration: another now-canonical mechanism relies on redox-active molecular shuttles, such as flavins (von Canstein et al. 2008; Marsili, Baron, et al. 2008), which have been shown to interact directly with cell-surface-exposed multiheme cytochromes (Okamoto et al. 2014; Edwards et al. 2015). Based on MHC and PCC genome content, and abundance in the MXC-1.1 planktonic fraction (**Table 1**; **Table 2** and **Figure 4**), we identify as the most likely current producers the two Acidobacteria *Geothrix* S15 and *Holophaga* S7, the novel betaproteobacterium Burkholderiales S1, the novel *Geobacter* S20 with 80 MHCs, and the novel Firmicutes *Desulfosporosinus* S24.

Using the same criteria, the organisms abundant in the planktonic fraction of MXC-1 that might have contributed to current production include Ignavibaceteria S9, Betaproteobacteria S12 and Burkholderiales S13 (a *Hydrogenophaga* sp.), the two genomically similar Anaerolineales (Chloroflexi) strains S11 and S13, and the two Deltaproteobacteria of genus *Desulfovibrio* (S13 and S14). It may be the case that some of the organisms, even those with putative EET-related genes (MHCs and PCCs), whether more abundant in the planktonic or the biofilm, are incapable of electrode- or mineral-based respiration on their own, but are nonetheless able to use the electrode as an electron acceptor by "plugging in" to an existing EET charge-transport network assembled by species such as *Geobacter* that are specialized for this lifestyle. Indeed, Chan et al. find evidence for this within populations of *G. sulfurreducens* containing both wild-type cells and EET-deficient knockout mutants (Chan et al. 2016).

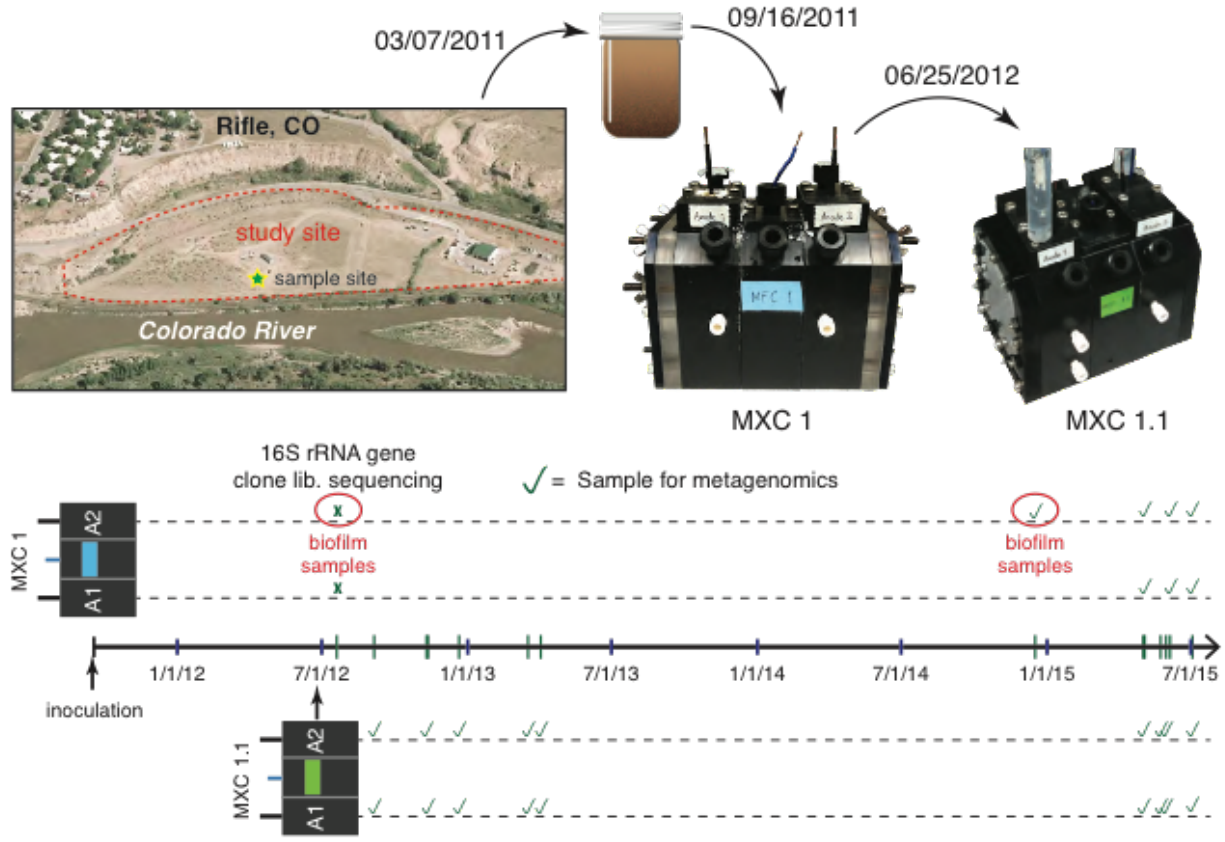

Figure 3.1 - Overview of the experiment. MXC-1 was inoculated from sediment recovered from the study site adjacent to the Colorado River near the town of Rifle (aerial photograph). Around the time that the biofilm was sampled for 16S rRNA analysis a second cell, MXC-1.1 was inoculated with planktonic cells from MXC-1 medium. The lower part of the figure is a timeline showing inoculation and sample-collection dates.

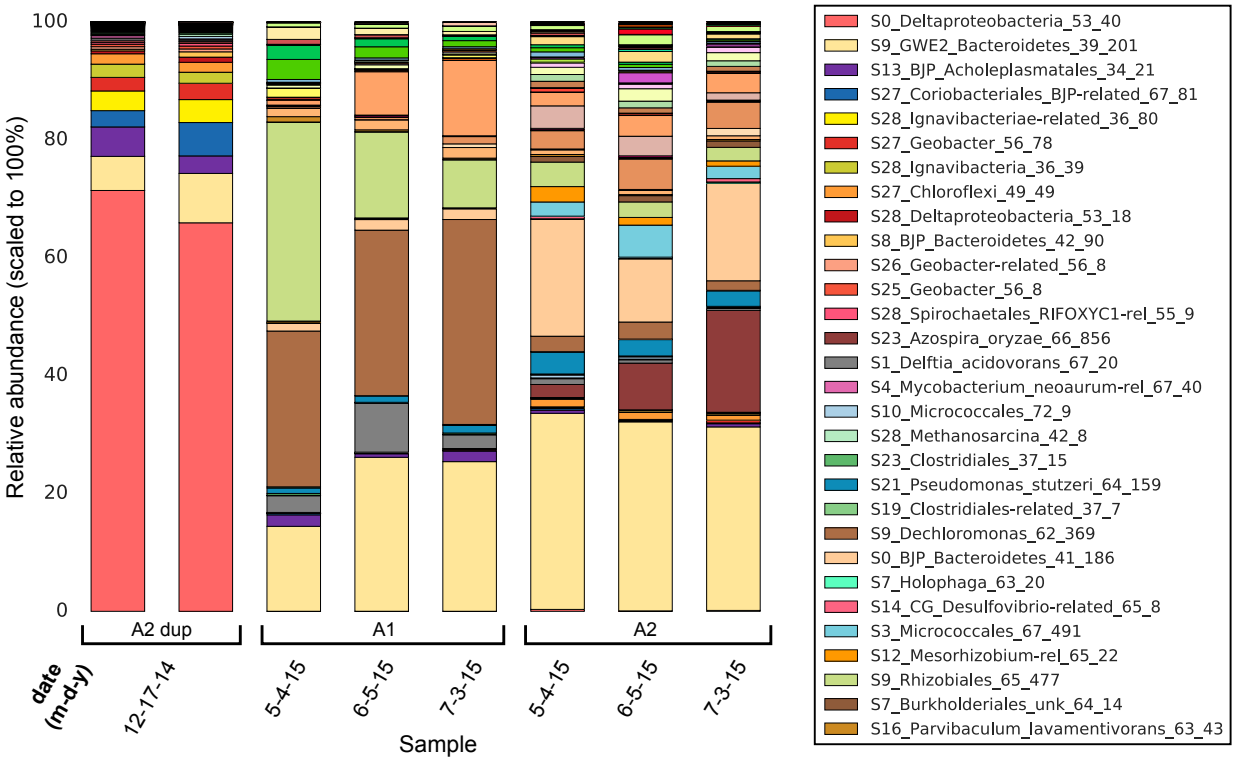

Figure 3.2 - Genome-resolved overview of the composition of MXC-1 and MXC-1.1 consortia shown as stacked bar charts. (**A**) There are major differences in the composition of biofilm (Anode 2 replicates: "A2 dup") and planktonic samples in MXC-1. The planktonic consortia within each chamber of MXC-1 remain fairly constant in composition over the two-month period covered by the samples, but differ from each other due to the presence of some distinct organisms. Genome order in each stacked bar is according to biofilm abundance, with the most abundant at the bottom. The figure legend contains only the 30 most abundant MXC-1 organisms, with the most abundant at the top. *Figure continued, next page.*

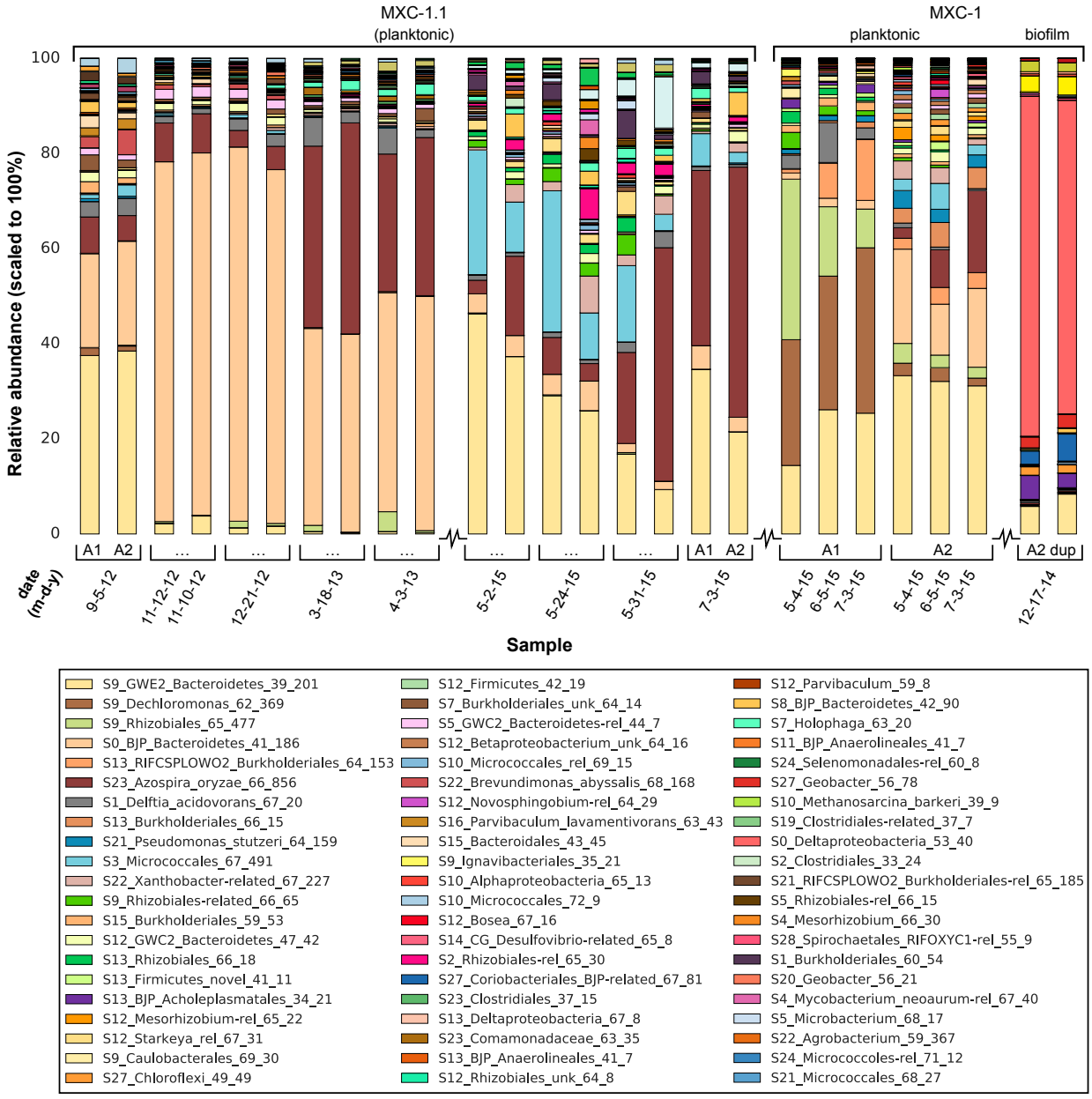

Figure 3.2 (*Continued*) – Genome-resolved overview of the composition of MXC-1 and MXC-1.1 consortia shown as stacked bar charts. (**B**) Comparison of the planktonic consortia in MXC-1 and MXC-1.1 (see **Table S2** for a listing of abundant shared strains) and the biofilms from MXC-1. Genome order in each bar is according to average abundance in MXC-1 planktonic samples. The jagged lines separating groups of bars indicate a long timespan between adjacent samples or a step back the timeline.

		Multiheme cytochromes				*Average abundances*		
Genome	**Phylum or Class**	**No. MHCs (≥ 3 hemes)**	**Average CXX(xx)CH**	**Max CXX(xx)CH**	**No. putative PCCs**	**MXC 1 biofilm**	**MXC 1 plank**	**MXC 1.1 plank**
S27_Geobacter_56_78	Deltaproteobacteria	81	15.2	53	6	34.48	1.00	0.85
S20_Geobacter_56_21	Deltaproteobacteria	80	12.8	45	6	0.25	0.47	2.54
S25_Geobacter_56_8	Deltaproteobacteria	75	8.8	30	3	6.26	0.17	0.63
S0_Deltaproteobacteria_53_40	Deltaproteobacteria	72	11.5	45	4	947.01	0.95	0.72
S26_Geobacter-related_56_8	Deltaproteobacteria	60	7.0	22	3	6.28	0.17	0.56
S27_Coriobacteriales_BJP-related_67_81	Actinobacteria	37	11.4	24	0	55.90	1.47	0.62
S28_Ignavibacteriae-related_36_80	Ignavibacteria	20	10.0	40	2	49.30	0.19	0.01
S28_Ignavibacteria_36_39	Ignavibacteria	18	9.9	33	0	28.56	0.15	0.02
S9_Ignavibacteriales_35_21	Ignavibacteria	17	10.4	40	1	0.25	3.06	0.00
S12_Betaproteobacterium_unk_64_16	Betaproteobacteria	17	7.2	10	1	0.24	4.43	0.10
S28_Deltaproteobacteria_53_18	Deltaproteobacteria	16	6.1	12	1	9.11	0.12	0.09
S13_BJP_Anaerolineales_41_7	Chloroflexi	14	7.2	18	0	0.28	1.28	0.06
S11_BJP_Anaerolineales_41_7	Chloroflexi	14	7.1	26	0	0.19	1.02	0.01
S5_Desulfovibrio_63_18	Deltaproteobacteria	14	5.1	9	0	0.04	0.05	5.94
S7_Holophaga_63_20	Acidobacteria	12	6.2	10	0	1.66	1.02	11.30
S15_Geothrix_rel_68_9	Acidobacteria	12	5.8	11	2	0.01	0.10	0.70
S1_Burkholderiales_60_54	Betaproteobacteria	11	7.5	10	1	0.40	0.57	8.35
S24_Desulfosporosinus_43_10	Firmicutes	11	4.6	8	0	0.02	0.01	0.84
S14_CG_Desulfovibrio-related_65_8	Deltaproteobacteria	10	5.7	16	0	1.47	1.84	0.03
S13_Deltaproteobacteria_67_8	Deltaproteobacteria	9	5.7	15	0	0.01	1.39	0.11
S13_Burkholderiales_66_15	Betaproteobacteria	6	15.0	49	1	0.47	22.91	0.41

Table 3.1 – Listing of organisms (Genome) in order of the number of multiheme cytochromes (MHCs) encoded in their genomes. Organism names are in the form of Sample_organism classification_GC_Cov, where organism classification was established to the most specific level possible, GC is the GC content of the genome and Cov is the coverage in the sample from which the representative genome was recovered. Genomes with less than six putative MHCs are not shown. Proteins were considered to be putative MHCs if their sequences contained at least three heme-binding motifs (CXX(xx)CH). The number of putative porin-cytochrome complexes ("PCCs") is also listed for each genome (green shading). Orange-gold color shading on columns highlights the number of MHCs, the average number of heme-binding motifs and the maximum number of heme-binding motifs in any protein. Note that all of the genomes with many MHCs are Geobacter-related strains. Notable also is a Burkholderiales genome that encodes relatively few MHCs, but two with many heme-binding motifs (24 and 49) that are adjacent to one another and to a putative outer-membrane porin (shown in **Figure 3.4**). Color shading on the abundance columns indicates which of these three sample types (biofilm or planktonic, "plank") each genotype was most abundant in.

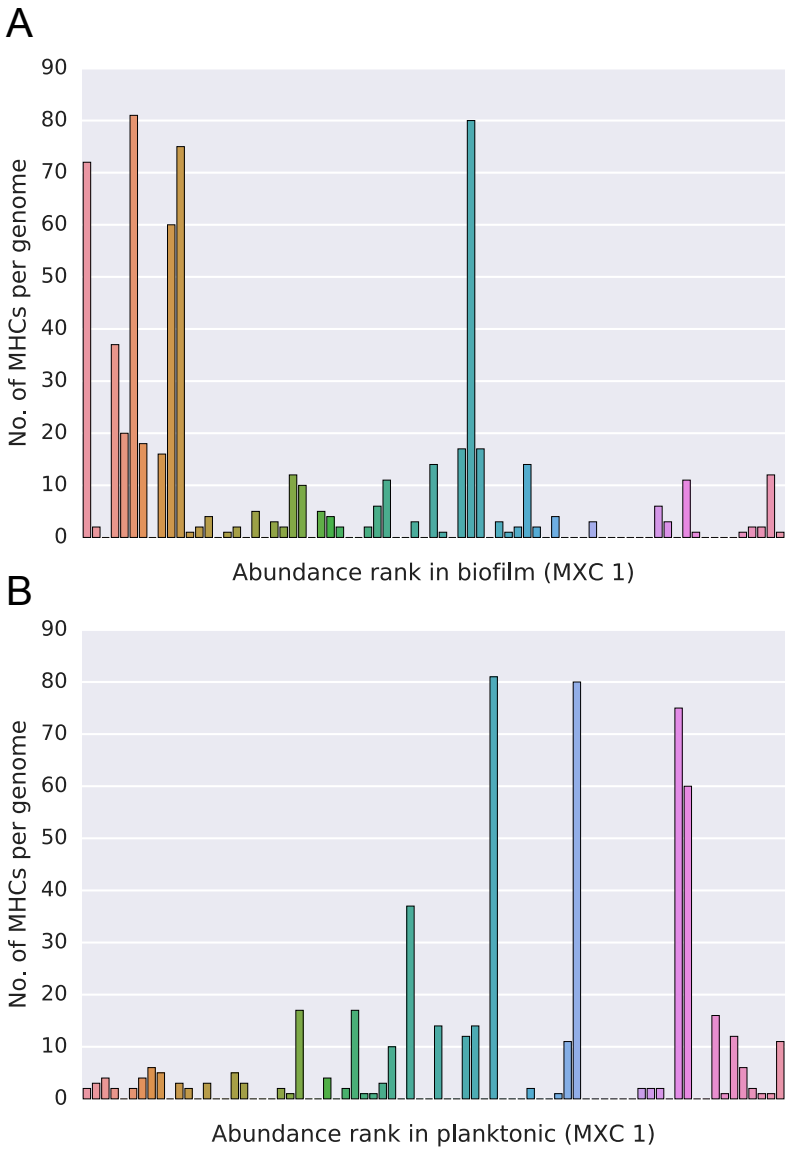

Figure 3.3 – Diagrams showing the number of multiheme cytochromes (MHCs) encoded in the genomes of biofilm and planktonic consortia, with organisms listed in order of their abundance. Note that the abundant organisms in the biofilm have a large number of MHCs whereas those that are abundant in the planktonic consortia have few MHCs.

					Average rel. abundances		
Genome (curated)	**OmbB**	**Ext B/E**	**ExtI**	**MtrB**	**MFC 1 biofilm**	**MFC 1 plank**	**MFC 1.1 plank**
S27_Geobacter_56_78	1	1	3	1	34.5	1.0	0.9
S0_Deltaproteobacteria_53_40	1	1	2	-	947.0	1.0	0.7
S20_Geobacter_56_21	1	1	3	1	0.2	0.5	2.5
S28_Deltaproteobacteria_53_18	1	-	-	-	9.1	0.1	0.1
S25_Geobacter_56_8	1	1	1	-	6.3	0.2	0.6
S26_Geobacter-related_56_8	2	-	1	-	6.3	0.2	0.6
S7_Holophaga_63_20	-	1	-	1	1.7	1.0	11.3
S1_Burkholderiales_60_54	-	-	-	1	0.4	0.6	8.4
S12_Betaproteobacterium_unk_64_16	-	-	-	1	0.2	4.4	0.1
S13_Burkholderiales_66_15	1	-	-	-	0.5	22.9	0.4
S28_Ignavibacteriae-related_36_80	1	-	-	1	49.3	0.2	0.0
S9_Ignavibacteriales_35_21	1	-	-	-	0.3	3.1	0.0
Avg TM domains:	*18.6*	*21.4*	*17.8*	*30.2*			
StDev:	*2.7*	*1.5*	*0.6*	*5.6*			

Table 3.2 – Summary statistics for putative porin cytochrome complexes (PCCs). Twelve of the 86 near-complete genomes contain at least one putative complex with homology to currently known outer-membrane PCC porin protein families from gram-negative bacteria (Liu et al. 2014 and Chan et al. 2016); see **Figure 3.4** for details). The number of putative porins from each family are listed by genome, along with the average and standard deviation of the number of beta-strand transmembrane domains predicted by PRED-TMBB (bottom rows). The average relative (rel.) abundances of each genome in MXC-1 biofilm or planktonic (plank.) and MXC-1.1 are also shown for context.

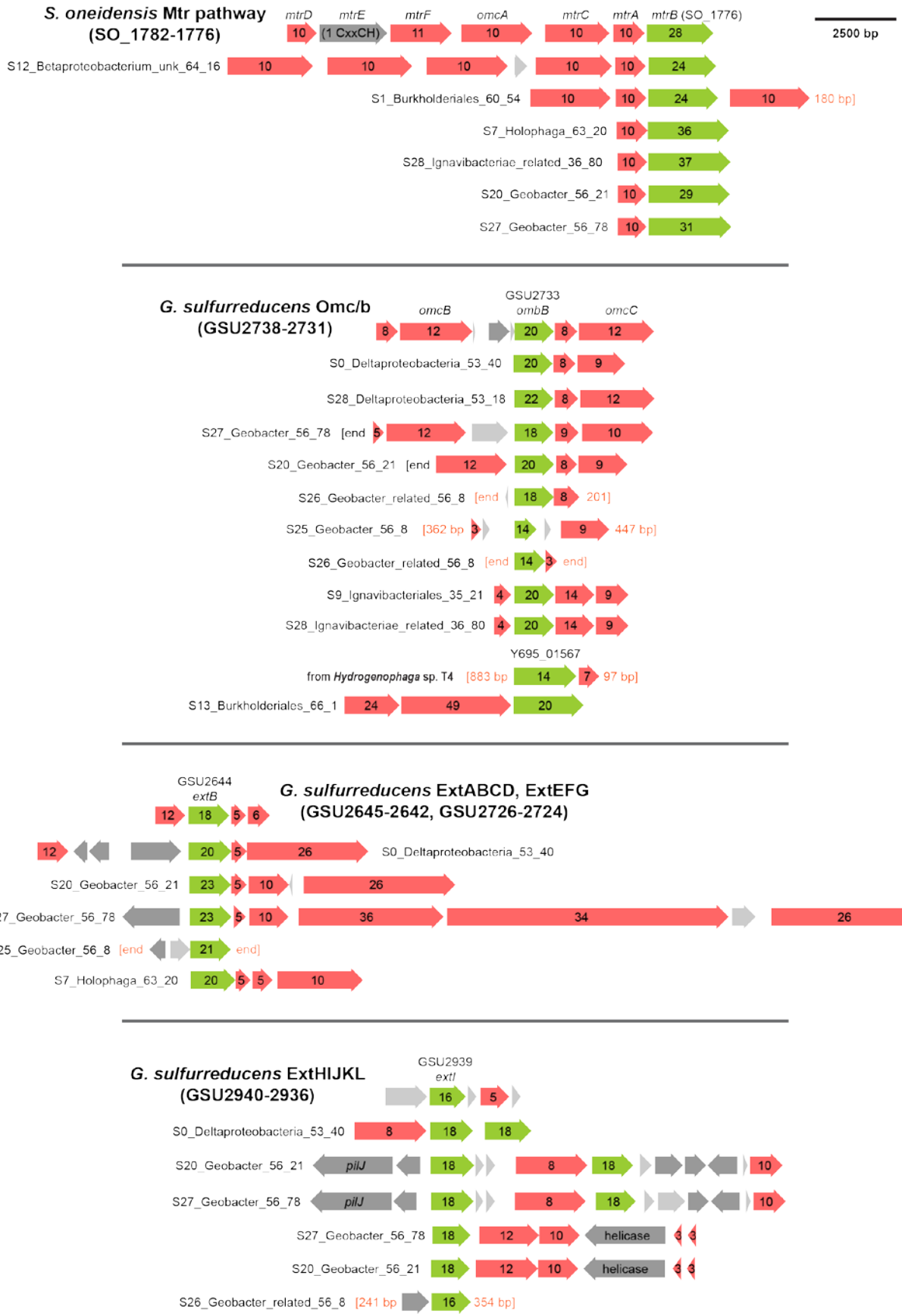
S. oneidensis Mtr pathway
(SO_1782-1776)
mtrD
mtrE
mtrF
omcA
mtrC
mtrA
mtrB (SO_1776)
2500 bp
S12_Betaproteobacterium_unk_64_16
S1_Burkholderiales_60_54
S7_Holophaga_63_20
S28_Ignavibacteriae_related_36_80
S20_Geobacter_56_21
S27_Geobacter_56_78
G. sulfurreducens Omc/b
(GSU2738-2731)
omcB
GSU2733
ombB
omcC
S0_Deltaproteobacteria_53_40
S28_Deltaproteobacteria_53_18
S27_Geobacter_56_78 [end
S20_Geobacter_56_21 [end
S26_Geobacter_related_56_8 [end
S25_Geobacter_56_8 [362 bp
S26_Geobacter_related_56_8 [end
S9_Ignavibacteriales_35_21
S28_Ignavibacteriae_related_36_80
Y695_01567
from Hydrogenophaga sp. T4 [883 bp
S13_Burkholderiales_66_1
GSU2644
extB
G. sulfurreducens ExtABCD, ExtEFG
(GSU2645-2642, GSU2726-2724)
S0_Deltaproteobacteria_53_40
S20_Geobacter_56_21
S27_Geobacter_56_78
S25_Geobacter_56_8 [end
S7_Holophaga_63_20
G. sulfurreducens ExtHIJKL
(GSU2940-2936)
GSU2939
extI
S0_Deltaproteobacteria_53_40
S20_Geobacter_56_21
S27_Geobacter_56_78
S27_Geobacter_56_78
S20_Geobacter_56_21
S26_Geobacter_related_56_8 [241 bp
pilJ
helicase

Figure 3.4 (*previous page*) – Porin-cytochrome gene clusters from MXC and reference genomes. The loci in some genomes show similarity to the locus in *Shewanella oneidensis* whereas others share gene content and gene order with one or more of the loci in *Geobacter sulfurreducens*. Green arrows represent porin proteins (the number indicates the predicted number of transmembrane domains), red arrows indicate multiheme *c*-type cytochromes (the numbers indicate the number of heme-binding motifs), dark grey arrows indicate other genes (*pilJ* is a pilus gene) and light grey arrows indicate proteins with no predicted function.

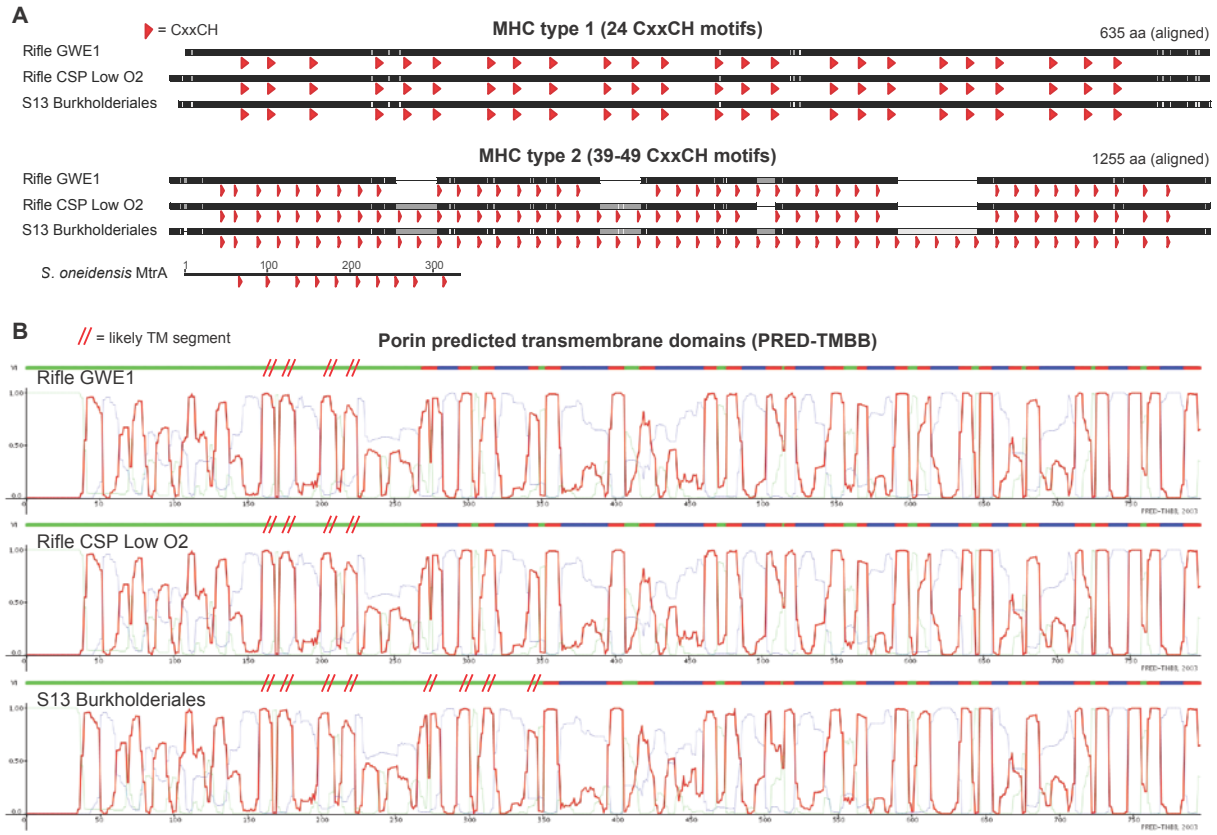

Figure 3.5 – Comparison of homologous MHC and porin protein sequences from three closely related Burkholderiales genomes. (**A**) Protein alignments of MHCs showing heme-binding motifs as red arrowheads emphasize the dense packing of hemes and the variability in number of heme-binding motifs for the larger proteins. MtrA from *Shewanella oneidensis* MR-1 is shown using the same horizontal scale as the larger MHCs. (**B**) Despite having highly similar porin sequences between the S13 and Rifle Burkholderiales genomes (97.6 and 97.7%), PRED-TMBB (default parameters) predicts 20 vs. 24 transmembrane domains (red regions at the top of each plot). This is likely not accurate, as the probability profiles in each plot are very similar. The red parallel hashes have been added to indicate further likely transmembrane regions, yielding the same number and locations for all three porins. Light green and blue traces related to predicted cytoplasmic or non-cytoplasmic localization

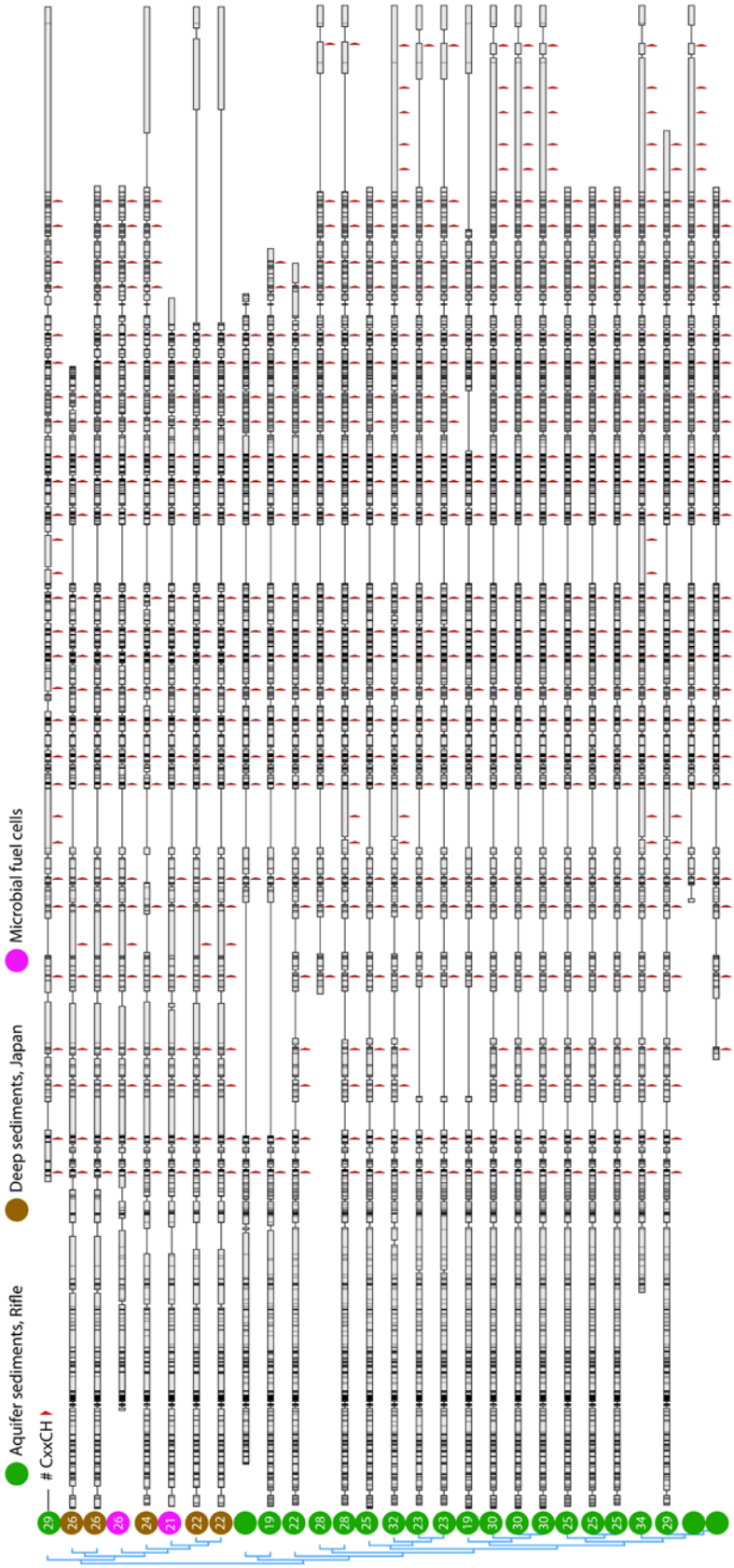
Aquifer sediments, Rifle
Deep sediments, Japan
Microbial fuel cells
CxxCH

Figure 3.6 (*previous page*) – Protein alignment of large multiheme cytochromes found in closely related Chloroflexi genomes. The most closely related MHCs to those from the MXC Anaerolineales genomes (magenta circles) were from organisms found in deep borehole sediments from Japan (brown circles) and next from Rifle sediment (green circles). As in **Figure 3.5**, the positions of heme-binding motifs are flagged with red arrowheads. The total number of motifs for each sequence is listed within each circle at left. There are few cases where the most closely related sequences differ by just a single heme, which may indicate that CxxCH motifs are more likely gained or lost in pairs or multiples during single evolutionary events.

						Rifle sample type					
Genomes with >96% rpS3 ID to Rifle organism (>98% highlighted)	**Course Taxonomy**	**No. MHCs (≥ 3 motifs)**	**Rel. abun., MXC-1 biofilm**	**Rel. abun., MXC-1 plank**	**Rel. abun., MXC-1.1 plank**	**Acetate GW**	**Sediment Ac**	**Sediment**	**LowO2 Gw**	**HighO2 GW**	**O2 GW**
S0_Deltaproteobacteria_53_40	Deltaproteobacteria	72.0	947.011	0.952	0.722	X	X	X			
S9_GWE2_Bacteroidetes_39_201	Bacteroidetes	2.0	95.477	257.577	156.658	X					X
S27_Geobacter_56_78	Deltaproteobacteria	81.0	34.479	0.996	0.854	X	X	X			
S28_Ignavibacteria_36_39	Ignavibacteria	18.0	28.559	0.146	0.017			X			
S28_Deltaproteobacteria_53_18	Deltaproteobacteria	16.0	9.111	0.118	0.092	X	X	X			
S8_BJP_Bacteroidetes_42_90	Bacteroidetes	2.0	7.730	1.151	10.350	X					X
S25_Geobacter_56_8	Deltaproteobacteria	60.0	6.259	0.168	0.630	X	X	X			
S28_Spirochaetales_RIFOXYC1-rel_55_9	Spirochaetes	1.0	5.022	0.576	0.491	X					X
S21_Pseudomonas_stutzeri_64_159	Gammaproteobacteria	5.0	2.182	19.645	2.215	X	X			X	
S21_Pseudomonas_stutzeri_64_159	Gammaproteobacteria	5.0	2.182	19.645	2.215	X	X		X	X	
S9_Dechloromonas_62_369	Betaproteobacteria	3.0	2.023	152.030	1.943		X	X	X	X	
S0_BJP_Bacteroidetes_41_186	Bacteroidetes	2.0	2.005	81.902	456.276	X					X
S14_CG_Desulfovibrio-related_65_8	Deltaproteobacteria	10.0	1.466	1.839	0.035	X					
S7_Burkholderiales_unk_64_14	Betaproteobacteria	2.0	0.747	5.103	9.793	X			X	X	
S15_Burkholderiales_59_53	Betaproteobacteria		0.558	11.232	4.681	X			X	X	
S13_Burkholderiales_66_15	Betaproteobacteria	6.0	0.468	22.914	0.409	X			X	X	X
S1_Burkholderiales_60_54	Betaproteobacteria	11.0	0.399	0.568	8.351	X	X			X	X
S13_RIFCSPLOWO2_Burkholderiales_64_153	Betaproteobacteria		0.307	47.199	0.724		X		X		
S18_Spirochatetes_52_9	Spirochaetes		0.287	0.145	0.852	X	X				X
S13_BJP_Anaerolineales_41_7	Chloroflexi	14.0	0.279	1.283	0.060	X					
S3_Spirochaetes_52_8	Spirochaetes		0.270	0.174	0.982	X	X		X		X
S20_Geobacter_56_21	Deltaproteobacteria	80.0	0.248	0.470	2.536	X	X	X			
S12_Betaproteobacterium_unk_64_16	Betaproteobacteria	17.0	0.244	4.431	0.103			X	X		
S12_GWC2_Bacteroidetes_47_42	Bacteroidetes	3.0	0.223	9.802	12.842	X					
S5_GWC2_Bacteroidetes-rel_44_7	Bacteroidetes	1.0	0.201	4.746	13.700	X					X
S21_RIFCSPLOWO2_Burkholderiales-rel_65_185	Betaproteobacteria	2.0	0.188	0.757	3.975	X			X	X	
S11_BJP_Anaerolineales_41_7	Chloroflexi	14.0	0.185	1.018	0.006	X					
S23_Comamonadaceae_63_35	Betaproteobacteria		0.143	1.351	2.915	X	X		X		
S4_Pseudomonas_61_25 (*rpS3 scaff2*)	Gammaproteobacteria	3.0	0.047	0.141	9.508	X	X		X	X	
S13_Firmicutes_novel_41_11	Firmicutes		0.038	8.593	0.288		X				
S15_Pseudomonas_62_25	Gammaproteobacteria	2.0	0.023	0.041	6.983				X		
S15_Pseudomonas_62_25	Gammaproteobacteria	2.0	0.023	0.041	6.983	X	X		X	X	
S24_Desulfosporosinus_43_10	Firmicutes	11.0	0.022	0.006	0.838		X				X
S22_Parvibaculum_lavamentivorans_63_78	Alphaproteobacteria		0.014	0.165	3.035				X	X	
S18_Pseudomonas_mendocina_63_22	Gammaproteobacteria	1.0	0.009	0.069	2.058	X	X		X	X	
S16_Stenotrophomonas_66_10	Gammaproteobacteria	2.0	0.009	0.190	1.079			X	X		
S15_Geothrix_rel_68_9	Acidobacteria	12.0	0.006	0.098	0.701		X				
S13_Deltaproteobacteria_67_8	Deltaproteobacteria	9.0	0.006	1.387	0.106	X					
					Totals:	**28**	**19**	**9**	**16**	**12**	**10**

Table 3.3 (*previous page*) – Genomes from MXC-1 and MXC-1.1 that are very closely related to genomes recovered from the Rifle, Colorado sediment and groundwater metagenomes. Genomes are listed if their ribosomal protein S3 (rpS3) sequence shared ≥ 96% rpS3 amino acid identity (ID) with a sequence from a genome assembled from the Rifle-site metagenomes (the site from which MXC-1 was inoculated), and are sorted by abundance in the biofilm. An "X" indicates that an MXC genome is represented in that Rifle metagenomic sample. Green shaded boxes indicate that the rpS3 protein sequences shared at least 98% identity with the corresponding Rifle genome. Included are 38 of the total 86 MXC genomes. The number of multiheme *c*-type cytochromes present in each MXC genome is show, as well as and their average relative abundance (Rel. abun.) in MXC-1 biofilm or planktonic (plank.) and MXC-1.1 samples. Rifle metagenomes were obtained from acetate (Ac)-stimulated sediment and groundwater (GW) and from groundwater with naturally low (LowO2 GW) and high (HighO2 GW) oxygen concentrations and from an oxygen injection experiment (O2 GW). The total number of MXC genomes found in each sample type is shown below each column.

REFERENCES

Aelterman, P. et al., 2008. The anode potential regulates bacterial activity in microbial fuel cells. *Applied Microbiology and Biotechnology*, 78(3), pp.409–18.

Altschul, S.F. et al., 1990. Basic local alignment search tool. *Journal of Molecular Biology*, 215(3), pp.403–410.

Anantharaman, K. et al., 2016. Thousands of microbial genomes shed light on interconnected biogeochemical processes in an aquifer system. *Nature Communications*, 7, p.13219.

Anderson, R.T. et al., 2003. Stimulating the In Situ Activity of Geobacter Species To Remove Uranium from the Groundwater of a Uranium-Contaminated Aquifer. *Applied and Environmental Microbiology*, 69(10), pp.5884–5891.

Baek, G. et al., 2016. Bioaugmentation of anaerobic sludge digestion with iron-reducing bacteria: process and microbial responses to variations in hydraulic retention time. *Applied Microbiology and Biotechnology*, 100(2), pp.927–937.

Bard, A.J. & Faulkner, L.R., 2001. *Electrochemical methods: fundamentals and applications* 2nd ed., Wiley New York.

Beliaev, A.S. & Saffarini, D.A., 1998. Shewanella putrefaciens mtrB Encodes an Outer Membrane Protein Required for Fe(III) and Mn(IV) Reduction. *Journal of Bacteriology*, 180(23), pp.6292–6297.

Bennetto, H.P., 1984. Microbial Fuel Cells. *Life Chemistry Reports*, 2(4), pp.363–453.

Beyenal, H. & Babauta, J.T., 2012. Microscale gradients and their role in electron-transfer mechanisms in biofilms. *Biochemical Society Transactions*, 40(6), pp.1315–8.

Bianchi, T.S., 2011. The role of terrestrially derived organic carbon in the coastal ocean: A changing paradigm and the priming effect. *Proceedings of the National Academy of Sciences*, 108(49), pp.19473–19481.

Bodemer, G.J. et al., 2010. The effect of detergents and lipids on the properties of the outer-membrane protein OmcA from Shewanella oneidensis. *Journal of Biological Inorganic Chemistry*, 15, pp.749–58.

Bonanni, P.S., Schrott, G.D., Robuschi, L., et al., 2012. Charge accumulation and electron transfer kinetics in Geobacter sulfurreducens biofilms. *Energy & Environmental Science*, 5, pp.6188–95.

Bonanni, P.S., Schrott, G.D. & Busalmen, J.P., 2012. A long way to the electrode: how do Geobacter cells transport their electrons? *Biochemical Society Transactions*, 40(6), pp.1274–9.

Bond, D.R. et al., 2002. Electrode-reducing microorganisms that harvest energy from marine sediments. *Science* , 295(5554), pp.483–5.

Bond, D.R., 2010. Electrodes as electron acceptors, and the bacteria who love them. In M. Mandl & A. Loy, eds. *Geomicrobiology: Molecular and Environmental Perspectives*. Springer.

Bond, D.R. & Lovley, D.R., 2003. Electricity Production by Geobacter sulfurreducens Attached to Electrodes. *Applied and Environmental Microbiology*, 69(3), pp.1548–1555.

Bonneville, S., Behrends, T. & Van Cappellen, P., 2009. Solubility and dissimilatory reduction kinetics of iron(III) oxyhydroxides: A linear free energy relationship. *Geochimica et Cosmochimica Acta*, 73(18), pp.5273–5282.

Bonneville, S., Van Cappellen, P. & Behrends, T., 2004. Microbial reduction of iron(III) oxyhydroxides: effects of mineral solubility and availability. *Chemical Geology*, 212(3–4),

pp.255–268.
Bouhenni, R.A. et al., 2010. The Role of Shewanella oneidensis MR-1 Outer Surface Structures in Extracellular Electron Transfer. *Electroanalysis*, 22(7–8), pp.856–864.
Bradford, M.M., 1976. A rapid and sensitive method for the quantitation of microgram quantities of protein utilizing the principle of protein-dye binding. *Analytical Biochemistry*, 72(1–2), pp.248–254.
Bretschger, O. et al., 2007. Current Production and Metal Oxide Reduction by Shewanella oneidensis MR-1 Wild Type and Mutants . *Applied and Environmental Microbiology*, 73(21), pp.7003–7012.
Bretschger, O. et al., 2015. Functional and taxonomic dynamics of an electricity-consuming methane-producing microbial community. *Bioresource Technology*, 195, pp.254–264.
Breuer, M., Rosso, K.M. & Blumberger, J., 2014. Electron flow in multiheme bacterial cytochromes is a balancing act between heme electronic interaction and redox potentials. *PNAS*, 111(2), pp.611–616.
Bridge, T.A.M. & Johnson, D.B., 1998. Reduction of soluble iron and reductive dissolution of ferric iron- containing minerals by moderately thermophilic iron-oxidizing bacteria. *Applied and Environmental Microbiology*, 64(6), pp.2181–2186.
Brown, C.T. et al., 2015. Unusual biology across a group comprising more than 15% of domain Bacteria. *Nature*, 523(7559), pp.208–211.
Bücking, C. et al., 2010. Involvement and specificity of Shewanella oneidensis outer membrane cytochromes in the reduction of soluble and solid-phase terminal electron acceptors. *FEMS Microbiology Letters*, 306(2), pp.144–151.
Bücking, C., Schicklberger, M. & Gescher, J., 2012. The Biochemistry of Dissimilatory Ferric Iron and Manganese Reduction in Shewanella oneidensis. In J. Gescher & A. Kappler, eds. *Microbial Metal Respiration*. Berlin, Heidelberg: Springer Berlin Heidelberg, pp. 49–82.
Busalmen, J.P. et al., 2010. ATR-SEIRAs characterization of surface redox processes in G. sulfurreducens. *Bioelectrochemistry*, 78, pp.25–29.
Busalmen, J.P. et al., 2008. C-Type Cytochromes Wire Electricity-Producing Bacteria to Electrodes. *Angewandte Chemie*, 120(26), pp.4952–4955.
Butler, J.E., Kaufmann, F. & Coppi, M., 2004. MacA , a Diheme c-Type Cytochrome Involved in Fe (III) Reduction by Geobacter sulfurreducens. *Journal of Bacteriology*, 186(12), pp.4042–4045.
Butler, J.E., Young, N.D. & Lovley, D.R., 2010. Evolution of electron transfer out of the cell: comparative genomics of six Geobacter genomes. *BMC Genomics*, 11(Iii), p.40.
Cabezas, A. et al., 2015. Geobacter, Anaeromyxobacter and Anaerolineae populations are enriched on anodes of root exudate-driven microbial fuel cells in rice field soil. *Environmental Microbiology Reports*, 7(3), pp.489–497.
von Canstein, H. et al., 2008. Secretion of flavins by Shewanella species and their role in extracellular electron transfer. *Applied and Environmental Microbiology*, 74(3), pp.615–23.
Chae, K.-J. et al., 2009. Effect of different substrates on the performance, bacterial diversity, and bacterial viability in microbial fuel cells. *Bioresource Technology*, 100, pp.3518–25.
Chan, C.H. et al., 2016. *Genome scale mutational analysis of Geobacter sulfurreducens reveals distinct molecular mechanisms for respiration of poised electrodes vs. Fe(III) oxides*,
Chaudhuri, S.K. & Lovley, D.R., 2003. Electricity generation by direct oxidation of glucose in mediatorless microbial fuel cells. *Nature Biotechnology*, 21(10), pp.1229–32.
Chung, K.W. et al., 2005. Novel Synthesis of Nanosized Cellular Iron Oxide/Oxyhydroxide Thin

Films. *Journal of The Electrochemical Society*, 152(8), p.C560.
Clarke, T.A. et al., 2011. Structure of a bacterial cell surface decaheme electron conduit. *Proceedings of the National Academy of Sciences*, 108(23), pp.9384–9389.
Coates, J.D. et al., 2001. Geobacter hydrogenophilus, Geobacter chapellei and Geobacter grbiciae, three new, strictly anaerobic, dissimilatory Fe(III)-reducers. *International Journal of Systematic and Evolutionary Microbiology*, 51, pp.581–588.
Commault, A.S. et al., 2013. Influence of anode potentials on selection of Geobacter strains in microbial electrolysis cells. *Bioresource Technology*, 139, pp.226–234.
Commault, A.S., Lear, G. & Weld, R.J., 2014. Comment on Microbial Community Composition Is Unaffected by Anode Potential. *Environmental Science & Technology*.
Cornell, R.M. & Schwertmann, U., 2003. *The Iron Oxides: Structure, Properties, Reactions, Occurences and Uses* 2nd ed., Weinheim, FRG: Wiley-VCH Verlag GmbH & Co. KGaA.
Coursolle, D. et al., 2010. The Mtr respiratory pathway is essential for reducing flavins and electrodes in Shewanella oneidensis. *Journal of Bacteriology*, 192(2), pp.467–74.
Croese, E. et al., 2011. Analysis of the microbial community of the biocathode of a hydrogen-producing microbial electrolysis cell. *Applied Microbiology and Biotechnology*, 92(5), pp.1083–1093.
Delcher, A.L. et al., 2002. Fast algorithms for large-scale genome alignment and comparison. *Nucleic Acids Research*, 30(11), pp.2478–2483.
DiChristina, T.J. et al., 1988. Dissimilative Iron Reduction by the Marine Eubacterium Alteromonas putrefaciens Strain 200. *Water Science & Technology*, 20(11/12), pp.69–79.
Ding, Y.-H.R. et al., 2008. Proteome of Geobacter sulfurreducens grown with Fe(III) oxide or Fe(III) citrate as the electron acceptor. *Biochimica et Biophysica Acta*, 1784(12), pp.1935–41.
Disalvo, E.A. & Videla, H.A., 1979. 266 - Relation between biological parameters and the bioelectrochemical fuel-cell response. *Bioelectrochemistry and Bioenergetics*, 6(2), pp.185–195.
Eddy, S.R., 2011. Accelerated Profile HMM Searches W. R. Pearson, ed. *PLoS Computational Biology*, 7(10), p.e1002195.
Edgar, R.C., 2004. MUSCLE: multiple sequence alignment with high accuracy and high throughput. *Nucleic Acids Research*, 32(5), pp.1792–1797.
Edgar, R.C., 2010. Search and clustering orders of magnitude faster than BLAST. *Bioinformatics*, 26(19), pp.2460–2461.
Edgar, R.C. et al., 2011. UCHIME improves sensitivity and speed of chimera detection. *Bioinformatics*, 27(16), pp.2194–2200.
Edwards, M.J. et al., 2015. Redox Linked Flavin Sites in Extracellular Decaheme Proteins Involved in Microbe-Mineral Electron Transfer. *Scientific Reports*, 5(July), p.11677.
Esteve-Núñez, A. et al., 2008. Fluorescent properties of c-type cytochromes reveal their potential role as an extracytoplasmic electron sink in Geobacter sulfurreducens. *Environmental Microbiology*, 10(2), pp.497–505.
Finneran, K.T., 2003. Rhodoferax ferrireducens sp. nov., a psychrotolerant, facultatively anaerobic bacterium that oxidizes acetate with the reduction of Fe(III). *International Journal of Systematic and Evolutionary Microbiology*, 53(3), pp.669–673.
Firer-Sherwood, M.A., Pulcu, G.S. & Elliott, S.J., 2008. Electrochemical interrogations of the Mtr cytochromes from Shewanella: opening a potential window. *Journal of Biological Inorganic Chemistry*, 13(6), pp.849–54.

Fortney, N.W. et al., 2016. Microbial Fe(III) oxide reduction potential in Chocolate Pots hot spring, Yellowstone National Park. *Geobiology*, 14(3), pp.255–275.
Franks, A.E. et al., 2009. Novel strategy for three-dimensional real-time imaging of microbial fuel cell communities: monitoring the inhibitory effects of proton accumulation within the anode biofilm. *Energy & Environmental Science*, 2(1), p.113.
Fricke, K., Harnisch, F. & Schröder, U., 2008. On the use of cyclic voltammetry for the study of anodic electron transfer in microbial fuel cells. *Energy & Environmental Science*, 1(1), p.144.
Grabovich, M. et al., 2006. Proposal of Giesbergeria voronezhensis gen. nov., sp. nov. and G. kuznetsovii sp. nov. and reclassification of [Aquaspirillum] anulus, [A.] sinuosum and [A.] giesbergeri as Giesbergeria anulus comb. nov., G. sinuosa comb. nov. and G. giesbergeri comb. nov. *International journal of systematic and evolutionary microbiology*, 56(Pt 3), pp.569–76.
Gregory, K. & Holmes, D.E., 2011. MICROBIAL RESPIRATION OF ANODES AND CATHODES IN ELECTROCHEMICAL CELLS. In J. F. Stolz & R. S. Oremland, eds. *Microbial Metal and Metalloid Metabolism: Advances and Applications*. Washington, D.C.: ASM Press.
Ha, P.T. et al., 2012. Treatment of alcohol distillery wastewater using a Bacteroidetes-dominant thermophilic microbial fuel cell. *Environmental Science & Technology*, 46(5), pp.3022–30.
Handley, K.M. et al., 2013. Biostimulation induces syntrophic interactions that impact C, S and N cycling in a sediment microbial community. *The ISME Journal*, 7(4), pp.800–16.
Harel, A. et al., 2014. Evolutionary history of redox metal-binding domains across the tree of life. *Proceedings of the National Academy of Sciences*, 111(19), pp.7042–7.
Harnisch, F. & Freguia, S., 2012. A basic tutorial on cyclic voltammetry for the investigation of electroactive microbial biofilms. *Chemistry, an Asian journal*, 7(3), pp.466–75.
Hartshorne, R.S. et al., 2009. Characterization of an electron conduit between bacteria and the extracellular environment. *Proceedings of the National Academy of Sciences*, 106(52), pp.22169–74.
Hartshorne, R.S. et al., 2007. Characterization of Shewanella oneidensis MtrC: a cell-surface decaheme cytochrome involved in respiratory electron transport to extracellular electron acceptors. *Journal of Biological Inorganic Chemistry*, 12(7), pp.1083–94.
Heidelberg, J.F. et al., 2002. Genome sequence of the dissimilatory metal ion-reducing bacterium Shewanella oneidensis. *Nature Biotechnology*, 20(11), pp.1118–1123.
Heidelberg, J.F. et al., 2004. The genome sequence of the anaerobic, sulfate-reducing bacterium Desulfovibrio vulgaris Hildenborough. *Nature Biotechnology*, 22(5), pp.554–9.
Hernsdorf, A.W. et al., 2017. Potential for microbial H2 and metal transformations associated with novel bacteria and archaea in deep terrestrial subsurface sediments. *The ISME Journal*, pp.1–15.
Holmes, D.E. et al., 2004. Microbial communities associated with electrodes harvesting electricity from a variety of aquatic sediments. *Microbial Ecology*, 48, pp.178–90.
Holmes, D.E. et al., 2007. Subsurface clade of Geobacteraceae that predominates in a diversity of Fe(III)-reducing subsurface environments. *The ISME Journal*, 1(8), pp.663–77.
Hori, T. et al., 2010. Identification of iron-reducing microorganisms in anoxic rice paddy soil by 13C-acetate probing. *The ISME Journal*, 4(2), pp.267–278.
Hori, T. et al., 2015. Isolation of microorganisms involved in reduction of crystalline iron(III) oxides in natural environments. *Frontiers in Microbiology*, 6(MAY), pp.1–16.

Hug, L.A. et al., 2016. A new view of the tree of life. *Nature Microbiology*, 1(5), p.16048.
Hug, L.A. et al., 2013. Community genomic analyses constrain the distribution of metabolic traits across the Chloroflexi phylum and indicate roles in sediment carbon cycling. *Microbiome*, 1(1), p.22.
Hyatt, D. et al., 2010. Prodigal: prokaryotic gene recognition and translation initiation site identification. *BMC Bioinformatics*, 11(1), p.119.
Inoue, K. et al., 2010. Purification and characterization of OmcZ, an outer-surface, octaheme c-type cytochrome essential for optimal current production by Geobacter sulfurreducens. *Applied and Environmental Microbiology*, 76(12), pp.3999–4007.
Ishii, S. et al., 2008. Characterization of a filamentous biofilm community established in a cellulose-fed microbial fuel cell. *BMC Microbiology*, 8(1), p.6.
Ishii, S. et al., 2014. Microbial population and functional dynamics associated with surface potential and carbon metabolism. *The ISME Journal*, 8(5), pp.963–978.
Islam, F.S. et al., 2004. Role of metal-reducing bacteria in arsenic release from Bengal delta sediments. *Nature*, 430(6995), pp.68–71.
Itoh, T. et al., 2011. Aciditerrimonas ferrireducens gen. nov., sp. nov., an iron-reducing thermoacidophilic actinobacterium isolated from a solfataric field. *International Journal of Systematic and Evolutionary Microbiology*, 61(6), pp.1281–1285.
Jangir, Y. et al., 2016. Isolation and Characterization of Electrochemically Active Subsurface Delftia and Azonexus Species. *Frontiers in Microbiology*, 7(MAY), pp.1–11.
Jung, S. & Regan, J.M., 2007. Comparison of anode bacterial communities and performance in microbial fuel cells with different electron donors. *Applied Microbiology and Biotechnology*, 77(2), pp.393–402.
Jung, S. & Regan, J.M., 2011. Influence of external resistance on electrogenesis, methanogenesis, and anode prokaryotic communities in microbial fuel cells. *Applied and Environmental Microbiology*, 77(2), pp.564–571.
Kan, J. et al., 2011. Current production by bacterial communities in microbial fuel cells enriched from wastewater sludge with different electron donors. *Environmental Science & Technology*, 45(3), pp.1139–46.
Kanehisa, M. et al., 2016. KEGG as a reference resource for gene and protein annotation. *Nucleic Acids Research*, 44(D1), pp.D457–D462.
Kashima, H. & Regan, J.M., 2015. Facultative Nitrate Reduction by Electrode-Respiring Geobacter metallireducens Biofilms as a Competitive Reaction to Electrode Reduction in a Bioelectrochemical System. *Environmental Science & Technology*, 49(5), pp.3195–3202.
Kato, S. et al., 2015. Potential for biogeochemical cycling of sulfur, iron and carbon within massive sulfide deposits below the seafloor. *Environmental Microbiology*, 17(5), pp.1817–1835.
Kato, S. et al., 2010. Respiratory interactions of soil bacteria with (semi)conductive iron-oxide minerals. *Environmental Microbiology*, 12(12), pp.3114–3123.
Katoh, K. & Standley, D.M., 2013. MAFFT Multiple Sequence Alignment Software Version 7: Improvements in Performance and Usability. *Molecular Biology and Evolution*, 30(4), pp.772–780.
Katuri, K.P. et al., 2010. Geobacter sulfurreducens biofilms developed under different growth conditions on glassy carbon electrodes: insights using cyclic voltammetry. *Chemical Communications*, 46(26), pp.4758–60.
Kawaichi, S. et al., 2013. Ardenticatena maritima gen. nov., sp. nov., a ferric iron- and nitrate-

reducing bacterium of the phylum “Chloroflexi” isolated from an iron-rich coastal hydrothermal field, and description of Ardenticatenia classis nov. *International Journal of Systematic Bacteriology and Evolutionary Microbiology*, 63, pp.2992–3002.
Kim, B.-C. et al., 2005. OmcF, a Putative c-Type Monoheme Outer Membrane Cytochrome Required for the Expression of Other Outer Membrane Cytochromes in Geobacter sulfurreducens. *Journal of Bacteriology*, 187(13), pp.4505–4513.
Kim, B.H. et al., 2004. Enrichment of microbial community generating electricity using a fuel-cell-type electrochemical cell. *Applied Microbiology and Biotechnology*, 63(6), pp.672–81.
Kim, J.D. et al., 2013. Anoxic photochemical oxidation of siderite generates molecular hydrogen and iron oxides. *Proceedings of the National Academy of Sciences*.
Kimura, H. et al., 2010. Microbial methane production in deep aquifer associated with the accretionary prism in Southwest Japan. *The ISME Journal*, 4(4), pp.531–541.
Klotz, M.G. et al., 2008. Evolution of an octahaem cytochrome c protein family that is key to aerobic and anaerobic ammonia oxidation by bacteria. *Environmental Microbiology*, 10(11), pp.3150–3163.
Konhauser, K., Newman, D. & Kappler, A., 2005. The potential significance of microbial Fe(III) reduction during deposition of Precambrian banded iron formations. *Geobiology*, 3, pp.167–177.
Kostka, J.E. & Green, S.J., 2011. Microorganisms and processes linked to uranium reduction and immobilization. In J. F. Stolz & R. S. Oremland, eds. *Microbial Metal and Metalloid Metabolism: Advances and Applications*. Washington, D.C.: ASM Press, pp. 117–138.
LaBelle, E. & Bond, D.R., 2009. Cyclic voltammetry for the study of microbial electron transfer at electrodes. In D. I. P. L. (Ed), ed. *Bio-electrochemical Systems: from extracellular electron transfer to biotechnological application*. Wageningen University, The Netherlands.
Lalonde, S. V & Konhauser, K.O., 2015. Benthic perspective on Earth’s oldest evidence for oxygenic photosynthesis. *Proceedings of the National Academy of Sciences*, 112(4), pp.995–1000.
Langmead, B. & Salzberg, S.L., 2012. Fast gapped-read alignment with Bowtie 2. *Nat Meth*, 9(4), pp.357–359.
Langmuir, D. & Whittemore, D.O., 1971. Variations in the Stability of Precipitated Ferric Oxyhydroxides. In *Nonequilibrium Systems in Natural Water Chemistry*. Advances in Chemistry. American Chemical Society, pp. 209–234.
Laviron, E., 1979. The use of linear potential sweep voltammetry and of a.c. voltammetry for the study of the surface electrochemical reaction of strongly adsorbed systems and of redox modified electrodes. *Journal of Electroanalytical Chemistry and Interfacial Electrochemistry*, 100(1–2), pp.263–270.
Laviron, E. & Roullier, L., 1980. General expression of the linear potential sweep voltammogram for a surface redox reaction with interactions between the adsorbed molecules. *Journal of Electroanalytical Chemistry and Interfacial Electrochemistry*, 115(1), pp.65–74.
Leang, C., Coppi, M. V & Lovley, D.R., 2003. OmcB, a c-Type Polyheme Cytochrome Involved in Fe (III) Reduction in Geobacter sulfurreducens. *Journal of Bacteriology*, 185(7), pp.2096–2103.
Lee, J. et al., 2003. Use of acetate for enrichment of electrochemically active microorganisms and their 16S rDNA analyses. *FEMS Microbiology Letters*, 223, pp.185–191.
Lentini, C.J., Wankel, S.D. & Hansel, C.M., 2012. Enriched Iron(III)-Reducing Bacterial

Communities are Shaped by Carbon Substrate and Iron Oxide Mineralogy. *Frontiers in Microbiology*, 3(DEC), pp.1–19.
Levar, C.E. et al., 2014. An Inner Membrane Cytochrome Required Only for Reduction of High Redox Potential Extracellular Electron Acceptors. *mBio*, 5(6), pp.e02034-14.
Levar, C.E. et al., 2017. Redox potential as a master variable controlling pathways of metal reduction by Geobacter sulfurreducens. *The ISME Journal*, 11(3), pp.741–752.
Levar, C.E., Rollefson, J.B. & Bond, D.R., 2012. Energetic and Molecular Constraints on the Mechanism of Environmental Fe(III) Reduction by Geobacter. In J. Gescher & A. Kappler, eds. *Microbial Metal Respiration*. Berlin, Heidelberg: Springer Berlin Heidelberg, pp. 29–48.
Liu, Y. et al., 2014. A trans-outer membrane porin-cytochrome protein complex for extracellular electron transfer by Geobacter sulfurreducens PCA. *Environmental Microbiology Reports*, 6(6), pp.776–785.
Liu, Y. et al., 2011. Linking spectral and electrochemical analysis to monitor c-type cytochrome redox status in living geobacter sulfurreducens biofilms. *ChemPhysChem*, 12(12), pp.2235–2241.
Lloyd, J.R. et al., 2003. Biochemical and genetic characterization of PpcA, a periplasmic c-type cytochrome in Geobacter sulfurreducens. *The Biochemical Journal*, 369(Pt 1), pp.153–61.
Logan, B.E. et al., 2006. Microbial Fuel Cells: Methodology and Technology. *Environmental Science & Technology*, 40(17), pp.5181–5192.
Logan, B.E. & Rabaey, K., 2012. Conversion of Wastes into Bioelectricity and Chemicals by Using Microbial Electrochemical Technologies. *Science* , 337(6095), pp.686–690.
Lovley, D.R., 1991. Dissimilatory Fe(III) and Mn(IV) reduction. *Microbiol. Mol. Biol. Rev.*, 55(2), pp.259–287.
Lovley, D.R. et al., 2011. Geobacter: the microbe electric's physiology, ecology, and practical applications. *Advances in Microbial Physiology*, 59, pp.1–100.
Lovley, D.R., 2011. Live wires: direct extracellular electron exchange for bioenergy and the bioremediation of energy-related contamination. *Energy & Environmental Science*.
Lovley, D.R. et al., 1991. Microbial reduction of uranium. *Nature*, 350, pp.413–416.
Lovley, D.R., Holmes, D.E. & Nevin, K.P., 2004. *Dissimilatory Fe(III) and Mn(IV) reduction*,
Lovley, D.R. & Phillips, E., 1988. Novel Mode of Microbial Energy Metabolism: Organic Carbon Oxidation Coupled to Dissimilatory Reduction of Iron or Manganese. *Applied and Environmental Microbiology*, 54(6), pp.1472–1480.
Lowe, T.M. & Eddy, S.R., 1997. tRNAscan-SE: a program for improved detection of transfer RNA genes in genomic sequence. *Nucleic Acids Research*, 25(5), pp.955–964.
Mahadevan, R. et al., 2006. Characterization of Metabolism in the Fe(III)-Reducing Organism Geobacter sulfurreducens by Constraint-Based Modeling. *Applied and Environmental Microbiology*, 72(2), pp.1558–1568.
Majzlan, J., 2012. Minerals and Aqueous Species of Iron and Manganese as Reactants and Products of Microbial Metal Respiration. In J. Gescher & A. Kappler, eds. *Microbial Metal Respiration*. Springer Berlin Heidelberg, pp. 1–28.
Malvankar, N.S., Lau, J., et al., 2012. Electrical Conductivity in a Mixed-Species Biofilm. *Applied and Environmental Microbiology*, 78(16), pp.5967–71.
Malvankar, N.S., Mester, T., et al., 2012. Supercapacitors Based on c-Type Cytochromes Using Conductive Nanostructured Networks of Living Bacteria. *ChemPhysChem*, 13(2), pp.463–468.

Malvankar, N.S. & Lovley, D.R., 2012. Microbial nanowires: a new paradigm for biological electron transfer and bioelectronics. *ChemSusChem*, 5(6), pp.1039–46.
Manzella, M.P., Reguera, G. & Kashefi, K., 2013. Extracellular electron transfer to Fe(III) oxides by the hyperthermophilic archaeon Geoglobus ahangari via a direct contact mechanism. *Applied and Environmental Microbiology*, 79(15), pp.4694–4700.
Marshall, C.W. & May, H.D., 2009. Electrochemical evidence of direct electrode reduction by a thermophilic Gram-positive bacterium, Thermincola ferriacetica. *Energy & Environmental Science*, 2(6), p.699.
Marsili, E., Rollefson, J.B., et al., 2008. Microbial biofilm voltammetry: direct electrochemical characterization of catalytic electrode-attached biofilms. *Applied and Environmental Microbiology*, 74(23), pp.7329–37.
Marsili, E., Baron, D.B., et al., 2008. Shewanella secretes flavins that mediate extracellular electron transfer. *Proceedings of the National Academy of Sciences*, 105(10), pp.3968–73.
Marsili, E., Sun, J. & Bond, D.R., 2010. Voltammetry and growth physiology of Geobacter sulfurreducens biofilms as a function of growth stage and imposed electrode potential. *Electroanalysis*, 22(7–8), pp.865–874.
McGlynn, S.E. et al., 2015. Single cell activity reveals direct electron transfer in methanotrophic consortia. *Nature*.
Mehta-Kolte, M.G. & Bond, D.R., 2012. Geothrix fermentans secretes two different redox active compounds to utilize electron acceptors across a wide potential window. *Applied and Environmental Microbiology*, 78(19), pp.6987–6995.
Methé, B.A. et al., 2009. Genome of Geobacter sulfurreducens : Metal Reduction in Subsurface Environments. *Science* , 1967(2003), pp.10–13.
Methé, B.A. et al., 2003. Genome of Geobacter sulfurreducens: metal reduction in subsurface environments. *Science* , 302(5652), pp.1967–9.
Miller, C.S. et al., 2011. EMIRGE: reconstruction of full-length ribosomal genes from microbial community short read sequencing data. *Genome Biology*, 12(5), p.R44.
Millo, D. et al., 2011. In situ spectroelectrochemical investigation of electrocatalytic microbial biofilms by surface-enhanced resonance raman spectroscopy. *Angewandte Chemie International Edition*, 50(11), pp.2625–2627.
Mitchell, A.C. et al., 2012. Role of outer membrane c-type cytochromes MtrC and OmcA in Shewanella oneidensis MR-1 cell production, accumulation, and detachment during respiration on hematite. *Geobiology*, 10(4), pp.355–70.
Moreno, C. et al., 1991. Simulation of the electrochemical behavior of multi-redox systems: Current potential studies on multiheme cytochromes. *European Journal of Biochemistry*, 202, pp.385–393.
Morgado, L. et al., 2010. Thermodynamic Characterization of a Triheme Cytochrome Family from Geobacter sulfurreducens Reveals Mechanistic and Functional Diversity. *Biophysical Journal*, 99, pp.293–301.
Myers, C.R. & Myers, J.M., 2003. Cell surface exposure of the outer membrane cytochromes of Shewanella oneidensis MR-1. *Letters in Applied Microbiology*, 37(3), pp.254–258.
Myers, C.R. & Myers, J.M., 1997. Cloning and sequence of cymA, a gene encoding a tetraheme cytochrome c required for reduction of iron(III), fumarate, and nitrate by Shewanella putrefaciens MR-1. *Journal of Bacteriology*, 179(4), pp.1143–1152.
Myers, C.R. & Nealson, K.H., 1988. Bacterial Manganese Reduction and Growth with Manganese Oxide as the Sole Electron Acceptor. *Science* , 240(4857), pp.1319–1321.

Myers, J.M. & Myers, C.R., 2001. Role for Outer Membrane Cytochromes OmcA and OmcB of Shewanella putrefaciens MR-1 in Reduction of Manganese Dioxide. *Applied and Environmental Microbiology*, 67(1), pp.260–269.

Navrotsky, A., Mazeina, L. & Majzlan, J., 2008. Size-driven structural and thermodynamic complexity in iron oxides. *Science* , 319(5870), pp.1635–8.

Nawrocki, E.P., 2009. *Structural RNA Homology Search and Alignment Using Covariance Models*. Washington University in St. Louis.

Nawrocki, E.P. & Eddy, S.R., 2013. Infernal 1.1: 100-fold faster RNA homology searches. *Bioinformatics*, 29(22), pp.2933–2935.

Nealson, K.H. & Little, B., 1997. Breathing Manganese and Iron: Solid-State Respiration. In *Advances in Applied Microbiology*. Academic Press, pp. 213–239.

Nealson, K.H. & Myers, C.R., 1990. Iron reduction by bacteria: a potential role in the genesis of banded iron formations. *American Journal of Science*, 290–A, pp.35–45.

Nevin, K.P. et al., 2010. Microbial Electrosynthesis: Feeding Microbes Electricity To Convert Carbon Dioxide and Water to Multicarbon Extracellular Organic Compounds. *mBio*, 1(2), pp.e00103–e00110.

Okamoto, A. et al., 2014. Bound Flavin Model Suggests Similar Electron-Transfer Mechanisms in Shewanella and Geobacter. *ChemElectroChem*, 1(11), pp.1808–1812.

Papa, S., Guerrieri, F. & Izzo, G., 1979. Redox bohr-effects in the cytochrome system of mitochondria. *FEBS Letters*, 105(2), pp.213–216.

Paquete, C.M. et al., 2014. Exploring the molecular mechanisms of electron shuttling across the microbe/metal space. *Frontiers in Microbiology*, 5(June).

Partin, C.A. et al., 2013. Uranium in iron formations and the rise of atmospheric oxygen. *Chemical Geology*, 362(0), pp.82–90.

Peng, Y. et al., 2012. IDBA-UD: a de novo assembler for single-cell and metagenomic sequencing data with highly uneven depth. *Bioinformatics*, 28(11), pp.1420–1428.

Podosokorskaya, O.A. et al., 2013. Characterization of Melioribacter roseus gen. nov., sp. nov., a novel facultatively anaerobic thermophilic cellulolytic bacterium from the class Ignavibacteria , and a proposal of a novel bacterial phylum I gnavibacteriae. *Environmental Microbiology*, 15(6), pp.1759–1771.

Potter, M., 1911. Electrical Effects Accompanying the Decomposition of Organic Compounds. *Proceedings of the Royal Society B*, 84(571), pp.260–276.

Qian, X. et al., 2011. Biochemical characterization of purified OmcS, a c-type cytochrome required for insoluble Fe(III) reduction in Geobacter sulfurreducens. *Biochimica et Biophysica Acta*, 1807(4), pp.404–412.

Raes, J. et al., 2007. Prediction of effective genome size in metagenomic samples. *Genome Biology*, 8(1), p.R10.

Reimers, C.E. et al., 2001. Harvesting energy from the marine sediment--water interface. *Environmental Science & Technology*, 35, pp.192–5.

Reinhold-Hurek, B. & Hurek, T., 2000. Reassessment of the taxonomic structure of the diazotrophic genus Azoarcus sensu lato and description of three new genera and new species, Azovibrio restrictus gen. nov., sp. nov., Azospira oryzae gen. nov., sp. nov. and Azonexus fungiphilus gen. nov., sp. *International journal of systematic and evolutionary microbiology*, 50 Pt 2, pp.649–59.

Reis, C. et al., 2002. Redox-Bohr effect in the nine haem cytochrome from Desulfovibrio desulfuricans 27774. *Inorganica Chimica Acta*, 339, pp.248–252.

Richter, H. et al., 2009. Cyclic voltammetry of biofilms of wild type and mutant Geobacter sulfurreducens on fuel cell anodes indicates possible roles of OmcB, OmcZ, type IV pili, and protons in extracellular electron transfer. *Energy & Environmental Science*, 2, p.506.
Rimboud, M. et al., 2015. Multi-system Nernst–Michaelis–Menten model applied to bioanodes formed from sewage sludge. *Bioresource Technology*.
Roden, E.E., 2006. Geochemical and microbiological controls on dissimilatory iron reduction. *Comptes Rendus Geoscience*, 338, pp.456–467.
Roden, E.E., 2012. Microbial iron-redox cycling in subsurface environments. *Biochemical Society Transactions*, 40(6), pp.1249–56.
Roden, E.E. & Zachara, J.M., 1996. Microbial Reduction of Crystalline Iron(III) Oxides: Influence of Oxide Surface Area and Potential for Cell Growth. *Environmental Science & Technology*, 30(5), pp.1618–1628.
Rotaru, A.-E. et al., 2014. Direct Interspecies Electron Transfer between Geobacter metallireducens and Methanosarcina barkeri. *Applied and Environmental Microbiology*, 80(15), pp.4599–4605.
Rotaru, A.-E. et al., 2012. Interspecies electron transfer via hydrogen and formate rather than direct electrical connections in cocultures of Pelobacter carbinolicus and Geobacter sulfurreducens. *Applied and Environmental Microbiology*, 78(21), pp.7645–7651.
Sacco, N.J., Bonetto, M.C. & Cortón, E., 2017. Isolation and Characterization of a Novel Electrogenic Bacterium, Dietzia sp. RNV-4 S. Yang, ed. *PLOS ONE*, 12(2), p.e0169955.
Santos, T.C. et al., 2015. Diving into the redox properties of Geobacter sulfurreducens cytochromes: a model for extracellular electron transfer. *Dalton Transactions*, 44(20), pp.9335–9344.
De Schamphelaire, L. et al., 2010. Microbial community analysis of anodes from sediment microbial fuel cells powered by rhizodeposits of living rice plants. *Applied and Environmental Microbiology*, 76(6), pp.2002–2008.
Schrott, G.D. et al., 2011. Electrochemical insight into the mechanism of electron transport in biofilms of Geobacter sulfurreducens. *Electrochimica Acta*, 56, pp.10791–10795.
Sharma, S., Cavallaro, G. & Rosato, A., 2010. A systematic investigation of multiheme c-type cytochromes in prokaryotes. *Journal of Biological Inorganic Chemistry*, 15, pp.559–571.
Shi, L. et al., 2016. Extracellular electron transfer mechanisms between microorganisms and minerals. *Nature Reviews Microbiology*, 14(10), pp.651–662.
Shi, L. et al., 2012. Mtr extracellular electron-transfer pathways in Fe(III)-reducing or Fe(II)-oxidizing bacteria: a genomic perspective. *Biochemical Society Transactions*, 40(6), pp.1261–1267.
Shi, L. et al., 2007. Respiration of metal (hydr)oxides by Shewanella and Geobacter: a key role for multihaem c-type cytochromes. *Molecular Microbiology*, 65(1), pp.12–20.
Shi, L. et al., 2009. The roles of outer membrane cytochromes of Shewanella and Geobacter in extracellular electron transfer. *Environmental Microbiology Reports*, 1(4), pp.220–227.
Shi, L., Fredrickson, J.K. & Zachara, J.M., 2014. Genomic analyses of bacterial porin-cytochrome gene clusters. *Frontiers in Microbiology*, 5(NOV), pp.1–10.
Snider, R.M. et al., 2012. Long-range electron transport in Geobacter sulfurreducens biofilms is redox gradient-driven. *Proceedings of the National Academy of Sciences*, 109(38), pp.15467–15472.
Srikanth, S. et al., 2008. Electrochemical characterization of Geobacter sulfurreducens cells immobilized on graphite paper electrodes. *Biotechnology and Bioengineering*, 99(5),

pp.1065–73.
Stamatakis, A., 2006. RAxML-VI-HPC: maximum likelihood-based phylogenetic analyses with thousands of taxa and mixed models. *Bioinformatics*, 22(21), pp.2688–2690.
Stamatakis, A., 2014. RAxML Version 8: A tool for Phylogenetic Analysis and Post-Analysis of Large Phylogenies. *Bioinformatics*.
Stevens, J.M. et al., 2004. C-type Cytochrome Formation: Chemical and Biological Enigmas. *Accounts of Chemical Research*, 37(12), pp.999–1007.
Straub, K.L. & Schink, B., 2004. Ferrihydrite-dependent growth of Sulfurospirillum deleyianum through electron transfer via sulfur cycling. *Applied and Environmental Microbiology*, 70(10), pp.5744–49.
Sturm, G. et al., 2012. Metal Reducers and Reduction Targets. A Short Survey About the Distribution of Dissimilatory Metal Reducers and the Multitude of Terminal Electron Acceptors. In J. Gescher & A. Kappler, eds. *Microbial Metal Respiration*. Berlin, Heidelberg: Springer Berlin Heidelberg, pp. 129–159.
Summers, Z.M. et al., 2010. Direct exchange of electrons within aggregates of an evolved syntrophic coculture of anaerobic bacteria. *Science* , 330(6009), pp.1413–5.
Suzek, B.E. et al., 2007. UniRef: comprehensive and non-redundant UniProt reference clusters. *Bioinformatics*, 23(10), pp.1282–1288.
Suzuki, Y. et al., 2003. Microbial Populations Stimulated for Hexavalent Uranium Reduction in Uranium Mine Sediment. *Applied and Environmental Microbiology*, 69(3), pp.1337–1346.
Tender, L.M. et al., 2002. Harnessing microbially generated power on the seafloor. *Nature Biotechnology*, 20, pp.821–5.
Thamdrup, B., 2000. Bacterial Manganese and Iron Reduction in Aquatic Sediments. In B. Schink, ed. *Advances in Microbial Ecology*. Advances in Microbial Ecology. Springer US, pp. 41–84.
Thomas, P.E., Ryan, D. & Levin, W., 1976. An improved staining procedure for the detection of the peroxidase activity of cytochrome P-450 on sodium dodecyl sulfate polyacrylamide gels. *Analytical Biochemistry*, 75(1), pp.168–176.
Thomas, S.H. et al., 2008. The mosaic genome of Anaeromyxobacter dehalogenans strain 2CP-C suggests an aerobic common ancestor to the delta-proteobacteria. *PloS ONE*, 3(5), p.e2103.
Tian, M. et al., 2015. The first metagenome of activated sludge from full-scale anaerobic/anoxic/oxic (A2O) nitrogen and phosphorus removal reactor using Illumina sequencing. *Journal of Environmental Sciences*, 35, pp.181–190.
Torres, C.I. et al., 2010. A kinetic perspective on extracellular electron transfer by anode-respiring bacteria. *FEMS Microbiology Reviews*, 34(1), pp.3–17.
Torres, C.I. et al., 2009. Selecting anode-respiring bacteria based on anode potential: phylogenetic, electrochemical, and microscopic characterization. *Environmental Science & Technology*, 43(24), pp.9519–24.
Torres, C.I., Kato Marcus, A. & Rittmann, B.E., 2008. Proton transport inside the biofilm limits electrical current generation by anode-respiring bacteria. *Biotechnology and Bioengineering*, 100(5), pp.872–81.
Valente, F.M. et al., 2001. A membrane-bound cytochrome c3: a type II cytochrome c3 from Desulfovibrio vulgaris Hildenborough. *ChemBioChem*, 2, pp.895–905.
Vargas, M. et al., 1998. Microbiological evidence for Fe(III) reduction on early Earth. *Nature*, 395(September), pp.65–67.
Virdis, B. et al., 2012. Non-invasive characterization of electrochemically active microbial

biofilms using confocal Raman microscopy. *Energy & Environmental Science*, pp.7017–7024.
Wagner, R.C., Call, D.F. & Logan, B.E., 2010. Optimal set anode potentials vary in bioelectrochemical systems. *Environmental Science & Technology*, 44(16), pp.6036–41.
Wang, X.J. et al., 2009. Phylogenetic diversity of dissimilatory ferric iron reducers in paddy soil of hunan, South China. *Journal of Soils and Sediments*, 9(6), pp.568–577.
Weber, K.A., Achenbach, L.A. & Coates, J.D., 2006. Microorganisms pumping iron: anaerobic microbial iron oxidation and reduction. *Nature Reviews Microbiology*, 4(10), pp.752–764.
Wei, J. et al., 2010. A new insight into potential regulation on growth and power generation of Geobacter sulfurreducens in microbial fuel cells based on energy viewpoint. *Environmental Science & Technology*, 44(8), pp.3187–91.
Weisburg, W.G. et al., 1991. 16S ribosomal DNA amplification for phylogenetic study. *Journal of Bacteriology*, 173(2), pp.697–703.
White, H.K. et al., 2009. Quantitative population dynamics of microbial communities in plankton-fed microbial fuel cells. *The ISME Journal*, 3(6), pp.635–46.
Williams, K.H. et al., 2011. Acetate Availability and its Influence on Sustainable Bioremediation of Uranium-Contaminated Groundwater. *Geomicrobiology Journal*, 28(5–6), pp.519–539.
Wingard, L.B., Shaw, C.H. & Castner, J.F., 1982. Bioelectrochemical fuel cells. *Enzyme and Microbial Technology*, 4(3), pp.137–142.
Wright, E.S., Yilmaz, L.S. & Noguera, D.R., 2012. DECIPHER, a Search-Based Approach to Chimera Identification for 16S rRNA Sequences. *Applied and Environmental Microbiology*, 78(3), pp.717–725.
Wrighton, K.C. et al., 2008. A novel ecological role of the Firmicutes identified in thermophilic microbial fuel cells. *The ISME Journal*, 2(11), pp.1146–56.
Wrighton, K.C., Engelbrektson, A.E., et al., 2011. ACCENTUATE THE POSITIVE: DISSIMILATORY IRON REDUCTION BY GRAM-POSITIVE BACTERIA. In J. F. Stolz & R. S. Oremland, eds. *Microbial Metal and Metalloid Metabolism: Advances and Applications*. Washington, D.C.: ASM Press, pp. 173–194.
Wrighton, K.C., Thrash, J.C., et al., 2011. Evidence for Direct Electron Transfer by a Gram-Positive Bacterium Isolated from a Microbial Fuel Cell. *Applied and Environmental Microbiology*, 77(21), pp.7633–7639.
Wrighton, K.C. et al., 2014. Metabolic interdependencies between phylogenetically novel fermenters and respiratory organisms in an unconfined aquifer. *The ISME Journal*, 8(7), pp.1452–1463.
Xing, D. et al., 2008. Electricity generation by Rhodopseudomonas palustris DX-1. *Environmental science & technology*, 42(11), pp.4146–51.
Yates, M.D. et al., 2012. Convergent development of anodic bacterial communities in microbial fuel cells. *The ISME Journal*, 6, pp.2002–13.
Yi, H. et al., 2009. Selection of a variant of Geobacter sulfurreducens with enhanced capacity for current production in microbial fuel cells. *Biosensors & Bioelectronics*, 24(12), pp.3498–503.
Yoho, R. et al., 2015. Anode biofilms of Geoalkalibacter ferrihydriticus exhibit electrochemical signatures of multiple electron transport pathways. *Langmuir*, p.151021123809009.
Yoho, R.A., Popat, S.C. & Torres, C.I., 2014. Dynamic Potential-Dependent Electron Transport Pathway Shifts in Anode Biofilms of Geobacter sulfurreducens. *ChemSusChem*, 7(12), pp.3413–9.

Yoshizawa, T. et al., 2014. Conversion of activated-sludge reactors to microbial fuel cells for wastewater treatment coupled to electricity generation. *Journal of Bioscience and Bioengineering*, 118(5), pp.533–539.
Zhang, Y. et al., 2009. Generation of electricity and analysis of microbial communities in wheat straw biomass-powered microbial fuel cells. *Applied and Environmental Microbiology*, 75(11), pp.3389–95.
Zhu, X., Yates, M.D., Hatzell, M.C., Ananda Rao, H., et al., 2014. Microbial Community Composition Is Unaffected by Anode Potential. *Environmental Science & Technology*, 48(2), pp.1352–1358.
Zhu, X., Yates, M.D., Hatzell, M.C., Rao, H.A., et al., 2014. Response to Comment on Microbial Community Composition Is Unaffected by Anode Potential. *Environmental Science & Technology*, 48(24), pp.14853–14854.
Zhu, X., Yates, M.D. & Logan, B.E., 2012. Set potential regulation reveals additional oxidation peaks of Geobacter sulfurreducens anodic biofilms. *Electrochemistry Communications*, 22, pp.116–119.